

# QGPU: Parallel logic in quantum LDPC codes

Boren Gu,<sup>1,2,3,\*</sup> Andy Zeyi Liu,<sup>4,5</sup> Armanda O. Quintavalle,<sup>1</sup> Qian Xu,<sup>6,7</sup> Jens Eisert,<sup>1</sup> and Joschka Roffe<sup>2,†</sup>

<sup>1</sup>*Dahlem Center for Complex Quantum Systems, Freie Universität Berlin, Berlin, 14195, Germany*

<sup>2</sup>*Quantum Software Lab, The University of Edinburgh, Edinburgh, EH8 9AB, United Kingdom*

<sup>3</sup>*Higgs Centre for Theoretical Physics, The University of Edinburgh, Edinburgh, EH9 3FD, United Kingdom*

<sup>4</sup>*Yale Quantum Institute, Yale University, New Haven, CT 06511, United States*

<sup>5</sup>*Department of Applied Physics, Yale University, New Haven, CT 06511, United States*

<sup>6</sup>*Institute for Quantum Information and Matter, California Institute of Technology, Pasadena, CA 91125, United States*

<sup>7</sup>*Walter Burke Institute for Theoretical Physics, California Institute of Technology, Pasadena, CA 91125, United States*

(Dated: March 6, 2026)

Quantum error correction is critical in the design and manufacture of scalable quantum computing systems. In recent years, there has been growing interest in quantum low-density parity-check codes as a resource-efficient alternative to the traditional surface code approach. However, their widespread adoption has been limited by the difficulty of compiling fault-tolerant logical operations. A key challenge is that logical qubits in quantum low-density parity-check codes do not necessarily correspond to distinct groups of physical qubits, which limits the number of logical operations that can be performed in parallel compared with the surface code. In this work, we introduce clustered-cyclic codes, a family of quantum low-density parity-check codes with finite-size instances such as  $[[136, 8, 14]]$  and  $[[198, 18, 10]]$  that are competitive with current state-of-the-art constructions. These codes are designed to support a directly addressable logical basis and therefore enable highly parallel logical measurement layers. To exploit this structure, we introduce parallel product surgery for quantum product codes. The protocol uses an additional copy of the data code patch as an auxiliary patch together with an engineered product connection structure to implement many logical Pauli-product measurements within a single surgery round at small and fixed overhead, enabling surface-code-style maximal parallelism for clustered-cyclic codes: up to  $k/2$  disjoint Pauli-product measurements can be scheduled in a single round under explicit algebraic conditions. To establish fault tolerance, we prove that parallel product surgery preserves the code distance when applied to hypergraph product codes and numerically verify that it preserves the distance for all listed clustered-cyclic code instances with logical dimension  $k = 8$ . Finally, we give an explicit example using the  $[[24, 8, 3]]$  clustered-cyclic code: by treating half of the logical qubits as auxiliaries, parallel product surgery enables arbitrary logical *CNOT* gates on disjoint pairs of qubits to be executed in parallel, and together with symmetry-derived operations, we show that these gates generate the full Clifford group fault-tolerantly.

## I. INTRODUCTION

Quantum error correction has emerged as one of the fastest-growing areas in quantum computing—and for compelling reasons. There is now overwhelming evidence that scalable, reliable quantum computation will only become a reality if fragile quantum information is protected through quantum error correction and fault tolerance [1–8]. Without these tools, large-scale quantum devices would remain fundamentally unstable. A landmark moment in the field was the introduction of the surface code in 1997: a planar topological code combining conceptual elegance with an unusually high error threshold [1, 4, 9]. For many years thereafter, it appeared—at least from a theoretical perspective—that the foundational questions of quantum error correction had largely been resolved. In the memorable words of Daniel Gottesman, what followed were the ‘middle ages’ of quantum error correction.

Yet, much like the historical Middle Ages, this period was far from being stagnant. Beneath the surface, substantial innovations were taking shape. In particular, the systematic study of *quantum low-density parity-check* (qLDPC) codes proved to be extraordinarily fruitful [10–13]. It became clear that

genuinely ‘good’ quantum codes could exist—codes whose distance and encoding rate both scale linearly with the number of physical qubits [13–15]. This development fundamentally reshaped expectations about what quantum codes could achieve. The true renaissance of quantum error correction, however, was catalysed by rapid experimental progress in quantum hardware, which in turn sparked a wave of new theoretical advances [16–18]. Nevertheless, strong code parameters alone are not sufficient and major bottlenecks remain. High thresholds and favourable scaling as such do not automatically translate into practical quantum computing. We require not only robust quantum memories, but codes that enable efficient logical quantum computation—ultimately, full universal fault-tolerant quantum computing [19–25].

A common approach for the compilation of fault-tolerant logical operations is organised around the *Pauli-product measurements* (PPMs) [26] framework for quantum computation: one performs rounds of (possibly multi-qubit) PPMs on encoded data, processes the classical outcomes, and updates a Pauli frame rather than physically correcting every byproduct. The computational workload is then naturally expressed as a sequence of measurement layers, each of which consists of a set of mutually commuting Pauli observables that can be measured simultaneously using code surgery methods [20, 27–29]. Clifford processing can be driven entirely within this measurement-and-tracking paradigm [21, 27, 30], while non-Clifford resources enter through designated primitives such as

\* [b.gu@fu-berlin.de](mailto:b.gu@fu-berlin.de)

† [joschka@roffe.eu](mailto:joschka@roffe.eu)

state injection, cultivation or code switching [22, 23, 25, 31]. This immediately elevates a single question to primary importance: how many logical PPMs can be implemented *in parallel per round* with controlled overhead?

For the surface code [1, 9, 20, 21], these ideas are conceptually very clean. Each logical qubit lives in its own patch, so it is spatially individually addressable. That provides a strong notion of parallelism: all single-qubit Cliffords can be applied locally and simultaneously across patches, and lattice surgery operations can be scheduled in parallel subject only to the interaction constraints between patches [21]. Concretely, lattice surgery realises joint logical Pauli measurements via geometric *merge* and *split* operations between patches [20]. As each merge consumes two patches, a single surgery round has a simple combinatorial ceiling: if  $k$  patches are available and each joint measurement pairs two patches, then at most  $\lfloor k/2 \rfloor$  disjoint merges can be performed simultaneously (assuming access to sufficient routing space). The architecture itself makes parallel logical control feel almost automatic.

Once we move to qLDPC codes, we gain encoding density, but we lose that clarity. Logical operators are not necessarily attached to specific sub-groups of qubits and are often heavily overlapping, so the idea of a ‘logical qubit’ as a distinct object becomes much less concrete [32, 33]. It is no longer obvious how to apply gates independently, and parallelism becomes harder to define and optimise. Here, two recurring bottlenecks arise. First, *logical operators* in many promising qLDPC codes [14] tend to lack a clean structure. Without a well-organised logical operator basis, fault-tolerant logical measurements do not follow a simple, uniform construction, and typically require designs tailored to the specific code and measurement being implemented [34–38]. Second, logical operations *fail to parallelise* automatically as for surface code computation. This limits computational throughput and increases effective overhead.

### A. Overview of results

In this work, we develop a code–logic co-design for fault-tolerant computation with qLDPC codes, guided by a single architectural goal: *high-throughput logical computation via parallel PPMs at small and fixed overhead*. We address this by introducing a subfamily of *lifted product* (LP) codes [14], the *clustered-cyclic* (CC) codes (Sec. IV), whose logical operator basis is engineered to behave like a surface code patch model (Fig. 1 (a)).

Building on this clustered basis, we introduce *parallel product surgery*, a generalised surgery technique [29] developed alongside this code family and applicable to all quantum product codes. The protocol uses an additional copy of the *data code patch* as an *auxiliary code patch*, together with an engineered *connection* structure, to implement many logical PPMs within a single surgery round at small and fixed overhead. A central outcome is that, for CC codes, the maximum per-round measurement parallelism matches that of surface-code lattice surgery: given  $k$  logical qubits, up to  $k/2$  joint logical Pauli measurements can be scheduled in a single round. Hence, par-

allel product surgery on CC codes addresses the parallelism bottleneck by imposing a structured logical operator basis, thereby enabling highly parallel logical measurements.

In Tables II and III and Figure 2, we report the most favourable cases of space-time overhead reduction of our protocol for suitably chosen PPMs on CC codes with respect to the state-of-the-art logical PPM gadgets [28, 39].

Our CC code family, combined with parallelised product surgery, embeds parallel logical control directly at the code level. In contrast to surface code computation, where parallelism resembles a multi core CPU with separate local processing units, our construction realises a single encoding block with intrinsic logical parallelism, more akin to a quantum GPU. Logical operations are not distributed across distinct patches but are natively supported within the global structure of the code. Building on the existing corpus of work on logical computation in qLDPC codes [28, 39–47], we believe this work represents an important step towards the development of universal instruction sets that will ultimately underpin utility-scale qLDPC-based quantum computers.

### B. Structure of this work

This manuscript is organised as follows: In Sec. II we summarise the key insights and main results. In Sec. III we review the algebraic and coding-theoretic background underlying our construction, including LP codes and their representation as chain complexes. Building on this, Sec. IV introduces CC codes and proves the existence of a clustered logical basis with the required patch-like structure. In Sec. V we present parallel product surgery for quantum product codes and specialise it to CC codes, deriving explicit parallel scheduling rules and conditions under which surface-code-level maximal parallelism is achieved. We also investigate the resource overhead of the proposed measurement procedures. Sec. VI analyses fault tolerance, including distance-preservation properties and the LDPC nature of parallel product surgery. In Sec. VII we provide finite-size case studies and compilation examples for full Clifford groups with automorphism and fold-transversal logical operations, illustrating how the CC structure and surgery primitives combine into practical fault-tolerant logical gadgets. Finally, we discuss the physical implementation of our proposed schemes in Sec. VIII and we discuss future directions to explore and give a summary of our work in Sec. IX.

## II. KEY RESULTS

Before proceeding, we briefly survey several recent approaches to parallel logical computation. These include schemes based on concatenated codes [48–50], colour codes defined on hyperbolic manifolds [51], and, in particular, *hypergraph product* (HGP) codes. A key advantage of HGP codes is that they admit a canonical logical operator basis, following the construction of Quintavalle *et al.* [32], which enables logical operators to be partitioned and addressed systematically. Leveraging this structure, a range of parallel protocols has

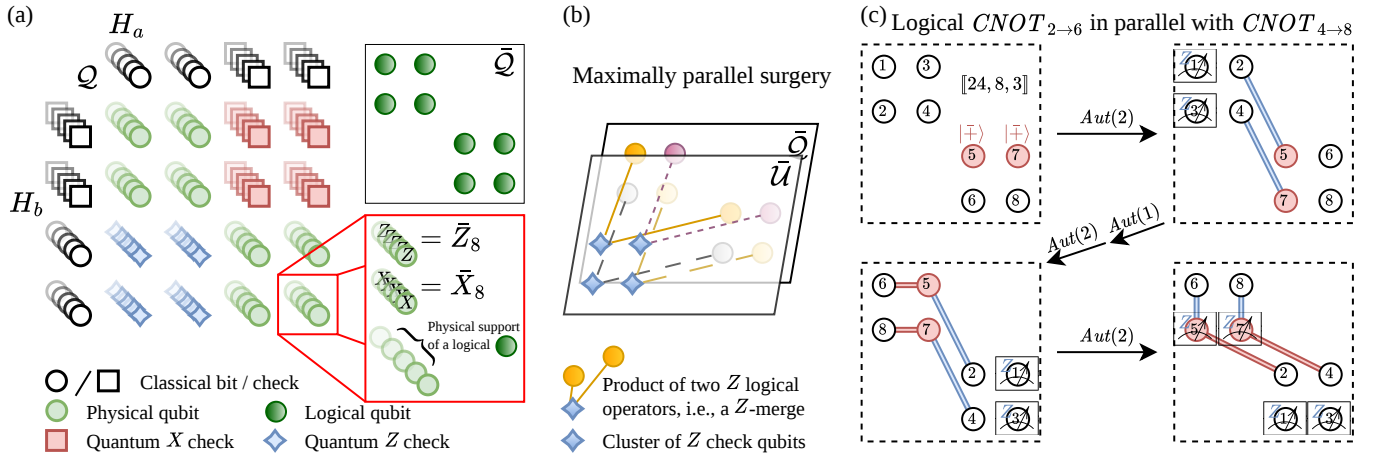


**FIG. 1. Illustration of the clustered logical operator basis of CC codes and maximally parallel surgery.** (a) Each CC code  $Q$  is constructed as the tensor product of two classical seed codes  $H_a$  and  $H_b$ . As an LP code defined over  $R = \mathbb{F}_2[x]/(x^p + 1)$ , passing to the binary representation lifts each ring element to a *cluster* of  $p$  physical qubits. Qubits and quantum checks can therefore be visualised as a square array of clusters inheriting the structure of the classical seed codes. Physical qubits partition into two sectors corresponding to the direct-sum structure in Equation (5). Every CC code admits a clustered logical operator basis in which each logical operator is supported on an entire cluster. If two basis elements anti-commute, their supports coincide on that whole cluster of physical qubits. Each logical qubit can thus be addressed directly via its associated physical cluster. (b) Maximally parallel surgery on CC codes performing four joint  $Z$  logical measurements across eight logical qubits. A second copy of the data patch is prepared as an auxiliary patch. Connections between  $Z$ -type checks of the auxiliary patch and data qubits in the original patch are determined by the product connection code  $\mathcal{P}$  with parity check matrices  $(H'_X, H'_Z)$ . Maximal parallelism is obtained when the parity check matrix of  $\mathcal{P}$  has full rank. The four measured logical pairs are distinguished by colours and connection lines. (c) Two logical  $CNOT$  gates executed in parallel with fixed space overhead for the  $[[24, 8, 3]]$  CC code. Logical  $CNOT_{2 \rightarrow 6}$  and  $CNOT_{4 \rightarrow 8}$  are implemented using both  $X$ - and  $Z$ -basis logical PPMs as described in Figure 4, treating logical qubits 1, 3, 5, 7 as auxiliaries. For example, a joint  $ZZ$  measurement between 2, 5 followed by a joint  $XX$  measurement between 5, 6, together with state initialisation and logical  $Z$  measurement on 5 implements the logical  $CNOT_{2 \rightarrow 6}$ . Together with automorphism-induced logical  $SWAP$  gates available in the  $[[24, 8, 3]]$  CC code, every stage of the protocol can be parallelised, including state initialisation, both types of joint logical measurements, and measurements of auxiliary qubits. Logical qubits are depicted as numbered circles, with red circles initialised in the  $|\bar{+}\rangle$  state vector. Blue and red double lines represent  $Z$ -type and  $X$ -type merges, respectively. The entire procedure requires only 48 additional physical qubits, consisting of 24 auxiliary data qubits and 24 auxiliary check qubits. A concrete construction for implementing arbitrary logical  $CNOT$  gates, and for parallelising arbitrary pairs of logical  $CNOT$  gates on four logical qubits of the  $[[24, 8, 3]]$  CC code, appears in Appendix K. Compilation of the full Clifford group on four logical qubits is illustrated in Section VII.

been developed for HGP codes, including approaches based on code switching [46], teleportation [52], and homomorphic logical measurements [30, 53]. Very recently, a constant-time-overhead surgery protocol has also been proposed for HGP codes, again exploiting their canonical logical operator basis [54].

Our work complements these studies by focusing instead on CC codes, which exhibit better finite-size code parameters than previously studied HGP codes [17]. We also note that a related randomised parallel surgery technique was introduced for high-rate qLDPC codes [55]; here we give an explicit construction of the required auxiliary system, thereby systematising that approach. Finally, Xu *et al.* [45] introduced a method for executing the same logical operations in parallel across multiple patches of high-rate qLDPC codes; by contrast, we develop a parallel scheme that realises many logical operations within a single code patch—enabling a quantum GPU style of computation.

### A. Clustered-cyclic code construction

In this subsection, we sketch the new family of codes we introduce in this work. We define CC codes as a constrained family of LP codes (Def. III.1) over the ring  $R = \mathbb{F}_2[x]/(x^p + 1)$  with prime lift parameter  $p$ , specified by cyclically structured seed matrices (Def. IV.1). We write  $CC(H_a, H_b)$  for a CC code with square seed matrices of sizes  $n_a$  and  $n_b$ , respectively. The binary CSS code  $CC(H_a, H_b)$  has parameters

$$[[N = 2pn_a n_b, k = 2n_a n_b, d \leq p]],$$

and constant check weight  $W = 2(w_a + w_b)$ , where  $w_a$  and  $w_b$  are the row weights of  $H_a$  and  $H_b$  respectively, which are uniform by construction.

Table I lists explicit CC codes with check weight  $W = 8$  identified via numerical search (App. F), including high-rate examples such as  $[[136, 8, 14]]$  and  $[[198, 18, 10]]$ , and compares their parameters with those of other known code families.

Fig. 3 presents phenomenological logical error rate simulations comparing these codes with the  $[[144, 12, 12]]$  Gross BB code, together with circuit-level memory simulations for the  $k = 8$  and  $k = 18$  CC code families.

The defining computational feature of CC codes is the existence of the clustered logical operator basis (Def. IV.2). Informally, the  $N$  physical qubits decompose into clusters of size  $p$ , and each logical operator in the basis is supported on an entire cluster, without overlapping with other logical operators of the same type. Whenever two logical operators in the basis anti-commute, their supports coincide on the full cluster (Fig. 1 (a)). The resulting interaction pattern closely resembles the structure of surface code architectures.

Theorem IV.3 establishes that every CC code  $CC(H_a, H_b)$  admits such a clustered logical basis. The clustered structure is the key ingredient enabling selective and parallel logical measurements. Scheduling and compilation reduce to combinatorial questions on clusters, rather than to unstructured manipulation of heavily overlapping, high-weight representatives.

### B. Parallel product surgery

To implement logical PPMs with high degrees of parallelism, we introduce a surgery primitive tailored to quantum product codes. Starting from a generalised CSS surgery framework (Def. V.1) [29], we choose the auxiliary patch to be a copy of the data patch and take the connection homomorphisms to be the parity check matrix of a same-size quantum product code (Def. V.2), which guarantees that the resulting merged complex defines a valid CSS surgery construction (Lem. V.3).

Product surgery nevertheless has limitations. Specifically, when used on HGP and CC codes [30, 55], two same-type logical operators can be merged only if they are supported in different sectors, or if they are aligned along the same row or column within a sector (Coro. V.11). To handle more general measurements, we introduce a hybrid gadget based on the gauging-based logical measurement technique [28], a state-of-the-art surgery method for arbitrary measurements, and augment it with parallel surgery whenever the target measurement contains sub-configurations compatible with product surgery.

For CC codes, we specialise to LP connection codes whose seed entries are restricted to 0, 1 over the ring  $R = \mathbb{F}_2[x]/(x^p + 1)$  (Def. V.4). This restriction ensures that merges are well defined on the clustered basis: products of logical operators supported on entire clusters can be realised as products of stabilisers introduced by the connection code (Theo. V.5). Concretely, each non-zero row of the connection code  $Z$ -check matrix  $H'_Z$  induces a merge of  $Z$ -type logical operators of the data patch. Consequently, the number  $M$  of logical PPMs being performed in one surgery round (Coro. V.7) is

$$M = \text{rank } H'_Z.$$

These properties provide a direct design rule:  $H'_Z$  decides the set of simultaneously measurable joint logical observables, and  $\text{rank } H'_Z$  quantifies the number of independent merges

achieved in that round. In short, for a CC code encoding  $k = 2n_a n_b$  logical qubits, up to

$$M_{\max} = k/2 = n_a n_b$$

$Z$ -type merges can be performed in a single round. This bound is achieved whenever the chosen product connection code satisfies  $\text{rank } H'_Z = n_a n_b$  (Theo. V.9).

As an example, for the  $[[136, 8, 14]]$  CC code, we observe that ‘boosting’ gauging-based logical measurements with parallel surgery reduces the auxiliary space overhead by approximately 150 physical qubits on average, when measuring combinations of single logical operators and pairs of joint logical operators (Fig. 2).

### C. Case study: $[[24, 8, 3]]$ and complete Clifford group over four logical qubits

To provide an explicit finite-size demonstration, we instantiate our construction on the  $[[24, 8, 3]]$  CC code. In this example, we exploit both fold-transversal logical gates [32, 56] and automorphism-induced logical gates [42] to realise fault-tolerant logical phase, Hadamard, and swap gates (App. J). Using these symmetries, we enlarge the set of merge configurations compatible with product surgery.

Treating four of the eight logical qubits as reusable auxiliaries, we obtain a four-logical-qubit data block on which we can implement arbitrary logical  $CNOT$  connectivity in parallel via parallel surgery (App. K, Fig. 1 (c)). Crucially, together with fold-transversal and automorphism-induced logical operations, these primitives generate the full Clifford group on the data block of four logical qubits (Sec. VII A), via a new generating set of the Clifford groups up to global phase (Theo. VII.1)

$$C_m/U(1) \cong \langle X_i, Z_i, CNOT_{i \rightarrow j}, S_i S_j^\dagger, H^{\otimes m} \rangle, \quad m \geq 3.$$

This case study therefore, illustrates end-to-end how the CC structure turns abstract qLDPC code parameters into an explicit, schedulable logical toolbox for Clifford operations with fixed per-round auxiliary overhead.

## III. PRELIMINARIES

### A. Ring, module and binary representation

We now outline the mathematical foundations of our code construction. Let  $G$  be a finite abelian group of order  $l$ . The group algebra of  $G$  over  $\mathbb{F}_2$ , denoted  $R = \mathbb{F}_2[G]$ , is a finite commutative ring. Throughout this work, we only consider such group algebras and free, finite-rank  $R$ -modules. A polynomial ring in  $x$  over  $\mathbb{F}_2$ , denoted  $\mathbb{F}_2[x]$ , consists of polynomials  $q = q_0 + q_1 x + \dots + q_m x^m$  with coefficients  $q_i \in \mathbb{F}_2$ . The quotient ring  $\mathbb{F}_2[x]/(x^l + 1)$  is obtained by imposing the relation  $x^l = 1$ . As a group algebra,  $\mathbb{F}_2[x]/(x^l + 1) \cong \mathbb{F}_2[C_l]$ , where  $C_l = \langle g \mid g^l = 1 \rangle$  is the cyclic group of order  $l$ .

An  $R$ -module may be viewed as a generalisation of a vector space in which the scalars are drawn from  $R$  rather than a

field. Homomorphisms between modules of the form  $R^n$  and  $R^m$  are represented by matrices  $M \in R^{m \times n}$ . We use the standard notion of rank over a commutative ring, defined as the largest  $r$  such that  $M$  contains an  $r \times r$  minor submatrix with non-zero determinant, and the matrix is called full rank if  $r = \min\{m, n\}$ .

Since  $R = \mathbb{F}_2[G]$  is an  $l$ -dimensional vector space over  $\mathbb{F}_2$  with basis  $\{g\}_{g \in G}$ , any  $R$ -linear map admits a faithful binary representation [57, Theorem 1.3.1]. We define the following binary representation of homomorphisms

$$\mathbb{B} : R^{m \times n} \rightarrow \mathbb{F}_2^{(lm) \times (ln)}; \quad M_{i,j} \mapsto \mathbb{B}(M_{i,j}) \in \mathbb{F}_2^{l \times l},$$

where  $\mathbb{B}(M_{i,j})$  is the faithful binary representation of the ring element  $M_{i,j}$  [14]. Accordingly,  $R$ -modules are lifted as  $\mathbb{B}(R^m) = \mathbb{F}_2^{lm}$ .

The group algebra  $R = \mathbb{F}_2[G]$  is equipped with a canonical involution  $*$  :  $R \rightarrow R$ , defined as the  $\mathbb{F}_2$ -linear extension of group inversion  $g \mapsto g^{-1}$ . For  $R \cong \mathbb{F}_2[x]/(x^l+1)$ , we identify  $x \leftrightarrow g$ , this involution acts as

$$* : q_0 + q_1x + \dots + q_mx^m \mapsto q_0 + q_1x^{l-1} + \dots + q_mx^{l-m}.$$

For a matrix  $M = (M_{i,j})_{m \times n}$ , we define its conjugate transpose as  $M^* = (M_{j,i}^*)_{n \times m}$ . The involution guarantees consistency between  $R$ -module conjugate transposition and the binary representation, satisfying

$$\mathbb{B}(M^*) = \mathbb{B}(M)^\top.$$

For example, let  $R = \mathbb{F}_2[x]/(x^3+1)$ , the binary representation of the following matrix and its conjugate transpose are, respectively,

$$M = \begin{pmatrix} 1 & 1+x \\ x^2 & x+x^2 \end{pmatrix}, \quad M^* = \begin{pmatrix} 1 & x \\ 1+x^2 & x+x^2 \end{pmatrix};$$

$$\mathbb{B}(M) = \begin{pmatrix} 1 & 0 & 0 & 1 & 1 & 0 \\ 0 & 1 & 0 & 0 & 1 & 1 \\ 0 & 0 & 1 & 1 & 0 & 1 \\ 0 & 0 & 1 & 0 & 1 & 1 \\ 1 & 0 & 0 & 1 & 0 & 1 \\ 0 & 1 & 0 & 1 & 1 & 0 \end{pmatrix}, \quad \mathbb{B}(M)^\top = \begin{pmatrix} 1 & 0 & 0 & 0 & 1 & 0 \\ 0 & 1 & 0 & 0 & 0 & 1 \\ 0 & 0 & 1 & 1 & 0 & 0 \\ 1 & 0 & 1 & 0 & 1 & 1 \\ 1 & 1 & 0 & 1 & 0 & 1 \\ 0 & 1 & 1 & 1 & 1 & 0 \end{pmatrix}.$$

## B. The chain complex representation of CSS codes

Chain complexes from homological algebra form the structural backbone of our construction. They already occupy a central role in quantum error correction, and here serve as the primary framework for designing CC codes.

A length- $n$  chain complex  $\mathcal{A} = (\{A_i\}, \{\partial_i\})$  is a sequence of  $R$ -modules,  $A_0, \dots, A_n$  and homomorphisms  $\partial_i : A_i \rightarrow A_{i-1}$ ,

$$A_n \xrightarrow{\partial_n} A_{n-1} \xrightarrow{\partial_{n-1}} \dots \xrightarrow{\partial_2} A_1 \xrightarrow{\partial_1} A_0,$$

satisfying the boundary condition  $\partial_i \circ \partial_{i+1} = 0$ . The  $i^{\text{th}}$  homology group,  $H_i(\mathcal{A})$ , and corresponding  $i^{\text{th}}$  cohomology group,  $H^i(\mathcal{A})$ , of this chain complex are defined as

$$H_i(\mathcal{A}) = \ker(\partial_i) / \text{im}(\partial_{i+1}),$$

$$H^i(\mathcal{A}) = \ker(\partial_{i+1}^*) / \text{im}(\partial_i^*).$$

Applying the binary representation entry-wise yields a length- $n$  chain complex  $\mathbb{B}(\mathcal{A})$  over  $\mathbb{F}_2$ ,

$$\mathbb{B}(A_n) \xrightarrow{\mathbb{B}(\partial_n)} \mathbb{B}(A_{n-1}) \xrightarrow{\mathbb{B}(\partial_{n-1})} \dots \xrightarrow{\mathbb{B}(\partial_2)} \mathbb{B}(A_1) \xrightarrow{\mathbb{B}(\partial_1)} \mathbb{B}(A_0).$$

Since  $\mathbb{B}(\cdot)$  preserves matrix multiplication, the boundary condition is preserved under binary lifting. Taking the binary representation of (co-) homology groups yields exactly the (co-) homology groups of  $\mathbb{B}(\mathcal{A})$ .

The simplest example here is a classical error-correcting code as a length-1 chain complex,

$$C : C_1 \xrightarrow{H} C_0,$$

where  $C_1 = R^n$ ,  $C_0 = R^m$  and  $H \in R^{m \times n}$  is the parity check matrix over  $R$ . By taking binary representation,  $\mathbb{B}(C)$  recovers the standard binary format of the code with check matrix  $\mathbb{B}(H) \in \mathbb{F}_2^{(lm) \times (ln)}$ . Binary classical codes are the special cases when  $R = \mathbb{F}_2$ .

An  $[[N, k, d]]$  quantum stabiliser code  $\mathcal{Q}$  is a  $2^k$ -dimensional logical subspace of the  $N$ -qubit physical Hilbert space [2–4, 26]. It is specified as the common +1 eigenspace of an Abelian subgroup  $\mathcal{S}$  of  $\mathcal{P}_N$  that does not contain  $-I$ . Logical operators are Pauli operators that act non-trivially on logical qubits while preserving the stabilisers. They are elements of the quotient group  $\mathcal{N}(\mathcal{S})/\mathcal{S}$ , where  $\mathcal{N}$  denotes the normaliser in  $\mathcal{P}_N$ . The distance  $d$  of the code is defined as the minimum Hamming weight of a logical operator in binary representation: it can be seen as a *quality measure* of the code, and higher distances are beneficial. When relevant, we distinguish  $d_x$  and  $d_z$  for logical operators of  $X$ - and  $Z$ -type.

In all that follows, we will consider instances of *Calderbank–Shor–Steane* (CSS) codes. They are an important family of stabiliser codes whose generators can be chosen to be purely  $X$ - or  $Z$ -type, described by check matrices  $H_X \in R^{m_X \times n}$  and  $H_Z \in R^{m_Z \times n}$ , respectively. Such codes are by far the most common type of quantum error correction code. Such codes admit a natural description as length-2 chain complexes,

$$\mathcal{Q} : \mathcal{Q}_2 \xrightarrow{H_Z^*} \mathcal{Q}_1 \xrightarrow{H_X} \mathcal{Q}_0.$$

The binary representation  $\mathbb{B}(\mathcal{Q})$  yields the standard stabiliser formalism for qubits, with  $\mathbb{B}(\mathcal{Q}_1)$  corresponding to the  $N = nl$  physical qubits, and  $\mathbb{B}(\mathcal{Q}_2)$  and  $\mathbb{B}(\mathcal{Q}_0)$  corresponding to  $Z$ - and  $X$ -type stabiliser checks, respectively. Each row of  $\mathbb{B}(H_X)$  ( $\mathbb{B}(H_Z)$ ) specifies an  $X$ -type ( $Z$ -type) stabiliser.

Stabiliser commutativity is equivalent to the condition

$$\mathbb{B}(H_X)\mathbb{B}(H_Z)^\top = 0 \iff H_X H_Z^* = 0,$$

which coincides with the boundary condition of the chain complex and is commonly referred to as the CSS condition.

For CSS codes, logical  $X$  and  $Z$  operators naturally appear as the cohomology and homology groups, respectively, of the associated chain complex,

$$\mathcal{L}_X := H^1(\mathcal{Q}) = \ker H_Z / \text{im} H_X^*,$$

$$\mathcal{L}_Z := H_1(\mathcal{Q}) = \ker H_X / \text{im} H_Z^*.$$

### C. Lifted product code

The lifted product is a technique for constructing CSS codes from pairs of *classical seed codes*. In this section, we derive it from the starting point of chain complexes.

Let  $\mathcal{A} = (\{A_i\}, \{\partial_i^A\})$  and  $\mathcal{B} = (\{B_i\}, \{\partial_i^B\})$  be length- $m_A$  and length- $m_B$  chain complexes over  $R$ , respectively. Their tensor product  $\mathcal{A} \otimes_R \mathcal{B}$  is defined as a length- $(m_A + m_B)$  chain complex over  $R$  with modules

$$\{(\mathcal{A} \otimes_R \mathcal{B})_m = \oplus_{i+j=m} A_i \otimes_R B_j\}_{m=0}^{m_A+m_B}$$

and homomorphisms

$$\{\partial_m^{AB} : (\mathcal{A} \otimes_R \mathcal{B})_m \rightarrow (\mathcal{A} \otimes_R \mathcal{B})_{m-1}\}_{m=1}^{m_A+m_B},$$

where  $\partial_m^{AB}$  is defined as

$$\partial_m^{AB}(a_i \otimes_R b_j) = \partial_i^A(a_i) \otimes_R b_j + a_i \otimes_R \partial_j^B(b_j),$$

for  $a_i \in A_i, b_j \in B_j$  and  $i + j = m$  [58]. This construction is also referred to as the total complex of the product complex. We then define the *lifted product* (LP) codes in this framework.

**Definition III.1** (Lifted product codes). Given classical codes  $\mathcal{A} : A_1 \xrightarrow{H_a} A_0$  and  $\mathcal{B} : B_1 \xrightarrow{H_b} B_0$  over  $R$ , a lifted product code, denoted  $Q = \text{LP}(H_a, H_b)$ , is defined as the total complex of  $\mathcal{A} \otimes_R \mathcal{B}$  given by

$$\begin{array}{ccccc} & & Q_0 & & \\ & & \uparrow H_X & & \\ & & Q_1 & & \\ & & \uparrow H_Z^* & & \\ & & Q_2 & & \\ A_1 \otimes_R B_0 & \xrightarrow{H_a \otimes_R I} & A_0 \otimes_R B_0 & \xleftarrow{I \otimes_R H_b} & A_0 \otimes_R B_1 \\ & \nwarrow I \otimes_R H_b & & \nearrow H_a \otimes_R I & \\ & & A_1 \otimes_R B_1 & & \end{array}, \quad (5)$$

where  $Q_1 = A_1 \otimes_R B_0 \oplus A_0 \otimes_R B_1$ .

The corresponding check matrices of  $Q$  as a CSS code are

$$\begin{aligned} H_X &= (H_a \otimes_R I \mid I \otimes_R H_b), \\ H_Z &= (I \otimes_R H_b^* \mid H_a^* \otimes_R I), \end{aligned}$$

where the vertical bar indicates horizontal concatenation of matrices. The CSS condition follows directly,

$$\begin{aligned} H_X H_Z^* &= (H_a \otimes_R I)(I \otimes_R H_b) + (I \otimes_R H_b)(H_a \otimes_R I) \\ &= H_a \otimes_R H_b + H_a \otimes_R H_b \\ &= 0, \end{aligned}$$

which coincides with the boundary condition of the chain complex.

Owing to the tensor product structure of LP codes, the logical operators can be characterised using the Künneth formula, a statement relating the homology of two objects to the homology of their product, in particular when  $R = \mathbb{F}_2[G]$ , for a finite odd order cyclic group  $G$ .

**Lemma III.2** (Künneth formula [58, 59]). Let  $R = \mathbb{F}_2[G]$  with  $G$  a finite odd order cyclic group. The (co-)homology group of the product complex  $Q = \mathcal{A} \otimes_R \mathcal{B}$  is subject to the isomorphism

$$\begin{aligned} H^m(\mathcal{A} \otimes_R \mathcal{B}) &\cong \bigoplus_{p+q=m} H^p(\mathcal{A}) \otimes_R H^q(\mathcal{B}), \\ H_m(\mathcal{A} \otimes_R \mathcal{B}) &\cong \bigoplus_{p+q=m} H_p(\mathcal{A}) \otimes_R H_q(\mathcal{B}). \end{aligned}$$

For LP codes, the logical operators are, therefore, given by

$$\begin{aligned} \mathcal{L}_X &= H^1(\mathcal{A}) \otimes_R H^0(\mathcal{B}) \oplus H^0(\mathcal{A}) \otimes_R H^1(\mathcal{B}), \\ \mathcal{L}_Z &= H_1(\mathcal{A}) \otimes_R H_0(\mathcal{B}) \oplus H_0(\mathcal{A}) \otimes_R H_1(\mathcal{B}). \end{aligned}$$

In terms of check matrices, this can be written explicitly as

$$\begin{aligned} \mathcal{L}_X &= (R^{n_a}/\text{im } H_a^*) \otimes_R \ker H_b^* \oplus \ker H_a^* \otimes_R (R^{n_b}/\text{im } H_b^*), \\ \mathcal{L}_Z &= \ker H_a \otimes_R (R^{n_b}/\text{im } H_b) \oplus (R^{n_a}/\text{im } H_a) \otimes_R \ker H_b. \end{aligned}$$

Interpreting the direct sum above as a partition of physical qubits into two sectors, as in Figure 1 (a), logical operators can be generated (up to stabilisers) by

$$\begin{aligned} \mathcal{L}_X &= \mathcal{L}_X^{\text{left}} \cup \mathcal{L}_X^{\text{right}} \\ &= \{(\bar{l}_a \otimes_R \bar{k}_b, \mathbf{0}) : \bar{l}_a \in R^{n_a}/\text{im } H_a^*, \bar{k}_b \in \ker H_b^*\} \\ &\quad \cup \{(\mathbf{0}, \bar{k}_a \otimes_R \bar{l}_b) : \bar{k}_a \in \ker H_a^*, \bar{l}_b \in R^{n_b}/\text{im } H_b^*\}, \\ \mathcal{L}_Z &= \mathcal{L}_Z^{\text{left}} \cup \mathcal{L}_Z^{\text{right}} \\ &= \{(k_a \otimes_R l_b, \mathbf{0}) : k_a \in \ker H_a, l_b \in R^{n_b}/\text{im } H_b\} \\ &\quad \cup \{(\mathbf{0}, l_a \otimes_R k_b) : l_a \in R^{n_a}/\text{im } H_a, k_b \in \ker H_b\}. \end{aligned} \quad (6)$$

**Remark III.3** (Hypergraph product codes). The *hypergraph product* (HGP) codes are LP codes defined over the binary field, i.e.,  $R = \mathbb{F}_2$ .

## IV. CLUSTERED-CYCLIC QUANTUM LDPC CODE

A central ingredient for fault-tolerant logical operations is the availability of a well-organised logical operator basis. In HGP codes, the tensor product structure induces a canonical decomposition of logical operators via the Künneth formula [32, 60]. This canonical logical operator basis supports structured parallel implementations of logical operations [30, 46, 55].

In this section, we introduce a subclass of LP codes, which we call *clustered-cyclic* (CC) codes. By imposing constraints on the classical seed codes and exploiting the tensor-product structure through the Künneth formula, we obtain a logical operator basis with explicit representatives and a well-controlled symmetric structure. These constraints are chosen with the aim of facilitating logical measurements, in particular joint measurements of pairs of same-type logical operators (e.g.,  $XX$ -type or  $ZZ$ -type), which can then be scheduled in a highly

parallel manner in our surgery-based setting introduced in Section V. As we show in Section VII A, these measurement primitives enable parallel implementations of logical Clifford operations for the  $[[24, 8, 3]]$  CC code when combined with fold-transversal and automorphism-induced logical operations. We begin with a formal definition of CC codes.

**Definition IV.1** (Clustered-cyclic code). A clustered-cyclic code is a lifted product code  $LP(H_a, H_b)$  where  $H_a$  and  $H_b$  are square matrices defined over a polynomial quotient ring with prime lift parameter  $p$ ,  $R = \mathbb{F}_2[x]/(x^p + 1)$ . Entries of these matrices are either binomial or zero and the supports of the non-zero terms are placed in a cyclic way such that each row or column in a matrix has exactly the same number of non-zero binomials and the matrices are full rank.

In order to avoid confusion, we denote the CC code as  $CC(H_a, H_b)$ , where the sizes of the seed matrices are  $n_a$  and  $n_b$  respectively. The parity check matrices of the CC code are then given by

$$\begin{aligned} H_X &= (H_a \otimes_R I_{n_b} \mid I_{n_a} \otimes_R H_b), \\ H_Z &= (I_{n_a} \otimes_R H_b^* \mid H_a^* \otimes_R I_{n_b}). \end{aligned}$$

Here  $H_a^*$  is the conjugate transpose of  $H_a$  and  $I_m$  is the identity matrix of size  $m$  over the ring  $R$ .

There are no restrictions on the sizes of two seed matrices, they can be chosen to be the same or different. For example, over  $R = \mathbb{F}_2[x]/(x^5 + 1)$ ,

$$H_a = \begin{pmatrix} x^3 + x^4 & x^2 + x^3 & 0 \\ 0 & x + x^2 & x^3 + x^4 \\ x + x^3 & 0 & x^3 + x^4 \end{pmatrix} \text{ and } H_b = \begin{pmatrix} 1 + x^2 & 0 \\ 0 & x^2 + x^4 \end{pmatrix},$$

are two classical seed codes that would combine to form a valid CC code as described in Definition IV.1.

Both matrices  $H_X$  and  $H_Z$  have size  $(n_a n_b) \times (2n_a n_b)$ . After taking the binary representation, these two matrices are mapped to matrices  $\mathbb{B}(H_X)$  and  $\mathbb{B}(H_Z)$  of size  $(pn_a n_b) \times (2pn_a n_b)$  over  $\mathbb{F}_2$ . Each row  $s$  of length  $N = 2pn_a n_b$  of  $\mathbb{B}(H_X)$  defines an  $X$ -type stabiliser  $X(s) = \bigotimes_{i=1}^N X_i^{s_i}$ ; each row  $v$  of the same length of  $\mathbb{B}(H_Z)$  defines a  $Z$ -type stabiliser  $Z(v) = \bigotimes_{i=1}^N Z_i^{v_i}$ . Following Theorem IV.3 and Corollary IV.6, the code  $CC(H_a, H_b)$  has parameters

$$[[N = 2pn_a n_b, k = 2n_a n_b, d \leq p]],$$

where  $N$  is the number of physical qubits,  $k$  is the number of logical qubits, and  $d$  is the code distance. When the code distance saturates its upper bound, we have  $N = kd$ . As shown in Table I, this scaling is achieved for small  $p$ , whereas for  $p \geq 11$  the distance becomes increasingly separated from  $p$ . Once the row weights of the seed matrices – i.e., the number of non-zero entries of each row – are fixed, with all rows having the same weight, CC codes have constant check weight for all values of the lift parameter  $p$  and seed matrix sizes  $n_a$  and  $n_b$ . In particular, if the row weights of  $H_a$  and  $H_b$  are  $w_a$  and  $w_b$ , respectively, the check weight of the resulting CC code  $LP(H_a, H_b)$  is

CC codes		BB codes	QRC
$k = 8$	$k = 18$		
$[[24, 8, 3]]$ (3)	-	$[[28, 6, 4]]$	-
$[[40, 8, 5]]$ (5)	-	$[[42, 6, 6]]$	-
$[[56, 8, 7]]$ (7)	$[[54, 18, 3]]$ (3)	$[[56, 6, 8]]$	$[[54, 8, 3]]$
$[[88, 8, 10]]$ (11)	$[[90, 18, 5]]$ (5)	$[[90, 8, 10]]$	$[[90, 8, 10]]$
$[[104, 8, 11]]$ (13)	$[[126, 18, 7]]$ (7)	$[[120, 8, 12]]$	$[[126, 8, 14]]$
$[[136, 8, 14]]$ (17)	$[[198, 18, 10]]$ (11)	$[[144, 12, 12]]$	-

TABLE I. Parameters of clustered-cyclic (CC) codes compared with *bicycle-bivariate* (BB) codes [16, 61] and *quantum radial codes* (QRC) [62]. Two CC code families are shown, with logical dimensions  $k = 8$  ( $n_a = n_b = 2$ ) and  $k = 18$  ( $n_a = n_b = 3$ ). For both families of CC codes, the check weight is 8 and the parameters are displayed as  $[[N, k, d]]$  ( $p$ ). The corresponding seed matrices are provided in Appendix H. Code distances for CC codes are obtained via numerical estimation using QDistRand [63], for accuracies of this estimation refer to Appendix F.

$$W = 2(w_a + w_b). \quad (7)$$

Table I lists numerically discovered examples of high-rate CC codes. The codes are ordered by their number of physical qubits and are compared with *bicycle-bivariate* (BB) codes [16, 61] and *quantum radial codes* (QRC) [62] of similar numbers of physical qubits. We observe a comparable logical error suppression between the  $[[136, 8, 14]]$  CC code,  $[[198, 18, 10]]$  CC code and the  $[[144, 12, 12]]$  Gross BB code in Fig. 3 (c).

### A. Clustered logical operator basis

Surface codes come with a particularly transparent set of logical operators: one can identify logical  $X$  and  $Z$  operators as string-like Pauli operators on the underlying 2D lattice, and this geometric picture directly underpins fault-tolerant logical primitives such as lattice surgery. By contrast, for most known families of high-rate qLDPC codes, logical operators are typically not given by an equally simple logical operator basis, which makes it difficult to systematically design and schedule logical operations. The purpose of this subsection is to show that CC codes admit a *clustered* logical operator basis, in which each logical operator has an explicit representative supported on a ‘cluster’ of  $p$  physical qubit as demonstrated in Figure 1 (a). This added structure plays the same organisational role as the geometric logical basis in surface codes: it provides a concrete set of measurement primitives that can be composed into fault-tolerant logical operations.

**Definition IV.2** (Clustered logical operator basis). A logical operator basis  $(\mathcal{L}_X, \mathcal{L}_Z)$  of a LP code defined over  $R = \mathbb{F}_2[x]/(x^p + 1)$  is *clustered* if its binary representation  $(\mathbb{B}(\mathcal{L}_X), \mathbb{B}(\mathcal{L}_Z))$  satisfy

1. Any operator in  $\mathbb{B}(\mathcal{L}_X)$  or  $\mathbb{B}(\mathcal{L}_Z)$  is supported on a ‘cluster’ of qubits: here, by a cluster we mean that the  $N$  physical qubits can always be partitioned consecutively into clusters of  $p$  physical qubits.
2. For any operator in  $\mathbb{B}(\mathcal{L}_X)$  there exists one and only one operator in  $\mathbb{B}(\mathcal{L}_Z)$  that anti-commutes with it, and vice versa. More precisely for every pairs of operators, one in  $\mathbb{B}(\mathcal{L}_X)$  and one in  $\mathbb{B}(\mathcal{L}_Z)$ , either their supports overlap on entire cluster of  $p$  physical qubits or do not overlap at all.

**Theorem IV.3** (Clustered logical operator basis of CC codes). clustered-cyclic codes  $\text{CC}(H_a, H_b)$  defined over  $R = \mathbb{F}_2[x]/(x^p + 1)$  have a clustered logical operator basis as defined in Definition IV.2.

*Proof.* As outlined in Corollary A.2, the kernel and image of the seed codes are given by

$$\begin{aligned} \text{rowspan } \text{diag}_{n_a}(\chi) &= \ker H_a = \ker H_a^*, \\ \text{rowspan } \text{diag}_{n_b}(\chi) &= \ker H_b = \ker H_b^*, \\ \text{rowspan } \text{diag}_{n_a}(1+x) &= \text{im } H_a = \text{im } H_a^*, \\ \text{rowspan } \text{diag}_{n_b}(1+x) &= \text{im } H_b = \text{im } H_b^*, \end{aligned}$$

where  $\chi = 1 + x + x^2 + \dots + x^{p-1}$ . We insert them back to Eq. (6) of the Künneth formula. As in  $R = \mathbb{F}_2[x]/(x^p + 1)$ ,  $\chi\chi = \chi$ , we find the basis for the both  $X$  and  $Z$  types of logical operators for  $\text{CC}(H_a, H_b)$  to be the rows of

$$L = \left( \begin{array}{c|c} \text{diag}_{n_a n_b}(\chi) & 0_{n_a n_b} \\ \hline 0_{n_a n_b} & \text{diag}_{n_a n_b}(\chi) \end{array} \right), \quad (8)$$

where  $0_{n_a n_b}$  denotes the zero matrix. This diagonal structure shows that each logical  $Z$  operator anti-commutes with exactly one logical  $X$  operator, since they overlap on a single  $\chi$ . After expressing each entry of  $R$  in binary form, this  $\chi$  corresponds to a cluster of  $p$  physical qubits. Furthermore, any two logical operators of the same type are supported on distinct clusters of equal size, with no overlap between them.  $\square$

**Remark IV.4.** Over  $R = \mathbb{F}_2[x]/(x^p + 1)$ , the binary representation of  $\chi$  is the matrix whose each entry is 1,  $\mathbb{B}(\chi)_{i,j} = 1$  for all  $i, j \in \{1, 2, \dots, p\}$ . The rank of  $\mathbb{B}(\chi)$  is simply 1. Hence, each row of  $L$  in Eq. (8) lifts into only one logical operator of Hamming weight  $p$  after mapping to the binary representation.

We now present specific instance of a  $[[12, 4, 3]]$  code as a concrete example of the CC code construction:

**Example IV.5.** Consider the code  $\text{CC}(H_a, H_b)$  defined over the ring  $R = \mathbb{F}_2[x]/(x^3 + 1)$  with seed matrices defined as follows

$$H_a = \begin{pmatrix} 1+x & 1+x^2 \\ 1+x^2 & 1+x \end{pmatrix} \text{ and } H_b = (1+x)$$

The  $X$ - and  $Z$ -type logical operators of this code over the ring are given by the rows of

$$L = \left( \begin{array}{cc|cc} \chi & 0 & 0 & 0 \\ 0 & \chi & 0 & 0 \\ \hline 0 & 0 & \chi & 0 \\ 0 & 0 & 0 & \chi \end{array} \right).$$

Mapping to the binary representation, the four logical operators of each type are represented as

$$\begin{aligned} \mathbb{B}(\bar{X}_1) &= \mathbb{B}(\bar{Z}_1) = \begin{pmatrix} 111 & 000 & 000 & 000 \\ 111 & 000 & 000 & 000 \\ 111 & 000 & 000 & 000 \end{pmatrix}, \\ \mathbb{B}(\bar{X}_2) &= \mathbb{B}(\bar{Z}_2) = \begin{pmatrix} 000 & 111 & 000 & 000 \\ 000 & 111 & 000 & 000 \\ 000 & 111 & 000 & 000 \end{pmatrix}, \\ \mathbb{B}(\bar{X}_3) &= \mathbb{B}(\bar{Z}_3) = \begin{pmatrix} 000 & 000 & 111 & 000 \\ 000 & 000 & 111 & 000 \\ 000 & 000 & 111 & 000 \end{pmatrix}, \\ \mathbb{B}(\bar{X}_4) &= \mathbb{B}(\bar{Z}_4) = \begin{pmatrix} 000 & 000 & 000 & 111 \\ 000 & 000 & 000 & 111 \\ 000 & 000 & 000 & 111 \end{pmatrix}, \end{aligned}$$

where each matrix now corresponds to one linearly independent binary logical operator of that type as mentioned in Remark IV.4. Hence, the binary clustered logical operator basis of this  $[[24, 8, 3]]$  CC code is

$$\begin{aligned} \bar{X}_1^{\mathbb{B}} &= \bar{Z}_1^{\mathbb{B}} = (111 \ 000 \ 000 \ 000), \\ \bar{X}_2^{\mathbb{B}} &= \bar{Z}_2^{\mathbb{B}} = (000 \ 111 \ 000 \ 000), \\ \bar{X}_3^{\mathbb{B}} &= \bar{Z}_3^{\mathbb{B}} = (000 \ 000 \ 111 \ 000), \\ \bar{X}_4^{\mathbb{B}} &= \bar{Z}_4^{\mathbb{B}} = (000 \ 000 \ 000 \ 111). \end{aligned}$$

From this clustered logical operator basis, we can infer that the code  $\text{CC}(H_a, H_b)$  has parameters  $[[12, 4, 3]]$ . In contrast to hypergraph product codes, there is no general method for determining the distance of an LP code directly from the distances of its seed codes. Instead, one typically relies on heuristic approaches to obtain upper bounds on the distance, for instance by using the QDistRand software package [63] or the BP+OSD distance estimation method introduced in [16]. Since the code under consideration is small, it is feasible to perform an exhaustive search over the logical operator space, which confirms that the distance is  $d = 3$ .

**Corollary IV.6** (Code parameters of CC codes). The codes  $\text{CC}(H_a, H_b)$  over  $R = \mathbb{F}_2[x]/(x^p + 1)$  have code parameters

$$[[N = 2pn_a n_b, k = 2n_a n_b, d \leq p]].$$

*Proof.* The logical dimension of an LP code is the dimension of the (co-)homology groups of the chain complex in its binary representation

$$k = \dim H^1[\mathbb{B}(Q)] = \dim H_1[\mathbb{B}(Q)].$$

The binary representation is a faithful representation preserving the kernel and images of homomorphisms

$$\mathbb{B}(\ker \partial_i) = \ker \mathbb{B}(\partial_i) \text{ and } \mathbb{B}(\text{im } \partial_i) = \text{im } \mathbb{B}(\partial_i),$$

as  $\forall v \in R^m$ ,  $\mathbb{B}[\partial(v)] = \mathbb{B}(\partial)\mathbb{B}(v)$ .

The dimensions of the (co-)homology groups defined above, as quotient groups of kernels by images, therefore coincide with the dimensions of the binary representations of the corresponding (co-)homology groups of the chain complex over ring modules,

$$k = \dim \mathbb{B}[H^1(Q)] = \dim \mathbb{B}[H_1(Q)].$$

As the binary representation of  $\chi = 1 + x + \dots + x^{p-1}$  has rank 1, the binary representation of the matrix of the logical operator basis in Eq. (8) has exactly  $2n_a n_b$  independent rows. From this, we see that

$$k = \text{rank } \mathbb{B}(L) = \text{rank } L = 2n_a n_b.$$

Each row of  $\mathbb{B}(L)$  has Hamming weight  $p$ , as the only non-zero entry in each row of  $L$  is  $\chi$ . This gives a distance upper bound for both types of logical operators.  $\square$

## V. PARALLEL SURGERY FOR PRODUCT CODES

In this section we present a surgery protocol tailored to product-code constructions, including HGP and LP codes. Existing surgery-based measurement schemes for qLDPC codes can achieve small space overheads for individual logical measurements. However, obtaining a high degree of parallelism at comparably low overhead is more subtle.

In generic qLDPC codes, logical operators often exhibit a complicated and highly overlapping structure. As a consequence, the set of logical operators that can be measured jointly in a single round is restricted by their mutual support overlap, commutation constraints, and the available auxiliary resources. This leads to an inherent trade-off between parallelism and auxiliary overhead [28, 34, 39, 55].

Our protocol enables parallel logical PPMs of the same Pauli type with a fixed per-round auxiliary overhead. For an underlying  $[[N, k, d]]$  product code, each surgery round requires  $2N$  auxiliary physical qubits, consisting of  $N$  data auxiliaries and  $N$  check auxiliaries. Crucially, this overhead does not scale with the number of PPMs performed within that round. The number of logical PPMs that can be executed simultaneously is therefore limited only by compatibility constraints between the chosen logical operators.

In the following sections we show that the clustered logical-operator basis derived in Section IV naturally supports such parallel measurements. For CC codes, we demonstrate levels of parallelism comparable to those achieved in distributed surface-code architectures: within a single surgery round, it is possible to measure the joint product of up to  $k/2$  pairs of two-logical operators of the same Pauli type.

## A. Parallel product surgery

The principal technical challenge in implementing a logical PPM via code surgery is to design a fault-tolerant measurement procedure that relies only on constant- or otherwise low-weight measurements. In other words, we seek to extract exactly the eigenvalue of the intended joint logical observable, such as  $(L_1 \otimes L_2)$ , without inadvertently leaking any additional logical information. Code surgery provides a family of techniques that achieve this by temporarily merging the data block with an auxiliary system so that, in the merged code, the desired joint logical operator  $(L_1 \otimes L_2)$  is promoted to an element of the stabiliser group [20, 29]. Its value can then be inferred through standard syndrome extraction, by measuring a suitable collection of low-weight stabilisers whose product yields the target PPM. We now describe how such merge operations can be formulated in the language of chain complexes.

Consider two CSS codes expressed as length-2 chain complexes

$$Q : Q_2 \xrightarrow{H_Z^*} Q_1 \xrightarrow{H_X} Q_0 \text{ and } \mathcal{U} : U_1 \xrightarrow{\partial_1} U_0 \xrightarrow{\partial_0} U_{-1},$$

where  $Q$  is the data code patch with non-zero logical dimension and  $\mathcal{U}$  is the auxiliary code patch, whose logical dimension can be either zero or non-zero.

**Definition V.1** (Code surgery and merged code [29]). Given a data code  $Q$  and an auxiliary code  $\mathcal{U}$ , the Z-type code surgery is uniquely defined by the complex

$$\begin{array}{ccccc} U_1 & \xrightarrow{\partial_1} & U_0 & \xrightarrow{\partial_0} & U_{-1} \\ & \searrow f_1 & & \searrow f_0 & \\ Q_2 & \xrightarrow{H_Z^*} & Q_1 & \xrightarrow{H_X} & Q_0 \end{array}, \quad (9)$$

where the diagram commutes, i.e.,  $f_0 \partial_1 = H_X f_1$ . Such a complex defines a CSS code, which we refer to as the merged code, with parity check matrices

$$\widetilde{H}_X = \begin{pmatrix} H_X & f_0 \\ & \partial_0 \end{pmatrix} \text{ and } \widetilde{H}_Z = \begin{pmatrix} H_Z & \\ f_1^* & \partial_1^* \end{pmatrix}.$$

The CSS condition of the merged code,  $\widetilde{H}_X \widetilde{H}_Z^* = 0$ , is satisfied as long as the above diagram commute. We can also denote the merged code as

$$\widetilde{\mathcal{M}} : Q_2 \oplus U_1 \xrightarrow{\widetilde{H}_Z^*} Q_1 \oplus U_0 \xrightarrow{\widetilde{H}_X} Q_0 \oplus U_{-1}.$$

The Z-type PPMs are therefore implemented by measuring the Z-type stabilisers corresponding to the rows of  $(f_1^* \ \partial_1^*)$ , where a designated subset of the rows of  $f_1^*$  realises the target joint logical operator on the data code patch.

We view the merged code as a subsystem code on the joint system consisting of the data code patch and the auxiliary code patch. Accordingly,  $\dim H_1[\mathbb{B}(\widetilde{\mathcal{M}})] = \widetilde{k} + \widetilde{r}$ , where  $\widetilde{k}$  is the number of logical qubits and  $\widetilde{r}$  the number of gauge qubits.

Passing to the binary representation  $\mathbb{B}(\cdot)$  of codes defined over the ring, and treating any logical operator of  $\widetilde{\mathcal{M}}$  supported on the auxiliary patch as a gauge operator, we obtain [29]

$$\begin{aligned} \widetilde{k} &= k + [\dim \ker [\mathbb{B}(\widetilde{H}_Z)]^\top - \dim \text{im} [\mathbb{B}(H_Z)]^\top], \\ &\quad - \dim \ker \mathbb{B}(\partial_1), \\ \widetilde{r} &= \dim [\ker \mathbb{B}(\partial_0)/\text{im} \mathbb{B}(\partial_1)] - \dim \ker [\mathbb{B}(H_X)]^\top \\ &\quad + [\dim \ker [\mathbb{B}(\widetilde{H}_X)]^\top - \dim \ker [\mathbb{B}(\partial_0)]^\top]. \end{aligned} \quad (10)$$

To interpret these terms, recall that if a family of Pauli generators is specified by a binary check matrix  $H$ , then any  $u \in \ker H^\top$  represents a multiplicative dependency among them: the product of generators selected by  $u$  is the identity (up to phase). Thus  $\dim \ker H^\top$  counts the *redundancy* of the generating set. In the merged code  $\widetilde{\mathcal{M}}$ , some stabiliser generators are inherited from the data patch, while additional generators arise from the auxiliary patch and the connection maps. The difference

$$\dim \ker [\mathbb{B}(\widetilde{H}_Z)]^\top - \dim \text{im} [\mathbb{B}(H_Z)]^\top$$

therefore measures the amount of Z-type stabiliser redundancy present in  $\widetilde{\mathcal{M}}$  that is not directly inherited from the data patch, i.e., the new dependencies created by the merge. The expression for  $\widetilde{r}$  is the corresponding X/Z-swapped analogue, comparing redundancies before and after merging with the roles of  $Q$  and  $\mathcal{U}$  interchanged, and  $\ker \mathbb{B}(\partial_0)/\text{im} \mathbb{B}(\partial_1)$  is the logical operator space of the auxiliary code patch.

Furthermore, the number of logical PPMs being executed during the surgery process is given by [55]

$$M = \dim \mathbb{B}(f_1)[\ker \mathbb{B}(\partial_1)]. \quad (11)$$

We refer to each PPM (possibly on single logical qubit) as a *merge* performed in an appropriate basis, following the standard code-surgery convention [20].

In the case when the data code  $Q$  is a CSS code under product construction, including HGP and LP codes, one can always build up code surgery for  $Q$  via introducing another copy of the same code as the auxiliary system  $\mathcal{U} = Q$  and taking the parity check matrices of another product code  $\mathcal{P}$  of the same size,  $(H'_X, H'_Z)$ , as  $(f_0, f_1^*)$ , respectively.

**Definition V.2** (Product connection code). Given an LP code  $Q$  with parity check matrices  $(H_X, H_Z)$  defined over  $R = \mathbb{F}_2[x]/(x^p + 1)$ , a corresponding *product connection code*  $\mathcal{P}$  is another LP code over  $R$  whose parity check matrices  $(H'_X, H'_Z)$  are in the same size with  $(H_X, H_Z)$ .

**Lemma V.3** (Parallel product surgery). Given an LP code  $Q$  and one corresponding product connection code  $\mathcal{P}$  with parity check matrices  $(H_X, H_Z)$  and  $(H'_X, H'_Z)$ , respectively, the following complex gives a valid surgery

$$\begin{array}{ccccc} Q_2^{\text{aux}} & \xrightarrow{H_Z^*} & Q_1^{\text{aux}} & \xrightarrow{H_X} & Q_0^{\text{aux}} \\ & \searrow^{H_Z^*} & & \searrow^{H'_X} & \\ Q_2 & \xrightarrow{H_Z} & Q_1 & \xrightarrow{H_X} & Q_0 \end{array} \quad (12)$$

The auxiliary code patch is another copy of the data code patch,  $Q^{\text{aux}} = Q$ . The corresponding CSS parity check matrices are

$$\widetilde{H}_X = \begin{pmatrix} H_X & H'_X \\ & H_X \end{pmatrix} \text{ and } \widetilde{H}_Z = \begin{pmatrix} H_Z & \\ H'_Z & H_Z \end{pmatrix}.$$

*Proof.* To show that the complex Eq.(12) yields a valid surgery operation, we need to show that the diagram commutes.

The product construction guarantees the commutativity of the diagram in Eq. (12) according to, on the one hand,

$$\begin{aligned} H_X H_Z^* &= (H_a \otimes_R I \mid I \otimes_R H_b) \begin{pmatrix} I \otimes_R H'_b \\ H'_a \otimes_R I \end{pmatrix} \\ &= (H_a \otimes_R I)(I \otimes_R H'_b) + (I \otimes_R H_b)(H'_a \otimes_R I) \\ &= H_a \otimes_R H'_b + H'_a \otimes_R H_b, \end{aligned}$$

and on the other hand, we have

$$\begin{aligned} H'_X H_Z^* &= (H'_a \otimes_R I \mid I \otimes_R H'_b) \begin{pmatrix} I \otimes_R H_b \\ H_a \otimes_R I \end{pmatrix} \\ &= (H'_a \otimes_R I)(I \otimes_R H_b) + (I \otimes_R H'_b)(H_a \otimes_R I) \\ &= H'_a \otimes_R H_b + H_a \otimes_R H'_b \\ &= H_a \otimes_R H'_b + H'_a \otimes_R H_b = H_X H'_Z^*. \end{aligned}$$

□

For parallel product surgery, we have  $\partial_1 = H_Z^*$ , leading to  $\partial_1 = \ker H_Z^*$ , which permits a high chance for

$$M = \dim \mathbb{B}(H_Z^*)[\ker \mathbb{B}(H_Z^*)] > 1.$$

This means that multiple PPMs can be carried out within a single surgery round, as illustrated in Section V B. Parallelism is therefore achieved at the logical level.

For CC codes, we further show in Section V C that an appropriate choice of the product connection code  $\mathcal{P}$  can exploit the clustered logical operator basis to saturate the natural upper bound on the number of merges per round,

$$M_{\max} = k/2,$$

whenever  $H'_Z$  is full rank. Finally, in Section V D, we characterise which configurations of PPMs are compatible with parallel product surgery for CC codes.

## B. Parallel product surgery procedure

Below, we present a product surgery procedure for product codes targeting Z-type PPMs via tracking stabiliser evolution explicitly. Whilst we consider Z-type merges here, the same process can be adapted directly to X-type merges. We assume the data patch is already prepared in the codespace of  $Q$  [29].

- 1. Initialisation:** Prepare an auxiliary patch of  $N$  physical qubits, intended to host the same product code as the data patch, i.e.,  $Q^{\text{aux}} = Q$ . At initialisation, these auxiliary qubits are not yet encoded into  $Q^{\text{aux}}$ ; instead, we prepare

the state vector  $|+\rangle^{\otimes N}$ . Equivalently, the auxiliary patch is stabilized by single-qubit  $X$  operators, so that only  $Z$ -type errors can accumulate on the auxiliary qubits prior to the first syndrome measurement. At this point, the joint system is stabilised by

$$H_X^1 = \begin{pmatrix} H_X & \\ & I \end{pmatrix} \text{ and } H_Z^1 = (H_Z \ 0).$$

- Measure the new  $Z$  stabilisers:** Measure each of the new  $Z$ -type stabilisers in the merged code from the rows  $(f_1^* \ \partial_1^*) = (H_Z' \ H_Z)$  of  $\widetilde{H_Z}$ . Since

$$\text{rowspan} \begin{pmatrix} H_X & H_X' \\ & I \end{pmatrix} = \text{rowspan} \begin{pmatrix} H_X & \\ & I \end{pmatrix},$$

and the rows  $(H_X \ H_X')$  commute with the newly measured  $Z$ -type stabilisers by construction, the only  $X$ -type stabilisers corresponding to rows  $(0 \ I)$  that anticommute with the measurements now be updated to  $(0 \ G)$ , where  $G$  indicates this intermediate step of stabiliser measurements of the merged code. The row of  $G$  generates the subspace that commutes with  $H_Z$ , i.e.,  $G$  is the matrix satisfying  $\ker G = \text{im } H_Z^* \subseteq \ker H_X$ . The physical system is now stabilised by

$$H_X^2 = \begin{pmatrix} H_X & H_X' \\ & G \end{pmatrix} \text{ and } H_Z^2 = \widetilde{H_Z} = \begin{pmatrix} H_Z & \\ & H_Z \end{pmatrix}.$$

The targetted PPMs are performed at this step as the product of  $Z$ -type stabiliser measurement outcomes corresponding to the rows of  $(H_Z' \ H_Z)$ , where a designated subset of the rows of  $H_Z'$  realises the target joint logical operators on the data code patch.

- Measure the new  $X$  stabilisers:** Measure the rows of  $(H_X \ H_X')$ . Since  $\text{im } G^* \setminus \text{im } H_X^* = \ker H_Z \setminus \text{im } H_X^* = \mathcal{L}_Z^{\text{aux}}$ , the rows of  $G$  which is not in the row space of  $H_X$  should be treated as fixed gauges, and we do not measure them. The physical system is now finally stabilised by

$$\widetilde{H_X} = \begin{pmatrix} H_X & H_X' \\ & H_X \end{pmatrix} \text{ and } \widetilde{H_Z} = \begin{pmatrix} H_Z & \\ & H_Z \end{pmatrix}.$$

- Measure the stabilisers of the merged code  $\widetilde{M}$  for  $d$  rounds:** We need to measure the stabilisers of the merged code  $\widetilde{M}$  for  $d$  rounds to ensure fault tolerance, where  $d$  is the distance of the data code patch  $Q$ .
- Split:** Measure the auxiliary qubits in  $X$  basis transversally to split the merged code back to the data code patch and auxiliary code patch. Apply Pauli corrections on the data code patch according to the measurement outcomes.

### C. Maximally parallel surgery for CC codes

The clustered logical operator bases of CC codes maximise the parallelism enabled by product surgery. Recall that a CC

code defined over the ring  $R = \mathbb{F}_2[x]/(x^p + 1)$  with code parameters

$$[[N = 2pn_a n_b, k = 2n_a n_b, d \leq p]]$$

is equipped with a basis for the both  $X$ - and  $Z$ -types of logical operators being the rows of

$$L = \left( \begin{array}{c|c} \text{diag}_{n_a n_b}(\chi) & 0_{n_a n_b} \\ \hline 0_{n_a n_b} & \text{diag}_{n_a n_b}(\chi) \end{array} \right),$$

where  $\chi = 1 + x + \dots + x^{p-1}$ . We now introduce parallel surgery for CC codes.

**Definition V.4.** [Parallel surgery for CC codes] Consider a CC code  $Q = \text{CC}(H_a, H_b)$  and another LP code  $\mathcal{P} = \text{LP}(H'_a, H'_b)$  defined over the same ring  $R = \mathbb{F}_2[x]/(x^p + 1)$ , as the product connection code. Each entry of  $H'_a$  and  $H'_b$  is either 0 or 1.

The parallel surgery is defined as

$$\begin{array}{ccccc} Q_2^{\text{aux}} & \xrightarrow{H_Z^*} & Q_1^{\text{aux}} & \xrightarrow{H_X} & Q_0^{\text{aux}} \\ & \searrow^{H_Z^*} & & \searrow^{H_X} & \\ Q_2 & \xrightarrow{H_Z^*} & Q_1 & \xrightarrow{H_X} & Q_0 \end{array},$$

where  $H'_X$  and  $H'_Z$  are the parity check matrices of the product connection code  $\mathcal{P}$ , and same as generic parallel product surgery,  $Q^{\text{aux}} = Q$ . The corresponding CSS parity check matrices of the merged code are

$$\widetilde{H_X} = \begin{pmatrix} H_X & H_X' \\ & H_X \end{pmatrix} \text{ and } \widetilde{H_Z} = \begin{pmatrix} H_Z & \\ & H_Z \end{pmatrix}.$$

**Theorem V.5** (Merge of  $Z$ -type logical operators). Each non-zero row in  $H'_Z$ , and the corresponding non-zero row in  $(H_Z' \ H_Z)$  defines a merge of some  $Z$ -type logical operators of the data code patch. They are measured as stabilisers of the merged code, and the measurement outcome corresponds to the value of the PPMs in the data code.

*Proof.* The goal is to express the targetted PPMs in a form where the only non-zero entries are  $\chi$ 's, for example  $\bar{Z}_1 \otimes \bar{Z}_3 = (\chi \ 0 \ \chi \ 0 \ \dots)$ , by writing them as products of stabilisers of the merged code, that is, as linear combinations of the rows of  $(H_Z' \ H_Z)$ . Each non-zero row in  $H'_Z$  corresponds to such a  $Z$ -type stabiliser. As each entry of  $H'_Z$  is either 0 or 1, owing to the constraints on  $H'_a$  and  $H'_b$ , we can always get a product of some  $Z$ -type logical operators of the data code patch by multiplying the rows of  $(H_Z' \ H_Z)$  that correspond to the non-zero rows of  $H'_Z$  with  $\chi$ : the 1's in the half coming from  $H'_Z$  will be converted to  $\chi$ 's, while the other half coming from  $H_Z$  is annihilated as any binomial times  $\chi$  is always zero over the ring  $R = \mathbb{F}_2[x]/(x^p + 1)$ .

From the binary viewpoint, the  $H'_Z$  half lifts to blocks of identity matrices, while each PPM is supported on entire clusters, appearing as contiguous blocks of 1's. For example, when  $p = 3$ ,

$$\bar{Z}_1^{\text{B}} \otimes \bar{Z}_3^{\text{B}} = (1 \ 1 \ 1 \ 0 \ 0 \ 0 \ 1 \ 1 \ 1 \ 0 \ 0 \ 0 \ \dots).$$

Consequently, ‘multiplication by  $\chi$ ’ on rows coming from  $H'_Z$  reduces to summing all rows within each identity block. By contrast, for rows coming from  $H_Z$ , the corresponding row-sum vanishes after lifting: the contributions cancel pairwise, so the total sum is zero.  $\square$

More concrete examples of PPMs as  $Z$ -type merges via parallel surgery of the  $[[24, 8, 3]]$  CC code are presented in Appendix I.

As each non-zero row in  $H'_Z$  defines a merge of some  $Z$ -type logical operators in the data patch. The total number of merges is thus determined by the rank of  $H'_Z$ .

**Corollary V.6.** The number of merges performed during the parallel surgery for CC codes is given by

$$M = \text{rank } H'_Z.$$

*Proof.* Eq. (11) for parallel surgery for CC codes reads

$$M = \dim \mathbb{B}(H_Z^*)[\ker \mathbb{B}(H_Z^*)].$$

The kernel of  $\mathbb{B}(H_Z^*)$  can be identified as  $\mathbb{B}(\ker H_a \otimes_R \ker H_b)$ . Let  $K$  be the basis matrix of  $\ker \mathbb{B}(H_Z^*)$ , we have

$$K = \mathbb{B}[\text{diag}_{n_a n_b}(\chi)],$$

as the basis matrices of  $\ker H_a$  and  $\ker H_b$  are given by  $\text{diag}_{n_a}(\chi)$  and  $\text{diag}_{n_b}(\chi)$ , respectively (Coro. A.2). Then we have

$$M = \dim \mathbb{B}(H_Z^*)[\ker \mathbb{B}(H_Z^*)] = \text{rank } \mathbb{B}(H_Z^*)K.$$

By Definition V.4, each entry of  $H'_Z$  is either 0 or 1, which means that  $H'_Z \text{diag}_{n_a n_b}(\chi) = \chi H'_Z$ , leading to

$$\text{rank } \mathbb{B}(H'_Z)K = \text{rank } \mathbb{B}(\chi H'_Z) = \text{rank } H'_Z = \text{rank } H'_Z.$$

$\square$

We also derive the number of logical qubits in the merged code, following Eq. (10).

**Corollary V.7.** The number of logical qubits in the merged code is

$$\tilde{k} = k - M = 2n_a n_b - \text{rank } H'_Z.$$

*Proof.* Recall the formula for the number of logical qubits in the merged code given in Eq. (10), for  $\partial_1 = H_Z^*$

$$\tilde{k} = k + \dim \ker [\mathbb{B}(\widetilde{H_Z})]^\top - 2 \dim \ker [\mathbb{B}(H_Z)]^\top,$$

where according to Lemma C.1,

$$\begin{aligned} \dim \ker [\mathbb{B}(\widetilde{H_Z})]^\top &= 2 \dim \ker [\mathbb{B}(H_Z)]^\top + \text{rank } [\mathbb{B}(H_Z)]^\top \\ &\quad - \text{rank } ([\mathbb{B}(H_Z)]^\top [\mathbb{B}(H'_Z)]^\top K). \end{aligned}$$

Here  $K = \mathbb{B}[\text{diag}_{n_a n_b}(\chi)]$  is the basis matrix of  $\ker (\mathbb{B}H_Z)^\top$ .

Again, as each entry of  $H'_Z$  is either 0 or 1, we have  $H'_Z \text{diag}_{n_a n_b}(\chi) = \chi H'_Z$ , whose columns are clearly not in the row space of  $H'_Z$ , and vice versa. Hence,

$$\begin{aligned} \text{rank } ([\mathbb{B}(H_Z)]^\top [\mathbb{B}(H'_Z)]^\top K) &= \text{rank } [\mathbb{B}(H_Z)]^\top \\ &\quad + \text{rank } [(\mathbb{B}H'_Z)^\top K]. \end{aligned}$$

Note that  $\text{rank } [(\mathbb{B}H'_Z)^\top K] = \text{rank } H'_Z = M$ , we have  $\dim \ker [\mathbb{B}(\widetilde{H_Z})]^\top = 2 \dim \ker [\mathbb{B}(H_Z)]^\top - \text{rank } H'_Z$ , leading us to

$$\tilde{k} = k - \text{rank } H'_Z = 2n_a n_b - \text{rank } H'_Z. \quad \square$$

The merge action of this parallel surgery has a symmetric action on the  $X$ -type gauge operators of the auxiliary code patch, which is straightforward from the conjugate transpose code of the merged code. That is with the  $X/Z$ -swapped analogue and with the roles of  $Q$  and  $Q^{\text{aux}}$  interchanged

$$\begin{array}{ccccc} Q_2^{\text{aux}} & \xleftarrow{H_Z} & Q_1^{\text{aux}} & \xleftarrow{H_X^*} & Q_0^{\text{aux}} \\ & \swarrow H_Z & & \swarrow H_X^* & \\ & Q_2 & \xleftarrow{H_Z} & Q_1 & \xleftarrow{H_X^*} & Q_0 \end{array}$$

Therefore, for each merge of  $Z$ -type logical operators in the data code patch, there is a corresponding reduction of number of gauge qubits in the auxiliary code patch.

And this reduced number of gauge qubits in the merged code is given as

$$\tilde{r} = k - M = 2n_a n_b - \text{rank } H'_X,$$

by a similar argument as in the proof of the number of logical qubits in the merged code. Here we remind that the auxiliary code patch has  $k$  gauge qubits before the merge as it is the same code as the data patch.

We now turn to the degree of parallelism enabled by the parallel surgery. A central primitive for PPM-induced logical operations is the joint measurement of the product of two logical operators [21]. For a CSS code encoding  $k$  logical qubits, the maximum number of disjoint logical pairs is  $k/2$ , obtained by partitioning the  $k$  logical qubits into pairs. This upper bounds the number of merges that can be performed in one surgery round by  $k/2$ .

**Definition V.8** (Maximally parallel). If PPMs are required to act on disjoint pairs of same-type logical operators, then at most

$$M_{\text{max}} = k/2$$

merges can be performed within a single surgery round. We say that a surgery protocol is maximally parallel if it enables  $k/2$  merges per round, for a CSS code encoding  $k$  logical qubits.

For CC codes, this upper bound is achieved provided that the product connection code  $\mathcal{P}$  used in the surgery has full rank check matrices. In particular, when

$$\text{rank } H'_Z = n_a n_b = k/2,$$

all targetted logical pairs can be merged in a single surgery round, thereby realising maximal parallel logical measurement.

**Theorem V.9** (Maximally parallel Z-type merges for CC codes). Consider the code  $\text{CC}(H_a, H_b)$  encoding  $k = 2n_a n_b$  logical qubits and we measure on Z logical basis. At most

$$M_{\max} = k/2 = n_a n_b$$

merges can be performed within a single surgery round with parallel surgery. This bound is achieved whenever the product connection code satisfies  $\text{rank } H'_Z = n_a n_b$ .

*Proof.* By Corollary V.7, the number of independent merges is determined by the rank of  $H'_Z$ . When  $\text{rank } H'_Z = n_a n_b$ , the merged code admits  $n_a n_b$  independent joint Z-type logical measurements, thereby achieving the upper bound. As we require  $H'_a$  and  $H'_b$  to be square matrices with only 0 or 1 being the entries,  $H'_Z$  is full rank if and only if at least one of  $H'_a$  and  $H'_b$  is full rank.

For example, a trivial choice for  $H'_a$  and  $H'_b$  could be

$$H'_a = I_{n_a} \text{ and } H'_b = I_{n_b}.$$

The logical action of such parallel surgery over a CC code is to merge every  $i^{\text{th}}$  Z-type logical operator in the left sector with the  $i^{\text{th}}$  Z-type logical operator in the right sector (Fig. 1 (b)).  $\square$

To illustrate the advantage enabled by maximal parallelisation, we compare the space-time overhead for performing a single merge of our protocol with state-of-the-art logical measurement protocols for qLDPC codes in Table II. The reduction in time overhead is immediate, since up to  $k/2$  merges can be performed within a single surgery round. Importantly, the improvement is not achieved merely by trading time for additional space: the overall space-time overhead is also reduced for CC codes. Throughout this comparison, we define the space overhead as the total number of auxiliary physical qubits required by the protocol, including both auxiliary data qubits and auxiliary check qubits.

Specifically, we compare the space-time overhead required to perform a single merge using the maximally parallel surgery protocol for the  $[[136, 8, 14]]$  CC code with that of the extractor protocol applied to the  $[[144, 12, 12]]$  Gross BB code, as shown in Table III. Such concrete, non-asymptotic, numbers can be helpful to assess the performance of scheme, reminiscent of the situation of the concrete numbers that have been suggested for the overheads of fault-tolerantly implementing certain protocols such as factoring 2048 bit RSA integers fault-tolerantly and other protocols [21, 64, 65].

**Remark V.10.** Recent work of Xu *et al.* [55] proposes a randomised, parallel surgery scheme with low overhead. By contrast, our parallel surgery for CC codes provides an explicit construction of the auxiliary code patch with a fixed per-round overhead.

Protocol	Space	Time	Space-time
This work	$2N$	$2d/k$	$4Nd/k$
Gauging [28]	$O(d \log^2 d)^\dagger$	$d$	$O(d^2 \log^2 d)$
Extractor [39]	$O(N \log^3 N)$	$d$	$O(Nd \log^3 N)$

TABLE II. Space-time overhead comparison between maximally parallel surgery for CC codes, gauging logical qubits [28], and the extractor protocol [39]. We consider the time overhead required to perform a single merge (either a single logical measurement or a joint measurement of two same-type logical operators). When maximal parallelisation is available, the effective time overhead is reduced by a factor of  $k/2$ . Specifically for CC codes listed in Table I, we observe that  $N \approx kd$ , leading to a space overhead around  $2kd$  and total space-time overhead around  $4d^2$  for a single merge using the maximally parallel surgery.

Code	Space (data, check)	Time	Space-time
$[[136, 8, 14]]$	272 (136, 136)	3.5	952
$[[144, 12, 12]]$	103 (54, 49)	12	1236

TABLE III. Space-time overhead comparison between maximally parallel surgery for the  $[[136, 8, 14]]$  CC code and the extractor protocol applied to the  $[[144, 12, 12]]$  Gross BB code [34, 39]. We consider the time overhead required to perform a single merge (either a single logical measurement or a joint measurement of two same-type logical operators).

#### D. Limitations of product surgery and hybrid gadget

The actual merge action being performed is directed by the product connection code  $\mathcal{P}$ . As illustrated in Corollary V.11, the fact that we can choose arbitrary  $H'_a$  and  $H'_b$  with 1's (the multiplicative identity over the ring  $R$ ) to be the only non-zero entries allows us to perform merge on any two same-type logical operators if they are in different sectors and one can merge at most  $k/2$  pairs of logical operators in one round. For logical operators supported within the same sector, the situation is more constrained. Two such logical operators can be merged if and only if they are aligned along the same row or column in the ring-level Tanner graph of the product construction. This alignment condition reflects the tensor-product structure of the auxiliary system and is consistent with previously observed constraints in logical operation protocols based on product-constructed auxiliary systems [30, 55].

**Corollary V.11** (Merge two Z-type logical operators). Let  $\bar{Z}_\alpha$  and  $\bar{Z}_\beta$  be two logical Z operators of a CC code. If they are supported in different sectors, or are aligned in the same row or column within a sector, then one can construct a connection product code  $\mathcal{P}$  with check matrix  $H'_Z$  such that there exists  $v \in \text{rowspan } H'_Z$  satisfying

$$\text{supp}(\bar{Z}_\alpha \otimes \bar{Z}_\beta) = \chi v.$$

*Proof (Informal).* The product connection code  $\mathcal{P}$  is a LP code with the same block size as the data code and inherits a product

structure. Its construction can be read off directly at the ring level of the Tanner graph. One begins with the target quantum connectivity pattern and then reconstructs the classical seed codes  $H'_a$  and  $H'_b$  according to the product construction rules of the Tanner graph formalism.

In Appendix B, we give an explicit algebraic construction of the product connection code  $\mathcal{P} = \text{LP}(H'_a, H'_b)$  corresponding to an arbitrary compatible merge.  $\square$

As a guiding example, we consider the  $[[24, 8, 3]]$  CC code. Although our parallel product surgery protocol permits only certain PPM configurations, these allowed configurations—together with the fold-transversal and automorphism-induced logical gates of the code—are already sufficient to generate the full Clifford group on four of the eight data logical qubits, while the remaining four logical qubits serve as auxiliaries. Details are provided in Section VII.

Motivated by this observation, we introduce a *hybrid logical measurement gadget*. The central idea is as follows: whenever a requested collection of PPMs contains a compatible sub-configuration (i.e., one realisable via product surgery), we first implement that subset using parallel product surgery, thereby benefiting from its constant overhead and intrinsic parallelism. Any remaining PPMs that fall outside the compatible subset are then carried out using standard logical measurement routines.

This hybrid strategy preserves full generality, while systematically exploiting the low-overhead structure of parallel surgery wherever possible. We refer to the resulting reduction in space overhead, relative to implementing all PPMs using only standard logical measurement routines, as a *boost*. Configurations that contain such a compatible subset are termed *boostable cases*.

Specifically, for the  $[[136, 8, 14]]$  CC code, Figure 2 illustrates that, for configurations compatible with product surgery, boosting gauging-based logical measurements [28] with parallel product surgery reduces the auxiliary space overhead by approximately 150 physical qubits on average when measuring combinations of single logical operators and pairs of joint logical operators. For this  $[[136, 8, 14]]$  CC code, there are

$$\sum_{m=0}^4 \frac{8!}{2^m m! (8-2m)!} 2^{8-2m} - 1 = 7192$$

non-trivial non-overlapping combinations of single logical operators and pairs of two logical operators in total. Among these, 867 combinations ( $867/7192 \approx 12\%$ ) are boostable via parallel surgery, meaning that each of these configurations contains at least one subset of measurements compatible with product surgery.

**Remark V.12** (Logical PPMs of the  $[[136, 8, 14]]$  CC code via gauging-based logical measurements [28]). We begin with the clustered logical operator basis in order to keep track of logical qubits and make fair comparison with the parallel product surgery. For any requested PPM, we form the target logical Pauli  $L$  (a single  $L_i$ , or for a pair the product  $L_i \otimes L_j$ ) in binary, and then *first replace it by a minimum Hamming weight*

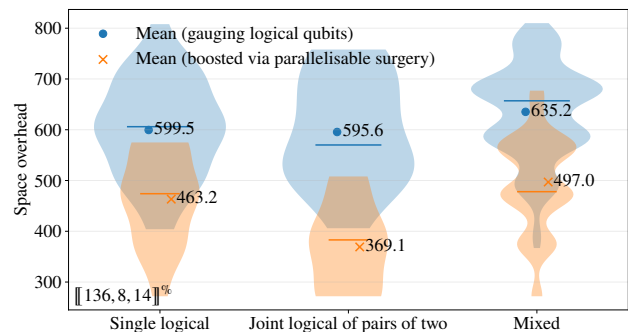


FIG. 2. Comparison of space overhead distributions between gauging-based logical measurements [28] (wide blue violins) and parallel surgery-boosted gauging (narrow orange violins) for the  $[[136, 8, 14]]$  CC code in the Z basis. Each violin represents the distribution over all allowed combinations of logical measurements that incur a given space overhead. The bullet (cross) indicates the mean value for each distribution and the horizontal lines are for the medians. *Single logical*: measurement of different combinations of single logical operators within one surgery round. *Joint logical of pairs of two*: measurement of different combinations of non-overlapping joint logical operators pairs within one surgery round. *Mixed*: combinations consisting of both single logical measurements and joint measurements on pairs of logical qubits as long as no measurement overlaps on any logical qubit. <sup>c</sup>Only configurations compatible with parallel product surgery are included in the comparison.

*representative in its stabiliser coset*:

$$L^* \in LS \quad \text{minimizing} \quad \text{HW}(L^*),$$

obtained by adding stabilisers to shrink support while preserving the logical operator.

We then instantiate the gauging measurement gadget of Williamson–Yoder (Alg. 1 of [28]): take  $V = \text{supp}(L^*)$ , choose an auxiliary constant-degree graph  $G$  on  $V$  satisfying the design constraints in Remark 2 of [28] (connectivity and expanding property, Cheeger constant  $h(G) \geq 1$ ), introduce one edge qubit per edge of the graph  $G$ , perform the gauging/ungauging measurements of Algorithm 1 to extract the eigenvalue of  $L^*$  (hence of  $L$ ), with the standard byproduct inferred from the edge outcomes.

The reported space overhead is the number of auxiliary edge qubits used.

**Example V.13** (Largest boost). The largest reduction in space overhead occurs for parallel Z-basis PPMs on the four joint logical-operator pairs (1, 7), (2, 8), (3, 5), and (4, 6) for the  $[[136, 8, 14]]$  CC code. Using the gauging-based logical measurement gadget [28], the total space overhead for measuring these four pairs is 758. Since this configuration is compatible with maximally parallel surgery, the same set of PPMs can instead be implemented with a fixed space overhead of 272, yielding a space overhead saving of 486.

## VI. FAULT TOLERANCE OF PARALLEL PRODUCT SURGERY

A surgery procedure for CSS codes, as defined in Definition V.1, is fault-tolerant if (i) all homomorphisms appearing in Eq. (9) are LDPC, and (ii) the procedure preserves the phenomenological distance at  $\Omega(d)$ . The first condition ensures bounded-degree circuit connectivity, thereby limiting error propagation under circuit-level noise. The second guarantees that error protection during surgery remains proportional to the distance  $d$  of the underlying code [6, 55].

Parallel product surgery satisfies the first condition provided that both the data code  $Q$  and the product connection code  $\mathcal{P}$  are LDPC. In particular, for CC codes with the parallel surgery construction, both  $Q$  and  $\mathcal{P}$  are LDPC by design.

In the following, we explicitly verify that parallel surgery for CC codes preserves the LDPC structure, and we provide numerical evidence that for all CC codes with 8 logical qubits listed in Table I, the merged code distance does not decrease.

**Remark VI.1.** In Appendix D, we show rigorously that the parallel product surgery is distance preserving for HGP codes, i.e., product surgery is fault-tolerant for HGP codes as long as both data HGP code  $Q$  and connection HGP code  $\mathcal{P}$  are LDPC.

### A. Fault tolerance of maximally parallel surgery for CC codes

CC codes are LDPC, as shown in Eq. (7), since the stabiliser check weight is a constant independent of the size of the parity-check matrices. Consequently, all homomorphisms defining both the data patch  $Q$  and the auxiliary patch  $\mathcal{U} = Q^{\text{aux}} = Q$  are LDPC.

The product connection code  $\mathcal{P}$  are defined such that its check weight

$$W_{\mathcal{P}} = \# \text{ of logical operators involved in a single merge.}$$

is a constant. In the most common scenarios, we measure either a single logical operator or the product of two logical operators, corresponding to  $W_{\mathcal{P}} = 1$  or  $W_{\mathcal{P}} = 2$ , respectively.

The parallel surgery of CC codes produces the merged code as a CSS code with parity check matrices

$$\widetilde{H}_X = \begin{pmatrix} H_X & H'_X \\ & H_X \end{pmatrix}, \quad \widetilde{H}_Z = \begin{pmatrix} H_Z & \\ H'_Z & H_Z \end{pmatrix}.$$

For CC codes with  $k = 8$  in Table I, there are  $2^{4+4} = 256$  distinct choices of  $(H'_X, H'_Z)$ . This follows from the fact that  $\mathcal{P} = \text{LP}(H'_a, H'_b)$ , and for  $k = 8$ , the seed matrices  $H'_a$  and  $H'_b$  are  $2 \times 2$  matrices whose entries are either 0 or 1.

For each CC code with parity check matrices  $(H_X, H_Z)$ , we exhaustively estimate the distance of all 256 corresponding merged code  $(\widetilde{H}_X, \widetilde{H}_Z)$  using QDistRnd [63]. In all cases tested, the merged code distance is no smaller than that of the original data code. Refer to Appendix F for accuracies of numerically estimated code distance.

## VII. FAULT-TOLERANT CLIFFORD OPERATIONS: EXPLICIT CONSTRUCTIONS AND CASE STUDIES

Fault-tolerant computation on stabiliser codes is naturally phrased in terms of how an operation acts by conjugation on Pauli operators. The  $m$ -qubit Clifford group  $C_m$  is the normaliser of the Pauli group  $\mathcal{P}_m = \langle X_i, Z_i \rangle_{i=1}^m$  in the unitary group, i.e.,  $U \in C_m \Leftrightarrow U\mathcal{P}_m U^\dagger = \mathcal{P}_m$ . For a stabiliser code, a logical Clifford operator is defined analogously as an unitary that preserves the logical Pauli group under conjugation, and is therefore fully specified by its action on a generating set of logical  $\bar{X}_i$  and  $\bar{Z}_i$ . Up to global phase, the Clifford group is generated by elementary single-qubit and entangling gates [7],

$$C_m/U(1) \cong \langle H_i, S_i, CNOT_{i \rightarrow j} \rangle, \quad i, j \in \{1, \dots, m\},$$

and we use an equivalent generating set tailored to our available primitives (paired phase gates  $\bar{S}_i \bar{S}_j^\dagger$ , a global Hadamard and logical  $CNOT$  gates) later in this section (Theo. VII.1).

Clifford processing can be driven entirely by layers of commuting PPMs together with classical feed-forward and Pauli-frame tracking, with auxiliary logical qubits repeatedly prepared in Pauli eigenstates and measured out [21, 26]. In the CC code setting, the required Pauli measurements are supplied by parallel product surgery, providing highly parallel fault-tolerant logical PPMs at fixed overhead, while code symmetries provide additional logical operations via fold-transversal and automorphism-induced operations.

In the remainder of this section, we make this explicit: we give concrete Clifford gadgets for the  $[[24, 8, 3]]$  CC code by combining parallel surgery with logical  $SWAP$  gates from automorphisms and fold-transversal  $CZ-S/H-SWAP$  gadgets, and show how four data logical qubits (with four reusable logical auxiliaries) realise a complete Clifford toolbox.

### A. Clifford operations from parallel surgery: the $[[24, 8, 3]]$ toy model

The  $[[24, 8, 3]]$  CC code encodes eight logical qubits. We partition them into four *data* logical qubits and four *auxiliary* logical qubits: we label the logical qubits 2, 4, 6, 8 as data, and the logical qubits 1, 3, 5, 7 as auxiliary.

The auxiliary logical qubits are repeatedly initialised in Pauli eigenstates, particularly the eigenvectors  $|\bar{0}\rangle$  or  $|\bar{+}\rangle$ . They are used to mediate entangling operations, like logical  $CNOT$  in Figure 4, and then measured and discarded, with all byproduct operators tracked in the Pauli frame.

We use five key ingredients, where the first two are primitives of the latter ones:

- (i) *Parallel product surgery*, which implements highly parallel logical PPMs with constant space overhead together with classical feed-forward. It serves as the basic primitive for parallel logical measurements, parallel logical state initialisation, and the parallel logical  $CNOT$  constructions used below.

- (ii) *Automorphism-induced logical SWAP gates*, which allow us to fault-tolerantly permute logical qubits, as illustrated in Appendix J3.
- (iii) *Maximally parallel logical CNOT gates* between arbitrary pairs of data logical qubits, implemented within the parallel surgery framework together with the logical SWAP gates. As outlined in detail in Appendix K, any two pairs of logical CNOT gates can be implemented in parallel for these four logical qubits at fixed space overhead.
- (iv) *Transversal  $\bar{S}_i \bar{S}_j^\dagger$  operations on arbitrary data logical qubit pairs*. They are obtained by compiling the fold-transversal CZ–S gadget with parallel state initialisation and logical SWAP gates (App. J1 and App. J3).
- (v) *Global Hadamard  $\bar{H}^{\otimes 8}$  (and hence  $\bar{H}^{\otimes 4}$  on the data subsystem)*. It is obtained by compiling fold-transversal H–SWAP gadget automorphism-induced logical SWAP gates (App. J2 and App. J3).

Altogether, we have the following set of logical operations

$$\{\bar{X}_i, \bar{Z}_i, \bar{CNOT}_{i \rightarrow j}, \bar{S}_i \bar{S}_j^\dagger, \bar{H}^{\otimes 4}\},$$

for the data logical qubits 2, 4, 6, 8. This is enough to generate the complete Clifford group of four logical qubits fault-tolerantly up to global phase, following Theorem VII.1.

**Theorem VII.1.** Let  $m \geq 3$ . Suppose the available operations on  $m$  qubits include  $X_i, Z_i$  for all  $i$ , arbitrary  $CNOT_{i \rightarrow j}$  for all  $i \neq j$ , the paired phase gates  $S_i S_j^\dagger$  for all  $i \neq j$ , and the global Hadamard  $H^{\otimes m}$ . Then these gates generate the full  $m$ -qubit Clifford group up to global phase:

$$C_m/U(1) \cong \langle X_i, Z_i, CNOT_{i \rightarrow j}, S_i S_j^\dagger, H^{\otimes m} \rangle.$$

*Proof.* See Appendix E.  $\square$

The [[24, 8, 3]] CC code therefore serves as a compact toy model demonstrating that parallel surgery, combined with a small number of fold-transversal and automorphism-induced operations, suffices to realise the full Clifford group on four of the eight logical qubits. Moreover, the maximally parallel logical CNOT layer discussed in Appendix K is enabled by the clustered logical basis of CC codes and the parallel surgery, which together allow multiple CNOT gates on disjoint data logical qubit pairs to be executed in parallel at fixed space overhead. For arbitrary Clifford logical operations, only an additional copy of the data code patch is required as an auxiliary patch  $Q'$ , incurring a  $2N$  space overhead: 24 auxiliary data qubits and 24 auxiliary check qubits.

## VIII. PHYSICAL IMPLEMENTATION

CC codes integrates desiderata from code construction itself with the practical requirements of implementing quantum logic. In this sense, it already follows a co-design principle. To make such codes fully practical, it is essential to align the

demands of quantum logic implementation with those of the underlying quantum hardware. Notably, the code we propose is particularly well suited to several leading quantum hardware architectures.

Indeed, our code–logic co-design is particularly well matched to platforms that support *dynamic, sparse reconfiguration* of the interaction graph. Particularly prominent such architecture of this type is provided by optical-tweezer neutral-atom arrays [24, 66, 67] and shuttling-based trapped-ion architectures [68–72], but also superconducting processors with tunable long-range couplers [16, 73]. The common theme is that these platforms can (i) operate with a low-degree ‘native’ connectivity graph during steady-state error correction, and (ii) temporarily instantiate additional sparse couplings when an algorithmic layer demands it. This exactly mirrors the operational pattern of our constructions: most of the time, each patch executes standard LDPC syndrome extraction on a bounded-degree graph, while parallel surgery requires turning on a structured set of inter-patch edges only during a designated interaction window.

There are further elements that render our code particularly attractive from the hardware-perspective, however. First, CC codes fall within the LP code family as qLDPC codes, so both data and check qubits have bounded degree and admit sparse syndrome-extraction graphs. This yields constant-weight stabilisers and supports highly parallel measurement schedules. Moreover, Xu *et al.* [17] show that reconfigurable neutral-atom arrays can implement the effectively non-local coupling patterns required by product qLDPC code syndrome extraction by rearranging atoms between circuit layers, so that the instantaneous interaction graph is adapted to the current stabiliser-measurement schedule while maintaining coherence [66]. In ion-trap *quantum charge-coupled device* (QCCD) architectures [71], shuttling provides an explicit mechanism for dynamically bringing the qubits required by a given parity check into a processing zone, again implementing a time-dependent sparse graph. In superconducting devices, tunable couplers and bus-mediated interactions offer a complementary route to activating and deactivating selected edges on demand [16, 73].

Second, the auxiliary subsystem required by parallel product surgery is deliberately non-specialised: it is simply another instance of the same data patch. This symmetry makes the hardware role of each patch interchangeable. From a systems perspective, this is attractive because it avoids dedicated ‘factory’ resources at the physical layer: any available patch can temporarily act as an auxiliary system, and the calibration targets (native syndrome extraction and native patch preparation/measurement) remain unchanged. On platforms with mid-circuit measurement and reset, this enables flexible scheduling strategies in which auxiliary patches are recycled round-by-round without altering the underlying code family.

Third, the product connection makes the inter-patch interface particularly natural in reconfigurable layouts. The same sparse algebraic structure that defines an LP code also defines sparse cross-connections between two copies, so that the joint-parity measurements required for surgery correspond to activating a prescribed, low-degree bipartite graph between a data patch and an auxiliary patch. Operationally, a surgery round

proceeds by (i) preparing the auxiliary patch and enabling the inter-patch couplings specified by the chosen product connection code while executing the required joint checks, and (ii) disabling those couplings and measuring out the auxiliary degrees of freedom. In this way, reconfigurability is used where it is most valuable—to transiently instantiate the inter-patch edges demanded by the product connection code—while each patch otherwise operates using its native intra-patch connectivity. This ‘mostly-static, briefly-rewired’ pattern is precisely the regime in which dynamically reconfigurable arrays are expected to offer the largest architectural advantage, and it provides a concrete pathway for implementing highly parallel logical PPM layers with fixed auxiliary overhead. This feature may well also be attractive for photonic platforms of fault tolerant quantum computing [74].

## IX. CONCLUSION AND OUTLOOK

This work sets out to explore a code–logic co-design perspective for fault-tolerant computation with qLDPC codes, motivated by the practical observation that, even when good code parameters are available, using a code for computation can still be constrained by (i) how transparently the logical operators can be represented and acted on, and (ii) how much parallelism can be achieved in logical measurement layers at a fixed, small overhead. Within this framing, CC codes are introduced as a LP code subfamily whose logical operator basis is engineered to have a ‘clustered’ organisation, with the aim of making selective and parallel logical measurements and scheduling more systematic.

A main operational primitive enabled by this structure is the parallel product surgery, which realises PPMs using an auxiliary copy of the data patch together with a tailored product connection code  $\mathcal{P}$ . In this framework, the rank of the connection-code check matrix  $H'_Z$  directly controls how many independent same-type merges can be executed within a single surgery round. For CC codes encoding  $k = 2n_a n_b$  logical qubits, the natural upper bound of number of merges  $M_{\max} = k/2 = n_a n_b$  is reached when  $\text{rank } H'_Z = n_a n_b$ , providing a simple algebraic criterion for when the protocol achieves maximal parallelism. This work also makes the resulting resource trade-offs relatively concrete by comparing space-time overheads to alternative logical-measurement approaches. At the level of scaling (Tab. II), maximal parallelisation reduces the effective time overhead per merge by  $k/2$  when many disjoint merges are executed concurrently. At the finite-size level (Tab. III), one representative comparison reports a space-time overhead of 952 for a single merge using maximally-parallel surgery on the  $[[136, 8, 14]]$  CC code (with auxiliary space 272 and time 3.5), versus 1236 for the extractor protocol applied to the  $[[144, 12, 12]]$  Gross BB code (with auxiliary space 103 but time 12), under the paper’s accounting conventions. While such comparisons depend on modelling and counting choices, they serve as a useful indication that the additional parallelism can translate into a non-trivial reduction in the combined space-time metric.

A second pragmatic ingredient is the hybrid gadget idea:

when a target measurement configuration is not directly compatible with the patterns admitted by product surgery, the protocol can still be used as a ‘booster’ for other measurement routines whenever the configuration contains a compatible sub-configuration. In the example for the  $[[136, 8, 14]]$  CC code (Fig. 2), among all possible 7192 combinations of single logical measurements and joint logical measurements of two-logical pairs considered, 867 ( $\approx 12\%$ ) are reported as boostable, and for those the boosted procedure reduces auxiliary space overhead by about 150 physical qubits on average in the reported distributions. This is inherently a partial-coverage strategy, but it suggests a modular way to reuse highly-parallel layers within broader measurement toolchains.

On fault tolerance, we show that the parallel product surgery procedure is fault-tolerant for HGP codes in full generality (App. D) as long as both data code and product connection codes are LDPC. For the CC code instances considered here, we further verify fault tolerance numerically for all listed  $k = 8$  CC codes by exhaustively checking all merged-code choices induced by  $(H'_X, H'_Z)$ .

The  $[[24, 8, 3]]$  CC case study illustrates how these ingredients combine into a compact fault-tolerant logical toolbox built from PPMs. In this measurement-based picture, Clifford processing is organised into layers of commuting PPMs with classical feed-forward and Pauli-frame tracking, using auxiliary logical qubits that are prepared and measured out repeatedly. Parallel surgery provides the required PPM primitives, while code symmetries supply additional logical operations, including automorphism-induced logical SWAPs and fold-transversal gadgets. A key feature is that surgery allows any two logical *CNOT* gates on disjoint qubit pairs to be executed in parallel. Together with arbitrary logical *CNOT* gates, paired  $S_i S_j^\dagger$  operations, and the global  $H^{\otimes 4}$ , this yields fault-tolerant full Clifford operation up to a global phase over four logical qubits, since these elements generate the full Clifford group (Theo. VII.1). These features are expected to contribute to bringing notions of fault tolerant quantum computing to a new level [8] and to render such schemes more practical.

At the same time, the manuscript is clear that product surgery comes with structural constraints that matter for compilation. Most explicitly, merges within the same sector require an alignment condition (e.g., sharing a row/column in the ring-level Tanner graph), whereas arbitrary inter-sector merges are allowed. This suggests that practical use will likely involve either (i) scheduling strategies that exploit the natural compatibility structure, or (ii) ‘routing’ steps (for instance, via logical permutations arising from code automorphisms) that map desired PPM layers into compatible patterns.

As a final comment, our work also raises some natural pathways for further investigation.

- Other structures of logical operator basis of high rate qLDPC codes and co-designed computational gadget.

Beyond the clustered logical operator basis studied here, other high-rate qLDPC families come with useful logical-basis structure. For instance, HGP codes admit a well-known canonical logical-operator basis [32], QRCs exhibit a structured basis that can be viewed as interpolating between clustered and

canonical forms [62], and recent work has also analysed logical basis structure for BB codes [33]. These structural insights suggest further opportunities for more efficient logical operations. At the same time, different basis choices naturally emphasize different desiderata: strong finite-size parameters, clear logical addressability, and large (computationally useful) automorphism groups do not always align within a single construction. A useful direction is therefore to treat the logical basis structure as a design input and to develop specialised computational gadgets that explicitly exploit the strengths of the chosen basis.

- Fault tolerance of generic parallel product surgery.

We proved that parallel product surgery is distance preserving for arbitrary HGP codes. Motivated by this general result and by our numerical evidence for the CC instances studied here, it is natural to conjecture that parallel product surgery remains distance preserving more broadly—for CC codes, and potentially for a wider class of quantum product codes. If true, this would point to a surgery gadget whose fault tolerance is not certified by the expansion properties of the auxiliary system, but instead emerges from the symmetry of the merged code as a whole. In this respect, the mechanism would be closer in spirit to surface code lattice surgery, where distance preservation is tied to the global geometry of the merged patch.

- Fast and parallel surgery at small space overhead for CC codes.

As illustrated in Section VB, each surgery round requires  $d$  rounds of stabiliser measurements to ensure fault tolerance. Very recently, several works have proposed techniques to reduce the time overhead of code surgery to a constant [54, 75, 76], although typically at the cost of increased space overhead. In particular, Ref. [54] demonstrates that surgery for HGP codes can achieve constant time overhead and almost constant space overhead, enabled by their canonical logical operator basis. This naturally raises the question of whether similar ideas can be applied to parallel product

surgery for CC codes, potentially reducing the time overhead while preserving the favourable space overhead.

- Other generating sets of the Clifford group.

We note that the generating set used in Theorem VII.1 may be particularly well suited to codes that admit many fold-transversal logical operations, since several of its elements can naturally arise from code symmetries. It would therefore be useful to identify alternative generating sets for the Clifford group whose generators are especially compatible with symmetry-based implementations [77]. For example, sets in which the required entangling and phase operations can be realised directly from automorphisms, fold-transversal gadgets, or other structured symmetry actions of the code. It is our hope that this work substantially advances the full experimental implementation of scalable quantum error correction.

#### ACKNOWLEDGEMENTS

We acknowledge helpful discussions with Robert I. Booth, Wang Fang, Shouzen (Bailey) Gu, Zhiyang (Sunny) He, Shilin Huang, Benjamin Ide, Yingjia Lin, Pavel Panteleev, Clément Poirson, Kaavya Sahay, Hasan Sayginel, Susan J. Sierra, Adithya Sireesh, and Ryan Tiew. We especially thank Stergios Koutsoumpas and Tamas Noszko for discussions and insightful comments. BG was supported by the Higgs Scholarship funded by the School of Physics and Astronomy, University of Edinburgh. BG and JR were supported by the project ‘Algorithmic fault-tolerance: quantum error correction beyond quantum memories’ funded by the UKRI Quantum Computing and Simulation (QCS) Hub (grant code: EP/T001062/1). BG and JR were also funded by the Innovate UK project ‘QEC Readout Testbed’ [reference number 10151107]. JR is currently funded by an EPSRC Quantum Career Acceleration Fellowship (grant code: UKRI1224). QX is funded in part by the Walter Burke Institute for Theoretical Physics at Caltech. The Berlin team has been supported by the the BMFTR (QSolid, MUNIQ-Atoms, PasQuops), the DFG (CRC 183 and SPP 2541), the Quantum Flagship (Millenion, PasQuans2), the Munich Quantum Valley, Berlin Quantum and the European Research Council (DebuQC).

- 
- [1] A. Y. Kitaev, *Annals of Physics* **303**, 2 (2003).  
 [2] D. Gottesman, “Opportunities and challenges in fault-tolerant quantum computation,” (2022), arXiv:2210.15844.  
 [3] J. Roffe, *Contemporary Physics* **60**, 226–245 (2019).  
 [4] E. T. Campbell, B. M. Terhal, and C. Vuillot, *Nature* **549**, 172 (2017).  
 [5] B. M. Terhal, *Rev. Mod. Phys.* **87**, 307 (2015).  
 [6] D. Gottesman, (2013), arXiv:1310.2984.  
 [7] M. A. Nielsen and I. L. Chuang, *Quantum computation and quantum information*, Cambridge Series on Information and the Natural Sciences (Cambridge University Press, 2000).  
 [8] J. Eisert and J. Preskill, (2025), arXiv:2510.19928.  
 [9] E. Dennis, A. Kitaev, A. Landahl, and J. Preskill, *J. Math. Phys.* **43**, 4452 (2002).  
 [10] J.-P. Tillich and G. Zemor, *IEEE Trans. Inf. Th.* **60**, 1193 (2014).  
 [11] P. Panteleev and G. Kalachev, *Quantum* **5**, 585 (2021).  
 [12] N. P. Breuckmann and J. N. Eberhardt, *PRX Quantum* **2**, 040101 (2021).  
 [13] A. Leverrier and G. Zémor, in *2022 IEEE 63rd Annual Symposium on Foundations of Computer Science (FOCS)* (IEEE, 2022) pp. 872–883.  
 [14] P. Panteleev and G. Kalachev, *IEEE Trans. Inf. Theor.* **68**, 213–229 (2022).

- [15] P. Panteleev and G. Kalachev, in *Proceedings of the 54th Annual ACM SIGACT Symposium on Theory of Computing*, STOC 2022 (Association for Computing Machinery, New York, NY, USA, 2022) p. 375–388.
- [16] S. Bravyi *et al.*, *Nature* **627**, 778 (2024).
- [17] Q. Xu, J. P. Bonilla Ataides, C. A. Pattison, N. Raveendran, D. Bluvstein, J. Wurtz, B. Vasić, M. D. Lukin, L. Jiang, and H. Zhou, *Nature Phys.* **20**, 1084 (2024).
- [18] G. P. Gehér, D. Byfield, and A. Ruban, (2025), arXiv:2507.19430.
- [19] B. Eastin and E. Knill, *Phys. Rev. Lett.* **102**, 110502 (2009).
- [20] C. Horsman, A. G. Fowler, S. Devitt, and R. V. Meter, *New J. Phys.* **14**, 123011 (2012).
- [21] D. Litinski, *Quantum* **3**, 128 (2019).
- [22] S. Bravyi and A. Kitaev, *Phys. Rev. A* **71**, 022316 (2005).
- [23] C. Gidney, N. Shutty, and C. Jones, (2024), arXiv:2409.17595.
- [24] P. S. Rodriguez *et al.*, *Nature* **645**, 620 (2025).
- [25] C. Li, J. Preskill, and Q. Xu, (2025), arXiv:2510.07269.
- [26] D. Gottesman, *Stabilizer codes and quantum error correction*, PhD thesis, California Institute of Technology (1997), arXiv:quant-ph/9705052.
- [27] L. Z. Cohen, I. H. Kim, S. D. Bartlett, and B. J. Brown, *Science Adv.* **8**, eabn1717 (2022).
- [28] D. J. Williamson and T. J. Yoder, (2024), arXiv:2410.02213.
- [29] B. Ide, M. G. Gowda, P. J. Nadkarni, and G. Dauphinais, *Phys. Rev. X* **15**, 021088 (2025).
- [30] Q. Xu, H. Zhou, G. Zheng, D. Bluvstein, J. P. B. Ataides, M. D. Lukin, and L. Jiang, *Phys. Rev. X* **15**, 021065 (2025).
- [31] S.-H. Lee, F. Thomsen, N. Fazio, B. J. Brown, and S. D. Bartlett, *PRX Quantum* **6**, 030317 (2025).
- [32] A. O. Quintavalle, P. Webster, and M. Vasmer, *Quantum* **7**, 1153 (2023).
- [33] J. N. Eberhardt and V. Steffan, (2024), arXiv:2407.03973.
- [34] A. Cross, Z. He, P. Rall, and T. J. Yoder, (2024), arXiv:2407.18393.
- [35] G. Zhang and Y. Li, *Phys. Rev. Lett.* **134**, 070602 (2025).
- [36] C. Poirson, J. Roffe, and R. I. Booth, (2025), arXiv:2505.01370.
- [37] A. Cowtan, (2024), arXiv:2407.09423.
- [38] P. Webster, L. Berent, O. Chandra, E. T. Hockings, N. Baspin, F. Thomsen, S. C. Smith, and L. Z. Cohen, arXiv preprint arXiv:2602.11457 (2026).
- [39] Z. He, A. Cowtan, D. J. Williamson, and T. J. Yoder, (2025), arXiv:2503.10390.
- [40] G. Zhang, Y. Zhu, and Y. Li, (2025), arXiv:2510.19442.
- [41] E. Swaroop, T. Jochym-O’Connor, and T. J. Yoder, *PRX Quantum* **7**, 010324 (2026).
- [42] H. Sayginel, S. Koutsoumpas, M. Webster, A. Rajput, and D. E. Browne, *PRX Quantum* **6**, 030343 (2025).
- [43] A. J. Malcolm, A. N. Glauddell, P. Fuentes, D. Chandra, A. Schotte, C. DeLisle, R. Haenel, A. Ebrahimi, J. Roffe, A. O. Quintavalle, S. J. Beale, N. R. Lee-Hone, and S. Simmons, (2025), arXiv:2502.07150.
- [44] Y. Yang, G. Zhang, and Y. Li, (2025), arXiv:2506.18061.
- [45] Q. Xu, H. Zhou, D. Bluvstein, M. Cain, M. Kalinowski, J. Preskill, M. D. Lukin, and N. Maskara, (2025), arXiv:2510.06159.
- [46] L. Golowich, K. Chang, and G. Zhu, (2025), arXiv:2510.06760.
- [47] J. P. B. Ataides *et al.*, (2025), arXiv:2502.09542.
- [48] H. Yamasaki and M. Koashi, *Nature Phys.* **20**, 247 (2024).
- [49] S. Yoshida, S. Tamiya, and H. Yamasaki, *npj Quant. Inf.* **11**, 88 (2025).
- [50] H. Goto, *Science Advances* **10**, eadp6388 (2024).
- [51] G. Zhu, S. Sikander, E. Portnoy, A. W. Cross, and B. J. Brown, *PRX Quantum* **5**, 040338 (2024).
- [52] L. Pecorari, F. P. Guerci, H. Perrin, and G. Pupillo, (2025), arXiv:2511.06124.
- [53] S. Huang, T. Jochym-O’Connor, and T. J. Yoder, *PRX Quantum* **4**, 030301 (2023).
- [54] K. Chang, Z. He, T. J. Yoder, G. Zhu, and T. Jochym-O’Connor, (2026), arXiv:2603.02157.
- [55] G. Zheng, L. Jiang, and Q. Xu, (2025), arXiv:2510.08523.
- [56] N. P. Breuckmann and S. Burton, *Quantum* **8**, 1372 (2024).
- [57] Y. A. Drozd and V. V. Kirichenko, *Finite Dimensional Algebras* (Springer, Berlin, Heidelberg, 1994).
- [58] A. Hatcher, *Algebraic Topology* (Cambridge University Press, 2019).
- [59] N. P. Breuckmann and J. N. Eberhardt, *IEEE Trans. Inf. Th.* **67**, 6653 (2021).
- [60] A. O. Quintavalle and E. T. Campbell, *IEEE Trans. Inf. Th.* **68**, 6569 (2022).
- [61] Z. Liang, K. Liu, H. Song, and Y.-A. Chen, *PRX Quantum* **6**, 020357 (2025).
- [62] T. R. Scruby, T. Hillmann, and J. Roffe, (2024), arXiv:2406.14445.
- [63] L. P. Pryadko, V. A. Shabashov, and V. K. Kozin, *J. Open Source Soft.* **7**, 4120 (2022).
- [64] C. Gidney, (2025), arXiv:2505.15917.
- [65] P. Webster, L. Berent, O. Chandra, E. T. Hockings, N. Baspin, F. Thomsen, S. C. Smith, and L. Z. Cohen, (2026), arXiv:2602.11457.
- [66] D. Bluvstein, A. A. Geim, S. H. Li, S. J. Evered, J. P. B. Ataides, G. Baranes, A. Gu, T. Manovitz, M. Xu, M. Kalinowski, S. Majidi, C. Kokail, N. Maskara, E. C. Trapp, L. M. Stewart, S. Hollerith, H. Zhou, M. J. Gullans, S. F. Yelin, M. Greiner, V. Vuletić, M. Cain, and M. D. Lukin, *Nature* **649**, 39 (2026).
- [67] G. Giudici, S. Veroni, G. Giudice, H. Pichler, and J. Zeiher, *PRX Quantum* **6**, 030308 (2025).
- [68] M. Ye and N. Delfosse, *Quantum* **9**, 1920 (2025).
- [69] M. Valentini, M. W. van Mourik, F. Butt, J. Wahl, M. Dietl, M. Pfeifer, F. Anmasser, Y. Colombe, C. Rössler, P. C. Holz, R. Blatt, A. Bermudez, M. Müller, T. Monz, and P. Schindler, *Phys. Rev. X* **15**, 041023 (2025).
- [70] O. Chandra, G. Muraleedharan, and G. K. Brennen, *Phys. Rev. Res.* **7**, 033247 (2025).
- [71] J. M. Pino, J. M. Dreiling, C. Figgatt, J. P. Gaebler, S. A. Moses, M. S. Allman, C. H. Baldwin, M. Foss-Feig, D. Hayes, K. Mayer, C. Ryan-Anderson, and B. Neyenhuis, *Nature* **592**, 209 (2021).
- [72] S. Dasu, M. DeCross, A. Y. Guo, A. Lavasani, J. Behrends, A. Benhemou, Y.-H. Chen, K. Mayer, C. N. Self, S. Simsek, B. Srivastava, M. Allman, J. Arkininstall, J. G. Bohnet, N. Q. Burdick, J. C. III, A. Chernoguzov, S. F. Cooper, R. D. Delaney, J. M. Dreiling, B. Estey, C. Figgatt, C. Foltz, J. P. Gaebler, A. Hall, C. A. Holliman, A. A. Husain, A. Isanaka, C. J. Kennedy, Y. Kodama, N. Kotibhaskar, N. K. Lysne, I. S. Madjarov, M. Mills, A. R. Milne, B. Neyenhuis, A. J. Park, A. Ransford, A. P. Reed, S. J. Sanders, C. H. Baldwin, D. Hayes, B. Criger, A. C. Potter, and D. Amaro, (2026), arXiv:2602.22211.
- [73] IBM Research, “IBM delivers new quantum processors, software, and algorithm breakthroughs on path to advantage and fault tolerance,” (2025).
- [74] S. Bartolucci, P. Birchall, H. Bombín, H. Cable, C. Dawson, M. Gimeno-Segovia, E. Johnston, K. Kieling, N. Nickerson, M. Pant, F. Pastawski, T. Rudolph, and C. Sparrow, *Nat. Commun.* **14**, 912 (2023).
- [75] N. Baspin, L. Berent, and L. Z. Cohen, (2025), arXiv:2510.04521 [quant-ph].
- [76] A. Cowtan, Z. He, D. J. Williamson, and T. J. Yoder, (2025), arXiv:2510.14895 [quant-ph].

- [77] T. Tansuwannont, T. Chan, and R. Takagi, (2026), [arXiv:2602.09788](https://arxiv.org/abs/2602.09788).
- [78] A. G. Manes and J. Claes, *Quantum* **9**, 1618 (2025).
- [79] M. Kang, Y. Lin, H. Yao, M. Gökdoğan, A. Meinking, and K. R. Brown, *Quantum* **9**, 1931 (2025).
- [80] C. Gidney, *Quantum* **5**, 497 (2021).
- [81] J. Roffe, D. R. White, S. Burton, and E. Campbell, *Phys. Rev. Res.* **2**, 043423 (2020).

### Appendix A: Kernel and image of the seed codes of the CC code

Here we characterise the kernel and image of seed code matrices of CC codes defined in Definition IV.1.

Let  $R = \mathbb{F}_2[x]/(x^p + 1)$  where  $p$  is prime, and  $\chi = 1 + x + \dots + x^{p-1}$ .

**Lemma A.1.** For any integers  $0 \leq \alpha < p$  and  $0 < \beta < p$ , the kernel of  $\text{diag}_n[x^\alpha(1+x^\beta)]$  is the row span of  $\text{diag}_n(\chi)$ . Its image is the row span of  $\text{diag}_n(1+x)$ .

*Proof.* Over  $R = \mathbb{F}_2[x]/(x^p + 1)$ , multiplication between  $\chi = 1 + x + \dots + x^{p-1}$  with any non-zero monomial remains  $\chi$ . Any binomial in the form  $x^\alpha(1+x^\beta)$  is annihilated by  $\chi$  as

$$x^\alpha(1+x^\beta)\chi = x^\alpha\chi + x^{\alpha+\beta}\chi = 2\chi = 0.$$

This gives  $\text{diag}_n[x^\alpha(1+x^\beta)]\text{diag}_n(\chi)^* = 0$ , indicating that the row span of  $\text{diag}_n(\chi)$  lives in the kernel of  $\text{diag}_n[x^\alpha(1+x^\beta)]$ . For the image, note each

$$x^\alpha(1+x^\beta) = x^\alpha(1+x)(1+x+\dots+x^{\beta-1})$$

is a multiple of  $1+x$ . Hence, the image of  $\text{diag}_n[x^\alpha(1+x^\beta)]$  is contained in the row span of  $\text{diag}_n(1+x)$ .

We check the row spans obtained above are exactly the kernel and image we want via the rank-nullity theorem over  $\mathbb{F}_2$ . As  $\mathbb{B}(\text{diag}_n[x^\alpha(1+x^\beta)]) : \mathbb{F}_2^{np} \rightarrow \mathbb{F}_2^{np}$ , we have

$$\begin{aligned} np &= \dim \text{im } \mathbb{B}(\text{diag}_n[x^\alpha(1+x^\beta)]) \\ &\quad + \dim \ker \mathbb{B}(\text{diag}_n[x^\alpha(1+x^\beta)]) \\ &= n(p-1) + n \\ &= \dim \text{im } \text{diag}_n(1+x) + \dim \text{im } \text{diag}_n(\chi). \end{aligned}$$

The dimensions match and the row spans are the kernel and image we are looking for.  $\square$

**Corollary A.2.** The kernel of a seed code of a CC code,  $H_a$ , defined in Definition IV.1 is the row span of  $\text{diag}_{n_a}(\chi)$ . Its image is the row span of  $\text{diag}_{n_a}(1+x)$ . The same holds for  $H_a^*$ .

*Proof.* Any binomial entry of  $H_a$  can be represented as  $x^\alpha(1+x^\beta)$  for some  $0 \leq \alpha < p$  and  $0 < \beta < p$ . As  $x^\alpha(1+x^\beta)\chi = 0$ , we know the row span of  $\text{diag}_{n_a}(\chi)$  lies in the kernel of  $H_a$ . Also, as  $x^\alpha(1+x^\beta) = x^\alpha(1+x)(1+x+\dots+x^{\beta-1})$  is a multiple of  $1+x$ . Hence, the image of  $H_a$  is contained in the row span of  $\text{diag}_{n_a}(1+x)$ .

We then end this proof by simply following the proof of Lemma A.1, as the dimension check with rank-nullity theorem over  $\mathbb{F}_2$  still holds. As for  $H_a^*$ , the conjugate transpose does not affect the form  $H_a$  takes. Hence, the statement still holds.  $\square$

### Appendix B: Merge two Z-type logical operators

**Corollary B.1** (Merge two Z-type logical operators). Let  $\bar{Z}_\alpha$  and  $\bar{Z}_\beta$  be two logical Z operators of a CC code. If they are supported in different sectors, or are aligned in the same row or column within a sector, then one can construct a product connection code  $\mathcal{P}$  with check matrix  $H'_Z$  such that there exists  $v \in \text{rowspan } H'_Z$  satisfying

$$\text{supp}(\bar{Z}_\alpha \otimes \bar{Z}_\beta) = \chi v.$$

*Proof.* For simplicity, we introduce the notation for logical operators as in Appendix I: given a data code patch with  $k = 2n_a n_b$  logical qubits, we separate its logical qubits into two sectors. Each Z-type logical operator is then denoted as

$$\bar{Z}_\alpha^{\text{left}} \text{ or } \bar{Z}_\alpha^{\text{right}} \text{ for } i \in \{1, \dots, n_a n_b\}.$$

If two logical operators are in different sectors,  $\bar{Z}_\alpha^{\text{left}}$  and  $\bar{Z}_\beta^{\text{right}}$ , we choose

$$(H_a^*)_{i_a, j_a} = 1 \text{ and } (H_b^*)_{i_b, j_b} = 1,$$

to be the only non-zero entries where

$$i_a = \left\lfloor \frac{\alpha}{n_b} \right\rfloor + 1, \quad j_a = \left\lfloor \frac{\beta}{n_b} \right\rfloor + 1,$$

$$i_b \equiv \alpha \pmod{n_b} \text{ and } j_b \equiv \beta \pmod{n_b}.$$

The  $((i_a - 1)n_b + i_b)^{\text{th}}$  row of  $H'_Z$  of this  $C' = \text{LP}(H'_a, H'_b)$  gives a row vector with the  $\alpha^{\text{th}}$  and  $\beta^{\text{th}}$  entries to be 1 and the only non-zero entries.

If two logical operators are both in the left sector,  $\bar{Z}_\alpha^{\text{left}}$  and  $\bar{Z}_\beta^{\text{left}}$  with  $\left\lfloor \frac{\alpha}{n_b} \right\rfloor = \left\lfloor \frac{\beta}{n_b} \right\rfloor$  (i.e., they are aligned in the same column), we simply choose

$$H_a^* = 0 \text{ and } (H_b^*)_{1, \alpha'} = (H_b^*)_{1, \beta'} = 1,$$

to be the only non-zero entries with  $\alpha \equiv \alpha' \pmod{n_b}$  and  $\beta \equiv \beta' \pmod{n_b}$ , where  $\alpha', \beta' \in \{1, 2, \dots, n_b\}$ . Then, the  $j_a^{\text{th}}$  row is what we want. However, if  $\left\lfloor \frac{\alpha}{n_b} \right\rfloor \neq \left\lfloor \frac{\beta}{n_b} \right\rfloor$  but  $\alpha \equiv \beta \pmod{n_b}$  (i.e., they are aligned in the same row), we let

$$(H_a^*)_{i_a, 1} = (H_a^*)_{j_a, 1} = 1 \text{ and } (H_b^*)_{1, \alpha'} = 1,$$

the sum of the  $(i_a n_b + 1)^{\text{th}}$  and  $(j_a n_b + 1)^{\text{th}}$  row from  $H'_Z$  gives the row vector we want.

If two logical operators are both in the right sector,  $\bar{Z}_\alpha^{\text{right}}$  and  $\bar{Z}_\beta^{\text{right}}$  with  $\left\lfloor \frac{\alpha}{n_b} \right\rfloor = \left\lfloor \frac{\beta}{n_b} \right\rfloor$  (i.e., they are aligned in the same column), we choose

$$(H_a^*)_{1, i_a} = 1 \text{ and } (H_b^*)_{\alpha', 1} = (H_b^*)_{\beta', 1} = 1,$$

and the sum of the  $(i_a n_b + \alpha')^{\text{th}}$  and  $(i_a n_b + \beta')^{\text{th}}$  row from  $H'_Z$  gives the row vector we want. If the logical operators are aligned in the same row on the right sector, i.e., if  $\left\lfloor \frac{\alpha}{n_b} \right\rfloor \neq \left\lfloor \frac{\beta}{n_b} \right\rfloor$  but  $\alpha \equiv \beta \pmod{n_b}$ , we simply choose

$$(H_a^*)_{1, i_a} = (H_a^*)_{1, j_a} = 1 \text{ and } H_b^* = 0,$$

and the  $\alpha^{\text{th}}$  row is what we want.  $\square$

### Appendix C: Lemma for merged code dimension

**Lemma C.1.** Given matrices  $A$  and  $B$  over a field, we have

$$\dim \ker \begin{pmatrix} A & B \\ & A \end{pmatrix} = 2 \dim \ker A + \text{rank } A - \text{rank } (A \ BK),$$

where  $K$  is the basis matrix of  $\ker A$ .

*Proof.* Let  $A \in \mathbb{F}^{m \times n}$ ,  $B \in \mathbb{F}^{m \times n}$ , and let  $K \in \mathbb{F}^{n \times k}$  be the basis matrix of  $\ker A$ , so that  $\ker A = \text{im } K$  and  $AK = 0$ . Consider the block matrix  $M := \begin{pmatrix} A & B \\ 0 & A \end{pmatrix}$ . For vectors  $\begin{pmatrix} u \\ v \end{pmatrix} \in \mathbb{F}^{2n}$  we have  $M \begin{pmatrix} u \\ v \end{pmatrix} = \begin{pmatrix} Au + Bv \\ Av \end{pmatrix}$ . Thus, for vectors  $\begin{pmatrix} u \\ v \end{pmatrix} \in \ker M$ , we have

$$\begin{cases} Au + Bv = 0, \\ Av = 0. \end{cases}$$

Since  $Av = 0$  implies  $v \in \ker A = \text{im } K$ , there exists  $w \in \mathbb{F}^k$  such that  $v = Kw$ . Substituting this into the first equation above, we find

$$Au + BKw = 0, \text{ i.e., } (A \ BK) \begin{pmatrix} u \\ w \end{pmatrix} = 0. \quad (\text{C1})$$

At this point, define a linear map  $S : \mathbb{F}^n \times \mathbb{F}^k \rightarrow \mathbb{F}^n \times \mathbb{F}^n$ ;  $S \begin{pmatrix} u \\ w \end{pmatrix} = \begin{pmatrix} u \\ Kw \end{pmatrix}$ . We now turn to showing that  $S$  restricts to a linear isomorphism

$$\ker (A \ BK) \cong \ker M.$$

We begin by proving that  $S$  maps  $\ker (A \ BK)$  into  $\ker M$ : if  $\begin{pmatrix} u \\ w \end{pmatrix}$  satisfies  $Au + BKw = 0$ , then

$$MS \begin{pmatrix} u \\ w \end{pmatrix} = \begin{pmatrix} Au + BKw \\ AKw \end{pmatrix} = 0,$$

since  $AK = 0$ . Hence, we find  $S \begin{pmatrix} u \\ w \end{pmatrix} \in \ker M$  for all  $\begin{pmatrix} u \\ w \end{pmatrix} \in \ker (A \ BK)$ .

Then  $S$  is surjective onto  $\ker M$ : given  $\begin{pmatrix} u \\ v \end{pmatrix} \in \ker M$ , Eq. (C1) indicates that there exists some  $\begin{pmatrix} u \\ w \end{pmatrix} \in \ker (A \ BK)$  such that  $S \begin{pmatrix} u \\ w \end{pmatrix} = \begin{pmatrix} u \\ v \end{pmatrix}$ . Lastly, we show that  $S$  is injective: if  $S \begin{pmatrix} u \\ w \end{pmatrix} = S \begin{pmatrix} u' \\ w' \end{pmatrix}$  then  $u = u'$  and  $Kw = Kw'$ , and since the columns of  $K$  are linearly independent (which is chosen to be a basis matrix) we get  $w = w'$ .

Therefore, we conclude  $\ker M \cong \ker (A \ BK)$  and hence,  $\dim \ker M = \dim \ker (A \ BK)$ .

Now compute the dimension of this kernel. The matrix  $(A \ BK)$  has  $n + k$  columns, with  $k = \dim \ker A$ . According

to rank-nullity theorem,

$$\begin{aligned} \dim \ker M &= \dim \ker (A \ BK) \\ &= (n + k) - \text{rank } (A \ BK) \\ &= 2 \dim \ker A + \text{rank } A - \text{rank } (A \ BK). \end{aligned}$$

□

### Appendix D: Product surgery is distance preserving for HGP codes

HGP codes are LP codes defined over  $R = \mathbb{F}_2$ . It is equipped with a canonical logical operator basis [32] which can be derived using Künneth formula as well. In this appendix, we show owing this logical operator basis, the parallel product surgery introduced in Lemma V.3 is always distance preserving for HGP codes.

Consider a HGP code with the following parity check matrices,

$$\begin{aligned} H_X &= (H_a \otimes I_{n_b} \mid I_{n_a} \otimes H_b), \\ H_Z &= (I_{n_a} \otimes H_b^\top \mid H_a^\top \otimes I_{n_b}). \end{aligned}$$

As given in Eq. (6), an arbitrary logical  $Z$  operator consisting of a product of logical  $Z$  operators and  $Z$  stabilisers takes the form of

$$\bar{Z} = \left( \sum_{i,j} \lambda_{i,j} x_i \otimes y_j + \sum_s w_s \otimes H_b \tilde{w}_s \right) := \begin{pmatrix} Z_1 \\ Z_2 \end{pmatrix},$$

where  $\{x_i\}$  and  $\{b_m\}$  are basis of classical codewords or  $H_a$  and  $H_b$ , respectively and  $\{y_j\}$  and  $\{a_l\}$  are sets of unit vectors whose linear combinations are outside the image of  $H_b$  and  $H_a$ , respectively.  $\lambda_{i,j}$  and  $\kappa_{lm}$  are arbitrary binary values [78].  $w = \sum_s w_s \otimes \tilde{w}_s$  is an arbitrary vector  $H_Z^\top$  acts on. Without loss of generality, assume some  $\sum_j \lambda_{i,j} x_j \neq 0$ . Since  $\sum_j \lambda_{i,j} x_j \neq 0$ ,  $\bar{Z}$  must have hamming weight  $\geq d_a$  (which is the classical code distance of  $H_a$ ) and there are therefore at least  $d_a$  distinct unit vectors  $e_t$  such that  $e_t \cdot (\sum_j \lambda_{i,j} x_j) = 1$  [78].

We now consider apply the parallel product surgery to this code while choosing another HGP code  $(H'_X, H'_Z)$  as product connection code  $\mathcal{P}$ :

$$\begin{array}{ccccc} Q_2^{\text{aux}} & \xrightarrow{H_Z^\top} & Q_1^{\text{aux}} & \xrightarrow{H_X} & Q_0^{\text{aux}} \\ & \searrow^{H_Z'^\top} & & \searrow^{H_X'} & \\ Q_2 & \xrightarrow{H_Z^\top} & Q_1 & \xrightarrow{H_X} & Q_0 \end{array}$$

The merged code is equipped with parity check matrices

$$\widetilde{H}_X = \begin{pmatrix} H_X & H'_X \\ & H'_X \end{pmatrix} \text{ and } \widetilde{H}_Z = \begin{pmatrix} H_Z & \\ H'_Z & H_Z \end{pmatrix}.$$

We want to show that the minimum weight of logical operators of this merged code is lower bounded by the distance of the data code. For a  $Z$ -type logical operator, the only problematic scenario is when a  $Z$ -type logical operator is constructed as

$$\bar{Z}^{\mathcal{M}} = \begin{pmatrix} \bar{Z} \\ 0 \end{pmatrix} + \begin{pmatrix} H_Z'^\top \\ H_Z^\top \end{pmatrix} u := \begin{pmatrix} Z^Q \\ Z^{\text{aux}} \end{pmatrix},$$

where the second term in the sum does not vanish in both patches [29, 55]. Expanding this arbitrary  $u = \sum_{s'} u_{s'} \otimes \tilde{u}_{s'}$ , we zoom in to the first row of  $Z^Q$ , corresponding to the first row of  $\tilde{Z}$  above,

$$Z_1^Q = \sum_{i,j} \lambda_{i,j} x_i \otimes y_j + \sum_s w_s \otimes H_b \tilde{w}_s + \sum_{s'} u_{s'} \otimes H'_b \tilde{u}_{s'}.$$

We apply  $(e_i^\top \otimes I_{m_b})$  to  $Z_1^Q$ . In any case  $(e_i^\top \otimes I_{m_b})Z_1^Q = 0$ , we know

$$\sum_{s'} (e_i^\top u_{s'}) H'_b \tilde{u}_{s'} \neq 0,$$

as  $(e_i^\top \otimes I_{m_b})Z_1 \neq 0$  [78]. This means  $(e_i^\top u_{s'}) \neq 0$  and leading to a non-vanishing part on the auxiliary patch

$$Z_1^{\text{aux}} = \sum_{s'} (e_i^\top u_{s'}) H_b \tilde{u}_{s'} \neq 0,$$

as  $H_Z^\top u$  is assumed to be non-zero. Hence, for each weight reduction of the logical operators supported on the data patch, there is always at least weight one compensation on the auxiliary patch. Hence, the  $Z$ -type distance is preserved throughout the parallel product surgery for HGP codes.

The  $X$ -type distance is always preserved for arbitrary CSS surgery if we are performing  $Z$ -type merges [29].

### Appendix E: Proof of Theorem VII.1

**Theorem VII.1.** Let  $m \geq 3$ . Suppose the available logical operations on  $m$  qubits include the single-qubit Paulis  $X_i, Z_i$  for all  $i$ , arbitrary  $CNOT_{i \rightarrow j}$  for all  $i \neq j$ , the paired phase gates  $S_i S_j^\dagger$  for all  $i \neq j$ , and the global Hadamard  $H^{\otimes m}$ . Then these gates generate the full  $m$ -qubit Clifford group up to global phase:

$$C_m/\text{U}(1) \cong \langle X_i, Z_i, CNOT_{i \rightarrow j}, S_i S_j^\dagger, H^{\otimes m} \rangle.$$

*Proof.* We use the standard description of Clifford operations via their conjugation action on the Pauli group. Modulo global phases  $\text{U}(1) = \{e^{i\theta} : \theta \in \mathbb{R}\}$ , any  $m$ -qubit Pauli can be written uniquely as  $X^x Z^z := \bigotimes_{k=1}^m X_k^{x_k} Z_k^{z_k}$  with  $(x, z) \in \mathbb{F}_2^m \times \mathbb{F}_2^m$ . We represent it by the binary vector  $(x | z) \in \mathbb{F}_2^{2m}$ . Two Paulis commute if and only if the symplectic form product  $x \cdot z' + z \cdot x'$  over  $\mathbb{F}_2$  vanishes. Every Clifford  $U$  conjugates Paulis to Paulis, hence induces a linear map  $(x | z) \mapsto (x' | z')$  preserving this symplectic form; equivalently,  $U$  induces a matrix  $\pi(U) \in \text{Sp}(2m, 2)$ , where  $\text{Sp}(2m, 2)$  is the symplectic group of  $\mathbb{F}_2^{2m}$ . The homomorphism  $\pi : C_m \rightarrow \text{Sp}(2m, 2)$  is surjective and its kernel is the Pauli subgroup up to global phase, so to generate  $C_m/\text{U}(1)$  it suffices to generate the full symplectic action and also have access to Paulis. The latter is trivial as we are given access to  $X_i, Z_i$ .

In this representation,  $CNOT_{i \rightarrow j}$  maps  $X_i \mapsto X_i X_j$  and  $Z_j \mapsto Z_i Z_j$ . Consequently arbitrary CNOTs generate the embedded subgroup of  $\text{Sp}(2m, 2)$ ,

$$L(\text{GL}(m, 2)) = \left\{ L(A) := \begin{pmatrix} A & 0 \\ 0 & (A^{-1})^T \end{pmatrix} : A \in \text{GL}(m, 2) \right\},$$

since elementary row-additions generate all  $A \in \text{GL}(m, 2)$ .

The global Hadamard swaps  $X_k \leftrightarrow Z_k$  for each  $k$ , so it swaps the two blocks, acting as

$$J := \pi(H^{\otimes m}) = \begin{pmatrix} 0 & I \\ I & 0 \end{pmatrix}.$$

For the phase gate  $S$ , it maps  $X$  operators into  $Y$  operators and fixes  $Z$  operators.  $S^\dagger$  have the same binary action. Thus  $S_i S_j^\dagger$  fixes  $x$  and updates  $z$  by  $z_i \mapsto z_i + x_i$  and  $z_j \mapsto z_j + x_j$ , i.e., we find

$$\pi(S_i S_j^\dagger) = \Lambda(D_{i,j}) := \begin{pmatrix} I & 0 \\ D_{i,j} & I \end{pmatrix}, \quad D_{i,j} = \text{diag}(e_i + e_j).$$

A direct block multiplication gives, for all  $A \in \text{GL}(m, 2)$  and all  $m \times m$  matrices  $C$ ,

$$L(A)\Lambda(C)L(A)^{-1} = \Lambda\left[(A^{-1})^\top C A^{-1}\right], \\ \Lambda(C_1)\Lambda(C_2) = \Lambda(C_1 + C_2),$$

with arithmetic over  $\mathbb{F}_2$ .

We claim these relations allow us to synthesize a single-qubit phase gate  $S_i$  for any  $i$  when  $m \geq 3$ . Choose three distinct qubits and relabel them as 1, 2, 3, and set  $C_0 := D_{12}$  so that  $\Lambda(C_0) = \pi(S_1 S_2^\dagger)$  is available. Consider the invertible  $3 \times 3$  matrices over  $\mathbb{F}_2$  given by

$$A_1 = \begin{pmatrix} 0 & 0 & 1 \\ 0 & 1 & 0 \\ 1 & 0 & 0 \end{pmatrix}, \quad A_2 = \begin{pmatrix} 1 & 0 & 1 \\ 0 & 0 & 1 \\ 1 & 1 & 0 \end{pmatrix}, \quad A_3 = \begin{pmatrix} 0 & 1 & 1 \\ 1 & 0 & 1 \\ 0 & 0 & 1 \end{pmatrix}.$$

Extend each to an  $m \times m$  matrix by  $\tilde{A}_k := \text{diag}(A_k, I_{m-3}) \in \text{GL}(m, 2)$  and define  $C_k := (\tilde{A}_k^{-1})^\top C_0 \tilde{A}_k^{-1}$ . One checks by explicit multiplication over  $\mathbb{F}_2$  that

$$C_1 + C_2 + C_3 = E_{1,1},$$

where  $E_{1,1}$  has a single 1 in the (1, 1) entry and zeros elsewhere. Therefore,

$$\Lambda(E_{1,1}) = \Lambda(C_1)\Lambda(C_2)\Lambda(C_3) \\ \in \langle \pi(CNOT_{i \rightarrow j}), \pi(S_i S_j^\dagger) \rangle.$$

But  $\Lambda(E_{1,1})$  is exactly the symplectic action of a single-qubit phase gate on qubit 1. Hence  $S_1$  (up to global phase, and up to a trackable Pauli frame) is generated by the given gates. Because  $SWAP$  gates can be synthesized from  $CNOT$  gates, conjugating by  $SWAP$  gates yields  $S_i$  for arbitrary  $i$ .

With  $S_i$  available, we now synthesize a single-qubit Hadamard  $H_i$  using the global  $H^{\otimes m}$ . At the symplectic level on one qubit, the Hadamard matrix satisfies

$$\begin{pmatrix} 0 & 1 \\ 1 & 0 \end{pmatrix} = \begin{pmatrix} 1 & 0 \\ 1 & 1 \end{pmatrix} \begin{pmatrix} 1 & 1 \\ 0 & 1 \end{pmatrix} \begin{pmatrix} 1 & 0 \\ 1 & 1 \end{pmatrix},$$

i.e.,  $\pi(H) = \Lambda(1)V(1)\Lambda(1)$ , where  $V(1) = J\Lambda(1)J$ . Embedding this identity on qubit  $i$  gives  $\pi(H_i) = \Lambda(E_{ii})V(E_{ii})\Lambda(E_{ii})$  and  $V(E_{ii}) = J\Lambda(E_{ii})J$ . Since  $J = \pi(H^{\otimes m})$  and  $\Lambda(E_{ii}) =$

$\pi(S_i)$ , we can implement  $V(E_{ii})$  as  $H^{\otimes m}S_iH^{\otimes m}$ , and thus (up to global phase)

$$H_i \equiv S_i (H^{\otimes m}S_iH^{\otimes m})S_i.$$

Therefore the generated group contains arbitrary  $CNOT_{i \rightarrow j}$  (by assumption), all single-qubit  $S_i$  and  $H_i$  (as shown), and all Paulis  $X_i, Z_i$  (by assumption). Since it is standard that the Clifford group  $C_m/U(1)$  is generated by  $\{CNOT_{i \rightarrow j}, H_i, S_i\}$  together with Paulis, we conclude that

$$C_m/U(1) \cong \langle X_i, Z_i, CNOT_{i \rightarrow j}, S_i S_j^\dagger, H^{\otimes m} \rangle.$$

□

**Remark E.1.** The condition  $m \geq 3$  is necessary. For  $m = 1$  there is no paired phase gate. For  $m = 2$ , the only paired phase has binary action  $\Lambda(\text{diag}(1, 1))$ , and conjugation by  $GL(2, 2)$  cannot produce  $\Lambda(E_{1,1})$  (the single-qubit phase action), so one cannot generate the full two-qubit Clifford group from these resources alone.

**Example E.2** (Generating  $S_1$  when  $m = 3$ ). Let

$$P_{12} := S_1 S_2^\dagger.$$

Choose the three invertible matrices  $A_1, A_2$  and  $A_3$  as in the proof and pick  $CNOT$ -only circuits  $U_i$  such that  $\pi(U_k) = L(A_i)$ :

$$\begin{aligned} U_1 &:= CNOT_{1 \rightarrow 3} CNOT_{3 \rightarrow 1} CNOT_{1 \rightarrow 3}, \\ U_2 &:= CNOT_{2 \rightarrow 3} CNOT_{3 \rightarrow 2} CNOT_{2 \rightarrow 1} CNOT_{1 \rightarrow 3}, \\ U_3 &:= CNOT_{1 \rightarrow 2} CNOT_{2 \rightarrow 1} CNOT_{3 \rightarrow 1} CNOT_{1 \rightarrow 2}. \end{aligned}$$

Define the conjugates

$$G_k := U_i P_{12} U_i^{-1} \quad (i = 1, 2, 3).$$

Then the product

$$S_1 \equiv G_1 G_2 G_3 = (U_1 P_{12} U_1^{-1})(U_2 P_{12} U_2^{-1})(U_3 P_{12} U_3^{-1})$$

implements  $S_1$  up to global phase and a trackable Pauli frame, using only  $\{CNOT_{i \rightarrow j}, S_i S_j^\dagger\}$  on three qubits.

## Appendix F: Confidence of numerically estimated code distances

In this appendix, we report confidence statistics for the numerical distance estimation of CC codes and of the merged codes arising from parallel surgery for CC codes. As described in [63], the probability  $P_{\text{fail}}$  that the distance  $D_{\text{QDistRnd}}$  returned by  $\text{QDistRnd}$  exceeds the true code distance is expected to be upper bounded by

$$P_{\text{fail}} < e^{-\bar{n}},$$

where  $\bar{n}$  denotes the average number of times a codeword of weight  $D_{\text{QDistRnd}}$  is found during the randomized search procedure [62].

Below in Table IV we report the confidence statistics for distance estimation for the CC codes listed in Table I, where the failure probability is negligible for all cases.

CC codes	$\bar{n}_X$	$e^{-\bar{n}_X}$	$\bar{n}_Z$	$e^{-\bar{n}_Z}$
[[24, 8, 3]]	26350	$< 10^{-10000}$	26390	$< 10^{-10000}$
[[40, 8, 5]]	6988	$< 10^{-3000}$	6999	$< 10^{-3000}$
[[56, 8, 7]]	1883	$< 10^{-800}$	1886	$< 10^{-800}$
[[88, 8, 10]]	283.8	$5.64 \times 10^{-124}$	284.9	$1.90 \times 10^{-124}$
[[104, 8, 11]]	152.0	$9.34 \times 10^{-67}$	156.6	$9.61 \times 10^{-69}$
[[136, 8, 14]]	20.84	$8.91 \times 10^{-10}$	20.15	$1.78 \times 10^{-9}$
[[54, 18, 3]]	2506	$< 10^{-1088}$	2491	$< 10^{-1081}$
[[90, 18, 5]]	739.4	$8.00 \times 10^{-322}$	735.4	$4.36 \times 10^{-320}$
[[126, 18, 7]]	210.8	$2.92 \times 10^{-92}$	211.7	$1.10 \times 10^{-92}$
[[198, 18, 10]]	36.22	$1.86 \times 10^{-16}$	36.56	$1.325 \times 10^{-16}$

TABLE IV. Confidence statistics for distance estimation of CC codes obtained using  $\text{QDistRnd}$ . For each CC code in Table I, we report the average multiplicity  $\bar{n}$  of the lowest-weight codeword found and the corresponding failure bound  $P_{\text{fail}} < e^{-\bar{n}}$  for both X- and Z-type logical operators. All estimates are based on  $10^5$  randomized trials in  $\text{QDistRnd}$ .

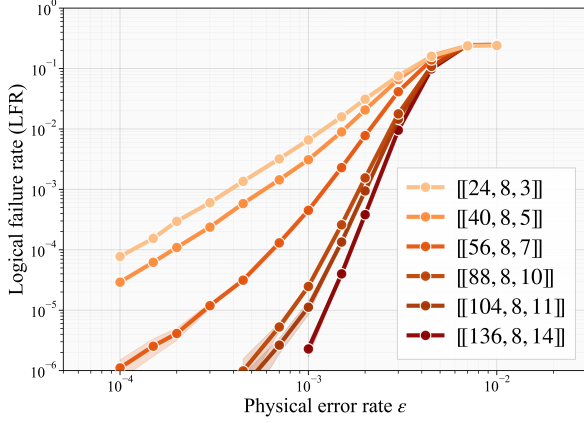
For each CC code with 8 logical qubits, there are  $2^8 = 256$  possible choices of product connection code  $\mathcal{P}$  in the parallel surgery construction. We estimate the code distance for all 256 corresponding merged codes.

In Table V, we report, for each CC data code, the minimum observed value of  $\bar{n}$  among the 256 merged codes and the corresponding worst-case failure bound  $P_{\text{fail}} < e^{-\bar{n}}$ , for both X- and Z-type logical operators.

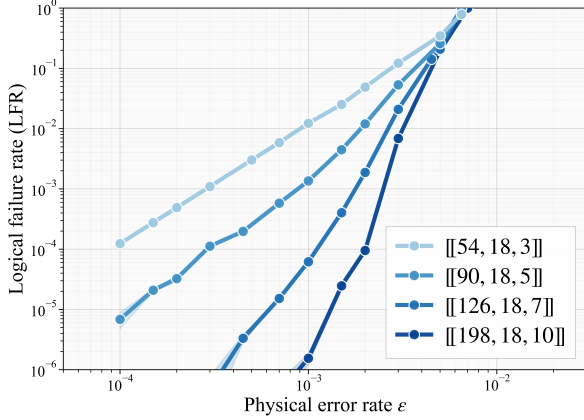
CC codes	$\{\bar{n}_X\}_{\min}$	$e^{-\{\bar{n}_X\}_{\min}}$	$\{\bar{n}_Z\}_{\min}$	$e^{-\{\bar{n}_Z\}_{\min}}$
[[24, 8, 3]]	24150	$< 10^{-10000}$	24080	$< 10^{-10000}$
[[40, 8, 5]]	6113	$< 10^{-2000}$	6113	$< 10^{-2000}$
[[56, 8, 7]]	1616	$< 10^{-700}$	1623	$< 10^{-700}$
[[88, 8, 10]]	225.7	$< 10^{-98}$	229	$< 10^{-99}$
[[104, 8, 11]]	130.1	$3.22 \times 10^{-56}$	123.5	$2.23 \times 10^{-54}$
[[136, 8, 14]]	8.630	$1.79 \times 10^{-4}$	8.700	$1.67 \times 10^{-4}$

TABLE V. Confidence statistics for distance estimation of merged codes obtained using  $\text{QDistRnd}$ . For each CC code with  $k = 8$  in Table I, we report the minimum observed multiplicity  $\{\bar{n}\}_{\min}$  of the lowest-weight codeword across all 256 merged codes arising from the parallel surgery construction, together with the corresponding worst-case failure bound  $P_{\text{fail}} < e^{-\{\bar{n}\}_{\min}}$  for both X- and Z-type logical operators. All estimates are based on  $10^5$  randomized trials.

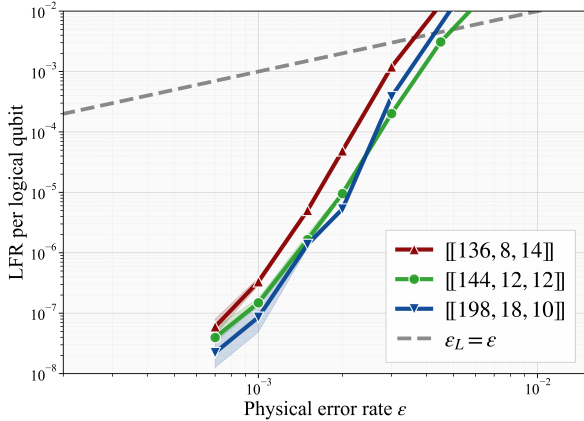
## Appendix G: Circuit-level memory simulations for CC codes



(a) The 8-logical CC code family.



(b) The 18-logical CC code family.



(c) LFR per logical qubit comparison.

**FIG. 3. Circuit-level memory performance of CC codes and comparison.** Logical failure rates per syndrome extraction cycle (LFRs) as a function of physical error rate  $\epsilon$  for the (a) 8-logical and (b) 18-logical CC code families under circuit-level depolarizing noise. (c) LFR per logical qubit  $\epsilon_{1,1}$  as a function of  $\epsilon$ . We compare the performance of the  $[[136, 8, 14]]$  and  $[[198, 18, 10]]$  CC codes with the  $[[144, 12, 12]]$  Gross BB code [16]. The dashed grey line denotes the break-even line  $\epsilon_{1,1} = \epsilon$ .

In this appendix we present the details for circuit-level memory logical error rate simulations, used for Figure 3.

### 1. Circuit scheduling

To evaluate the circuit-level memory performance of CC codes, we perform repeated-syndrome simulation using a framework built upon and extending QITS [79]. In each syndrome extraction round, stabiliser eigenvalues are measured by coupling data qubits to auxiliary qubits via *CNOT* gates dictated by the Tanner graph of the code. To schedule these entangling operations fault-tolerantly, the *CNOT* gates are partitioned into layers such that no qubit participates in more than one *CNOT* within a layer. Therefore, minimising the total number of layers, i.e., circuit depth per round, is essential because every additional layer introduces an idling time-step during which inactive qubits accumulate errors. We implement a greedy edge-colouration algorithm on the Tanner graph that achieves equal or shorter circuit depth than the generic scheduling strategies provided in QITS. The procedure is as follows.

1. **Directional partitioning:** Partition Tanner-graph edges into 4 disjoint groups  $v \in \{N, S, E, W\}$  that represent distinct interaction directions in the construction, with direction-indexed edge lists. This partitioning arises naturally in the HGP and LP constructions, in which two-qubit gates can be classified as horizontal or vertical Tanner graph edges.
2. **Conflict graph construction:** For each direction  $v$ , build a conflict graph  $\mathcal{G}_v$  whose vertices are *CNOT* gates in direction  $v$ , and connect two vertices if and only if the corresponding *CNOT* gates share a qubit, indicating a scheduling conflict.
3. **DSATUR graph colouring:** A vertex colouring of  $\mathcal{G}_v$  is computed using the Degree of Saturation (DSATUR) greedy heuristic, implemented via NetworkX. Each colour class defines a set of mutually non-conflicting *CNOT* gates that can be executed simultaneously in a single time-step.
4. **Circuit assembly:** The *CNOT* depth is  $\gamma_{CNOT} = \sum_v \phi(\mathcal{G}_v)$ , where  $\phi(\mathcal{G}_v)$  is the chromatic number returned by the DSATUR colouring for direction  $v$ . Within each round, the Hadamard gates conjugating the *X*-type auxiliaries and the mid-round auxiliary measurements and resets each contribute one additional time-step.

### 2. Decoding and post-processing

We use Stim [80] to compile the syndrome-extraction circuit and sample from it. And all results reported in this work are decoded by BP+OSD [81] on the full space-time parity-check matrices derived from the detector error model (DEM). We employ the following hyperparameters across all simulations

Parameter	Value
BP update rule	Min-sum
Min-sum scaling factor	0.625
Maximum BP iterations	200
OSD method	OSD-CS
OSD order	5

To ensure accurate resolution of the threshold and sub-threshold logical failure rates, we choose the number of syndrome measurement rounds  $\eta = 42$  if  $\epsilon < 4 \times 10^{-3}$  and  $\eta = 20$  if  $\epsilon > 4 \times 10^{-3}$ . From the empirical estimate of the total logical failure rate over  $\eta$  rounds,  $\epsilon_\gamma$ , we first define the *logical failure rate per round* (LFR). Assuming independent failure events across rounds in the small-error regime, the probability of zero logical failures occurring in a single cycle is  $1 - \text{LFR}$ . Over  $\eta$  rounds, this yields a total success probability

of  $(1 - \text{LFR})^\eta = 1 - \epsilon_\gamma$ , giving

$$\text{LFR} = 1 - (1 - \epsilon_\gamma)^{1/\eta}.$$

To further facilitate a fair comparison across codes with varying numbers of logical qubits,  $k$ , it is useful to convert this into an effective per-logical-qubit error rate per syndrome cycle,  $\epsilon_{1,1}$ . Following the approach outlined in Ref. [43], we extend the assumption of uniform, independent failures to the  $k$  individual logical qubits. The probability of no logical failures occurring on any specific qubit in a single round is  $1 - \epsilon_{1,1}$ . Equating the total block success probability over  $\eta$  rounds to  $(1 - \epsilon_{1,1})^{k\eta}$  yields

$$1 - \epsilon_\gamma = (1 - \epsilon_{1,1})^{k\eta},$$

which is directly inverted to give the single-qubit, single-round logical failure rate:

$$\epsilon_{1,1} = 1 - (1 - \epsilon_\gamma)^{1/k\eta}.$$

#### Appendix H: Examples of CC codes

Tables VI and VII list the seed matrices  $H_a$  and  $H_b$  over  $R = \mathbb{F}_2[x]/(x^p + 1)$  for the CC codes presented in Table I. For convenience, we denote the code parameters together with the corresponding lift parameter in the form  $[[N, k, d]](p)$ .

TABLE VI. Seed matrices  $H_a$  and  $H_b$  defined over  $R = \mathbb{F}_2[x]/(x^p + 1)$  for example CC codes with  $k = 8$  listed in Table I.

CC code	$[[24, 8, 3]](3)$	$[[40, 8, 5]](5)$	$[[56, 8, 7]](7)$	$[[88, 8, 10]](11)$	$[[104, 8, 11]](13)$	$[[136, 8, 14]](17)$
$H_a$	$\begin{pmatrix} 1+x^2 & x+x^2 \\ 1+x & x+x^2 \end{pmatrix}$	$\begin{pmatrix} x+x^3 & x+x^4 \\ x+x^4 & x+x^4 \end{pmatrix}$	$\begin{pmatrix} x+x^5 & x+x^3 \\ 1+x^2 & 1+x^3 \end{pmatrix}$	$\begin{pmatrix} x+x^5 & x^5+x^6 \\ x^2+x^3 & x^5+x^9 \end{pmatrix}$	$\begin{pmatrix} x+x^5 & x^2+x^5 \\ x+x^4 & x^9+x^{10} \end{pmatrix}$	$\begin{pmatrix} x^{13}+x^{16} & x^5+x^{15} \\ x^6+x^{16} & 1+x^3 \end{pmatrix}$
$H_b$	$\begin{pmatrix} 1+x^2 & x+x^2 \\ 1+x & 1+x \end{pmatrix}$	$\begin{pmatrix} 1+x & x^3+x^4 \\ 1+x^4 & 1+x^4 \end{pmatrix}$	$\begin{pmatrix} x^2+x^5 & 1+x \\ x^5+x^6 & x^4+x^6 \end{pmatrix}$	$\begin{pmatrix} 1+x^3 & x^8+x^{10} \\ x^5+x^7 & x^3+x^7 \end{pmatrix}$	$\begin{pmatrix} x^2+x^8 & 1+x^8 \\ x+x^9 & x+x^3 \end{pmatrix}$	$\begin{pmatrix} x+x^7 & x^8+x^{10} \\ x^8+x^{10} & x^5+x^{16} \end{pmatrix}$

TABLE VII. Seed matrices  $H_a$  and  $H_b$  defined over  $R = \mathbb{F}_2[x]/(x^p + 1)$  for example CC codes with  $k = 18$  listed in Table I.

CC code	$[[54, 18, 3]](3)$	$[[90, 18, 5]](5)$	$[[126, 18, 7]](7)$	$[[198, 18, 10]](11)$
$H_a$	$\begin{pmatrix} x+x^2 & 0 & 1+x \\ x+x^2 & 1+x & 0 \\ 0 & 1+x^2 & 1+x^2 \end{pmatrix}$	$\begin{pmatrix} 1+x & 0 & 1+x^4 \\ 1+x^3 & 1+x^2 & 0 \\ 0 & 1+x^4 & 1+x^2 \end{pmatrix}$	$\begin{pmatrix} x+x^4 & 0 & x^2+x^4 \\ x+x^3 & x^2+x^5 & 0 \\ 0 & 1+x^5 & 1+x^3 \end{pmatrix}$	$\begin{pmatrix} x^4+x^9 & 0 & x^5+x^7 \\ x^4+x^6 & x^2+x^8 & 0 \\ 0 & x^7+x^{10} & x^3+x^8 \end{pmatrix}$
$H_b$	$\begin{pmatrix} 1+x & 1+x^2 & 0 \\ 0 & x+x^2 & 1+x^2 \\ 1+x^2 & 0 & x+x^2 \end{pmatrix}$	$\begin{pmatrix} 1+x^4 & 1+x^2 & 0 \\ 0 & 1+x^3 & 1+x \\ 1+x & 0 & 1+x^3 \end{pmatrix}$	$\begin{pmatrix} x^5+x^6 & x^5+x^6 & 0 \\ 0 & x+x^3 & 1+x \\ x+x^2 & 0 & x^4+x^6 \end{pmatrix}$	$\begin{pmatrix} x^3+x^4 & x^6+x^{10} & 0 \\ 0 & x^2+x^3 & x^8+x^{10} \\ 1+x^7 & 0 & x^9+x^{10} \end{pmatrix}$

#### Appendix I: Examples of parallel surgery for CC codes

In this appendix, we give some concrete examples of parallel surgery with CC code as data code patch and auxiliary code patch. For simplicity, we separate the logical qubits of a CC code with code parameters  $[[N = 2pn_a n_b, k = 2n_a n_b, d \leq p]]$  into two sectors, left and right, with each sector contacting  $n_a n_b$  logical qubits. Each  $X$ -type logical operator is denoted as

$$\bar{X}_i^{\text{left}} \text{ or } \bar{X}_i^{\text{right}} \text{ for } i \in \{1, \dots, n_a n_b\}.$$

Each Z-type logical operator is denoted as

$$\bar{Z}_i^{\text{left}} \text{ or } \bar{Z}_i^{\text{right}} \text{ for } i \in \{1, \dots, n_a n_b\}.$$

**Example I.1** ([[24, 8, 3]], maximally 4 pairs of merges with overhead of 24 qubits and 24 checks). Consider the [[24, 8, 3]] CC code given in Table VI. The basis for the logical operators are given by

$$L = \left( \begin{array}{cccc|cccc} \chi & & & & & & & \\ & \chi & & & & & & \\ & & \chi & & & & & \\ & & & \chi & & & & \\ & & & & \chi & & & \\ & & & & & \chi & & \\ & & & & & & \chi & \\ & & & & & & & \chi \end{array} \right), \quad (11)$$

where  $\chi = 1 + x + x^2$ . We perform 4 pairs of joint logical measurements on all the logical qubits, i.e., merging  $\bar{Z}_i^{\text{left}}$  with  $\bar{Z}_i^{\text{right}}$  for  $i = 1, 2, 3, 4$  by choosing  $Q^{\text{aux}} = Q = \text{CC}(H_a, H_b)$  and  $\mathcal{P} = \text{LP}(H'_a, H'_b)$  where

$$H'_a = H'_b = I_2.$$

The corresponding merged code with parity check matrices

$$\widetilde{H}_X = \begin{pmatrix} H_X & H'_X \\ & H_X \end{pmatrix} \text{ and } \widetilde{H}_Z = \begin{pmatrix} H_Z & \\ H'_Z & H_Z \end{pmatrix},$$

defines a  $[[\widetilde{N} = 48, \widetilde{k} = 4, \widetilde{r} = 4, \widetilde{d} = 3]]$  merged code, where  $\widetilde{N}, \widetilde{k}, \widetilde{r}$  and  $\widetilde{d}$  are the number of physical qubits, number of logical qubits, number of gauges and code distance, respectively. The bottom half of  $\widetilde{H}_Z$  is given by

$$(H'_Z \ H_Z) = \left( \begin{array}{ccc|ccc|cccc|cccc} 1 & & & 1 & & & 1+x & 1+x^2 & & & 1+x & & & 1+x^2 \\ & 1 & & & 1 & & x+x^2 & 1+x^2 & & & & 1+x & & 1+x^2 \\ & & 1 & & & & & & 1+x & 1+x^2 & x+x^2 & & x+x^2 & 1+x^2 \\ & & & 1 & & & & & x+x^2 & 1+x^2 & & x+x^2 & & x+x^2 \\ & & & & 1 & & & & & & & & & \end{array} \right).$$

Data patch
Auxiliary patch

Therefore,  $\text{supp}(\bar{Z}_i^{\text{left}} \otimes \bar{Z}_i^{\text{right}}) = \chi (H'_Z \ H_Z)_{i, \bullet}$ . For example, we have

$$\begin{aligned} \text{supp}(\bar{Z}_2^{\text{left}} \otimes \bar{Z}_2^{\text{right}}) &= \chi (0 \ 1 \ 0 \ 0 | 0 \ 1 \ 0 \ 0 | x+x^2 \ 1+x^2 \ 0 \ 0 | 0 \ 1+x \ 0 \ 1+x^2) \\ &= (0 \ \chi \ 0 \ 0 | 0 \ \chi \ 0 \ 0 | 0 \ 0 \ 0 \ 0 | 0 \ 0 \ 0 \ 0) \\ &= (0 \ \chi \ 0 \ 0 | 0 \ 0 \ 0 \ 0 | 0 \ 0 \ 0 \ 0 | 0 \ 0 \ 0 \ 0) + (0 \ 0 \ 0 \ 0 | 0 \ \chi \ 0 \ 0 | 0 \ 0 \ 0 \ 0 | 0 \ 0 \ 0 \ 0). \end{aligned}$$

The binary action of this ‘multiplying by  $\chi$ ’ is simply taking the sum of the rows in the binary representation of the  $i^{\text{th}}$  row of  $(H'_Z \ H_Z)$ . Namely, for each merge  $\bar{Z}_i^{\text{left}} \otimes \bar{Z}_i^{\text{right}}$  we measure  $p = 3$  stabilisers of the merged code and the product of which is the Pauli product of this pair of Z-type logical operators. One thing worth mentioning is, if we initialise the data patch in  $|\overline{\uparrow}\rangle^{\otimes 8}$ , by measuring out the joint Pauli operators  $\bar{Z}_i^{\text{left}} \otimes \bar{Z}_i^{\text{right}}$ , we end up with 4 logical Bell states [21].

**Example I.2** ([[24, 8, 3]], 4 single-qubit logical measurements with overhead of 24 qubits and 24 checks). Consider the [[24, 8, 3]] CC code given in Table VI. The basis for the logical operators are given by  $L = \text{diag}_8(\chi)$  as in Eq. (11). We perform parallel logical measurements on 4 logical operators, i.e., measuring  $\bar{Z}_i^{\text{left}}$  for  $i = 1, 2, 3, 4$  by choosing  $Q^{\text{aux}} = Q = \text{CC}(H_a, H_b)$  and  $\mathcal{P} = \text{LP}(H'_a, H'_b)$  where

$$H'_a = 0 \text{ and } H'_b = I_2.$$

The corresponding merged code with parity check matrices

$$\widetilde{H}_X = \begin{pmatrix} H_X & H'_X \\ & H_X \end{pmatrix} \text{ and } \widetilde{H}_Z = \begin{pmatrix} H_Z & \\ H'_Z & H_Z \end{pmatrix},$$

defines a  $[[\tilde{N} = 48, \tilde{k} = 4, \tilde{r} = 4, \tilde{d} = 3]]$  merged code. The bottom half of  $\widetilde{H}_Z$  is given by

$$(H'_Z \ H_Z) = \left( \underbrace{\begin{array}{ccc|ccc} 1 & & & 0 & & \\ & 1 & & & 0 & \\ & & 1 & & & \\ & & & 1 & & \\ \hline & & & & & \end{array}}_{\text{Data patch}} \underbrace{\begin{array}{ccc|ccc} 1+x & 1+x^2 & & 1+x & & 1+x^2 \\ x+x^2 & 1+x^2 & & x+x^2 & 1+x & 1+x^2 \\ & & 1+x & 1+x^2 & & \\ & & x+x^2 & 1+x^2 & x+x^2 & x+x^2 \\ \hline & & & & & \end{array}}_{\text{Auxiliary patch}} \right).$$

Therefore,  $\text{supp}(\bar{Z}_i^{\text{left}}) = \chi(H'_Z \ H_Z)_{i,\bullet}$ . For example,

$$\begin{aligned} \text{supp}(\bar{Z}_2^{\text{left}}) &= \chi(0 \ 1 \ 0 \ 0 \mid 0 \ 0 \ 0 \ 0 \mid x+x^2 \ 1+x^2 \ 0 \ 0 \mid 0 \ 1+x \ 0 \ 1+x^2) \\ &= (0 \ \chi \ 0 \ 0 \mid 0 \ 0 \ 0 \ 0 \mid 0 \ 0 \ 0 \ 0 \mid 0 \ 0 \ 0 \ 0). \end{aligned}$$

Same as before, the binary action of this ‘multiplying by  $\chi$ ’ is simply taking the sum of the rows in the binary representation of the  $i^{\text{th}}$  row of  $(H'_Z \ H_Z)$ . Namely, for each logical operator  $\bar{Z}_i^{\text{left}}$  we measure  $p = 3$  stabilisers of the merged code and the product of which is the Pauli product of this  $Z$ -type logical operator.

**Example 1.3** ( $[[24, 8, 3]]$ , 2 pairs of merges with overhead of 24 qubits and 24 checks). Consider the  $[[24, 8, 3]]$  CC code given in Table VI. The basis for the logical operators are given by  $L = \text{diag}_8(\chi)$ . We perform two pairs of joint logical measurements on the logical operators on the right sector, i.e., measuring  $\bar{Z}_1^{\text{right}} \otimes \bar{Z}_3^{\text{right}}$  and  $\bar{Z}_1^{\text{right}} \otimes \bar{Z}_3^{\text{right}}$  in parallel by choosing  $\mathcal{Q}^{\text{aux}} = \mathcal{Q} = \text{CC}(H_a, H_b)$  and  $\mathcal{P} = \text{LP}(H'_a, H'_b)$  where

$$H'_a = \begin{pmatrix} 1 & 0 \\ 1 & 0 \end{pmatrix} \text{ and } H'_b = 0.$$

The corresponding merged code with parity check matrices

$$\widetilde{H}_X = \begin{pmatrix} H_X & H'_X \\ & H_X \end{pmatrix} \text{ and } \widetilde{H}_Z = \begin{pmatrix} H_Z & \\ H'_Z & H_Z \end{pmatrix},$$

defines a  $[[\tilde{N} = 48, \tilde{k} = 6, \tilde{r} = 6, \tilde{d} = 3]]$  merged code. The bottom half of  $\widetilde{H}_Z$  is given by

$$(H'_Z \ H_Z) = \left( \underbrace{\begin{array}{ccc|ccc} 0 & & & 1 & 1 & \\ & 0 & & & 1 & 1 \\ & & 0 & & & 0 \\ & & & 0 & & 0 \\ \hline & & & & & \end{array}}_{\text{Data patch}} \underbrace{\begin{array}{ccc|ccc} 1+x & 1+x^2 & & 1+x & & 1+x^2 \\ x+x^2 & 1+x^2 & & x+x^2 & 1+x & 1+x^2 \\ & & 1+x & 1+x^2 & & \\ & & x+x^2 & 1+x^2 & x+x^2 & x+x^2 \\ \hline & & & & & \end{array}}_{\text{Auxiliary patch}} \right),$$

where  $H'_Z$  only has rank 2. According to Theorem V.5 and Theorem V.7, there is only 2 merges being performed, which left  $8 - 2 = 6$  logical qubits with the merged code. To measure the joint Pauli product,

$$\text{supp}(\bar{Z}_1^{\text{right}} \otimes \bar{Z}_3^{\text{right}}) = \chi(H'_Z \ H_Z)_{1,\bullet} \text{ and } \text{supp}(\bar{Z}_2^{\text{right}} \otimes \bar{Z}_4^{\text{right}}) = \chi(H'_Z \ H_Z)_{2,\bullet}.$$

In this example, we perform measurements of two pairs of joint logical operators with the same overhead as in previous cases (24 physical qubits and 24 checks). This illustrates a key feature of the parallel surgery protocol: for a fixed data-code patch, the total resource cost of a single round of PPMs remains constant. The actual efficiency of the implementation then depends on how the algorithm is compiled so that more PPMs can be executed within that fixed overhead. An ideal scenario is to maximise the merge being performed each round, with  $k/2$  to be the maximum number of merges being performed, as laid out in Theorem V.9.

## Appendix J: Fold-transversal and automorphism Clifford operations for the $[[24, 8, 3]]$ CC code

The clustered logical operator basis of CC codes makes it straightforward to interpret the logical action of physical operations on the physical qubits. In this appendix, we illustrate the fold-transversal [32, 56] and automorphism gates [42] of the  $[[24, 8, 3]]$

CC code, which together with parallel surgery of CC codes, compiles the full Clifford group of four logical qubits while treating other four logical qubits as auxiliary logical qubits in Section VII.

To be entirely concrete, in the following, we consider the  $[[24, 8, 3]]$  CC code with seed codes given in VI, whose parity check matrices are

$$H_X = \left( \begin{array}{cccc|cc} 1+x^2 & & x+x^2 & & 1+x^2 & x+x^2 \\ & 1+x^2 & & x+x^2 & 1+x & 1+x \\ 1+x & & x+x^2 & & & 1+x^2 & x+x^2 \\ & 1+x & & x+x^2 & & 1+x & 1+x \end{array} \right)$$

$$H_Z = \left( \begin{array}{cccc|ccc} 1+x & 1+x^2 & & & 1+x & & 1+x^2 \\ x+x^2 & 1+x^2 & & & & 1+x & & 1+x^2 \\ & & 1+x & 1+x^2 & x+x^2 & & x+x^2 & \\ & & x+x^2 & 1+x^2 & & x+x^2 & & x+x^2 \end{array} \right).$$

### 1. $CZ$ - $S$ phase-type fold-transversal gate

This  $[[24, 8, 3]]$  CC code is equipped with a  $CZ$ - $S$  logical gate,

$$\bar{S}_1 \bar{S}_4 \bar{S}_5^\dagger \bar{S}_8^\dagger \bar{C}Z_{2,3} \bar{C}Z_{6,7},$$

via applying  $S$ ,  $S^\dagger$  and  $CZ$  gates on physical qubits in a fold-transversal way [32, 56]. Recall the action of  $S$  and  $CZ$  gates in terms of stabilisers and parity check matrices:

1. The phase gate  $S$ , that maps  $X$  operators into  $Y$  operators and fixes  $Z$  operators. Consider a diagonal binary matrix  $\mathbb{B}(A_S)$ , whose non-zero entries  $(i, i)$  corresponding to the application of  $S$  gates on the  $i^{\text{th}}$  physical qubits. The parity check matrices after application of  $S$  gates are updated to  $\mathbb{B}(H_X) \mapsto \mathbb{B}(H_X)$  and  $\mathbb{B}(H_Z) \mapsto \mathbb{B}(H_Z) + \mathbb{B}(H_X)\mathbb{B}(A_S)\mathbb{B}(H_X)^\top$ .
2. The  $CZ$  gate, a two qubit gate that maps  $X \otimes I \mapsto X \otimes Z$ ,  $I \otimes X \mapsto Z \otimes X$  and acts trivially on  $Z$  operators. In terms of parity check matrices,  $\mathbb{B}(H_X)$  does not change while  $\mathbb{B}(H_Z) \mapsto \mathbb{B}(H_Z) + \mathbb{B}(H_X)\mathbb{B}(A_{CZ})\mathbb{B}(H_X)^\top$ , where  $\mathbb{B}(A_{CZ})$  is a symmetric binary matrix describing the action of  $CZ$  gates.

Specifically, for this  $[[24, 8, 3]]$  CC code, we apply  $S$  gate on the diagonal clusters of physical qubits of the left sector,  $S^\dagger$  on the diagonal clusters of physical qubits of the right sector and  $CZ$  gates between off-diagonal clusters of physical qubits in each sector. They correspond to the binary representation of matrices over  $R = \mathbb{F}_2[x]/(x^3 + 1)$ ,  $A_S$  and  $A_{CZ}$ , respectively. Here

$$A_S = \left( \begin{array}{cccc|cccc} 1 & & & & & & & \\ & 0 & & & & & & \\ & & 0 & & & & & \\ & & & 1 & & & & \\ & & & & 1 & & & \\ & & & & & 0 & & \\ & & & & & & 0 & \\ & & & & & & & 1 \end{array} \right) \text{ and } A_{CZ} = \left( \begin{array}{cccc|cccc} 0 & & & & & & & \\ & 0 & 1 & & & & & \\ & 1 & 0 & & & & & \\ & & & 0 & & & & \\ & & & & 0 & & & \\ & & & & & 0 & 1 & \\ & & & & & & 1 & 0 \\ & & & & & & & 0 \end{array} \right).$$

It is simple to verify that to total action  $\mathbb{B}(A_{CZ-S}) = \mathbb{B}(A_{CZ}) + \mathbb{B}(A_S)$  preserves the  $Z$ -type stabilisers as

$$\mathbb{B}(H_X)\mathbb{B}(A_{CZ-S})\mathbb{B}(H_X)^\top = \mathbb{B}(H_X A_{CZ-S} H_X^*) = 0.$$

$X$ -type stabilisers are untouched. Therefore, above  $CZ$ - $S$  gate is a valid logical operation preserves the stabiliser group. And the overall phase cancels out due to same number of  $S$  and  $S^\dagger$  gates. For the clustered basis of this code, as in Eq. (II), the logical action is interpreted to be  $\bar{S}_1 \bar{S}_4 \bar{S}_5^\dagger \bar{S}_8^\dagger \bar{C}Z_{2,3} \bar{C}Z_{6,7}$ .

### 2. $H$ - $SWAP$ Hadamard-type fold-transversal gates

This  $[[24, 8, 3]]$  CC code is equipped with a  $H$ - $SWAP$  logical gate,

$$SWAP_{1,6} SWAP_{4,7} SWAP_{5,8} SWAP_{6,7} \prod_{i=1}^8 \bar{H}_i,$$

via applying global  $H$  on all physical qubits and some physical  $SWAP$  gates [32, 56].

Recall the action of  $H$  and  $SWAP$  gates in terms of stabilisers and parity check matrices:

1. The Hadamard gate  $H$ , that maps  $X$  operators into  $Z$  operators and vice-versa. The parity check matrices are exchanged,  $\mathbb{B}(H_X) \mapsto \mathbb{B}(H_Z)$  and  $\mathbb{B}(H_Z) \mapsto \mathbb{B}(H_X)$ .
2. The  $SWAP_{i,j}$  gate, that swaps the  $i^{\text{th}}$  physical qubit with  $j^{\text{th}}$  physical qubit. In terms of parity check matrices, both types of parity check matrices have the  $i^{\text{th}}$  column swapped with the  $j^{\text{th}}$  column.

Utilising AutQEC [42], we find the following physical operations which gives the logical  $H$ – $SWAP$  introduced above for the logical basis in Eq. (11),

$$SWAP_{18,21}SWAP_{17,20}SWAP_{16,19}SWAP_{15,22}SWAP_{14,24}SWAP_{13,23}$$

$$SWAP_{12,19}SWAP_{11,21}SWAP_{10,20}SWAP_{3,16}SWAP_{2,18}SWAP_{1,17} \prod_{i=1}^{24} H_i.$$

### 3. Automorphism logical $SWAP$ gates

Utilising AutQEC [42], for the  $[[24, 8, 3]]$  code, we find the following logical  $SWAP$  gates generated by only triggering physical  $SWAP$  gates. In Appendix K, we illustrate explicitly how these logical  $SWAP$  gates together with the parallel surgery compile into parallel  $CNOT$  gates.

$$Aut(1) = S\bar{W}AP_{1,6}S\bar{W}AP_{3,5}S\bar{W}AP_{2,8}S\bar{W}AP_{4,7}S\bar{W}AP_{5,8}S\bar{W}AP_{6,7};$$

$$Aut(2) = S\bar{W}AP_{2,3}S\bar{W}AP_{6,7};$$

$$Aut(3) = S\bar{W}AP_{5,3}S\bar{W}AP_{8,2},$$

where  $Aut(1)$  actually swaps left and right sector of logical qubits up to certain reordering within the sectors. The physical operations of these logical  $SWAP$ s are respectively

$$Aut(1)_{\text{phys}} = SWAP_{1,17}SWAP_{1,10}SWAP_{1,20}SWAP_{2,16}SWAP_{2,11}SWAP_{2,19}SWAP_{3,18}SWAP_{3,12}SWAP_{3,21}$$

$$SWAP_{4,22}SWAP_{4,7}SWAP_{4,15}SWAP_{5,24}SWAP_{5,8}SWAP_{5,14}SWAP_{6,23}SWAP_{6,9}SWAP_{6,13};$$

$$Aut(2)_{\text{phys}} = SWAP_{2,3}SWAP_{4,7}SWAP_{5,9}SWAP_{6,8}SWAP_{11,12}SWAP_{13,14}SWAP_{16,21}SWAP_{17,20}SWAP_{18,19}SWAP_{23,24};$$

$$Aut(3)_{\text{phys}} = SWAP_{4,22}SWAP_{5,23}SWAP_{6,24}SWAP_{7,15}SWAP_{8,13}SWAP_{9,14}.$$

### Appendix K: Parallel logical $CNOT$ gates for $[[24, 8, 3]]$ CC code

A logical  $CNOT$  can be performed via logical PPMs between an auxiliary logical qubit initialised in  $|\bar{\uparrow}\rangle$  state with the control logical qubit and the target logical qubit, respectively, as illustrated in Figure 4.

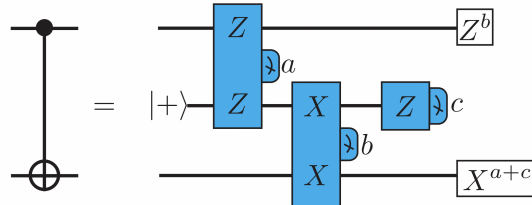


FIG. 4. Circuits for implementing the PPM-induced  $CNOT$  [30].

In this appendix, we investigate the  $[[24, 8, 3]]$  CC code as a toy model. We present concrete procedures for performing logical  $CNOT$  gates between any two logical qubits from the logical qubits 2, 4, 6, 8 while treating the logical qubits 1, 3, 5, 7 as auxiliary logical qubits. The PPMs are performed via parallel surgery and we make use of the fold-transversal gates and automorphism gates of the  $[[24, 8, 3]]$  CC code discovered in Appendix J. As the whole procedure can be accomplished with single patch of auxiliary code, the space overhead is fixed to be  $N = 24$  physical qubits and  $N = 24$  additional checks. Furthermore, we show

that we can maximally parallelise the logical  $CNOT$  gates such that any arrangement that partitions the four data logical qubits into two ordered pairs can be applied logical  $CNOT$  gates in parallel. Specifically, we present

$$\begin{aligned}
 &CNOT_{6 \rightarrow 2} \text{ in parallel with } CNOT_{8 \rightarrow 4} \text{ or } CNOT_{6 \rightarrow 4} \text{ in parallel with } CNOT_{8 \rightarrow 2}, \\
 &CNOT_{2 \rightarrow 6} \text{ in parallel with } CNOT_{4 \rightarrow 8}, \\
 &CNOT_{2 \rightarrow 8} \text{ in parallel with } CNOT_{4 \rightarrow 6}, \\
 &CNOT_{8 \rightarrow 6} \text{ in parallel with } CNOT_{2 \rightarrow 4} \text{ or } CNOT_{6 \rightarrow 8} \text{ in parallel with } CNOT_{4 \rightarrow 2}, \\
 &CNOT_{2 \rightarrow 4}, CNOT_{2 \rightarrow 6} \text{ or } CNOT_{2 \rightarrow 8}, \\
 &CNOT_{8 \rightarrow 4}, CNOT_{8 \rightarrow 2} \text{ or } CNOT_{8 \rightarrow 6},
 \end{aligned}$$

one by one in the following examples. These logical  $CNOT$  gates are enough to generate arbitrary logical  $CNOT$  gates between two logical qubits from the logical qubits 2, 4, 6, 8. For all processes presented below, the logical qubits 1, 3, 5, 7 are treated as auxiliary logical qubits, which do not carry logical information. The logical qubits 2, 4, 6, 8 are data qubits which we use for computation.

**Example K.1** (Logical  $CNOT_{6 \rightarrow 2} // CNOT_{8 \rightarrow 4}$  or logical  $CNOT_{6 \rightarrow 4} // CNOT_{8 \rightarrow 2}$ ). Below we illustrate the procedure for performing logical

$$\begin{aligned}
 &CNOT_{6 \rightarrow 2} \text{ in parallel with } CNOT_{8 \rightarrow 4} \text{ or} \\
 &CNOT_{6 \rightarrow 4} \text{ in parallel with } CNOT_{8 \rightarrow 2},
 \end{aligned}$$

in the  $[[24, 8, 3]]$  CC code via parallel surgery.

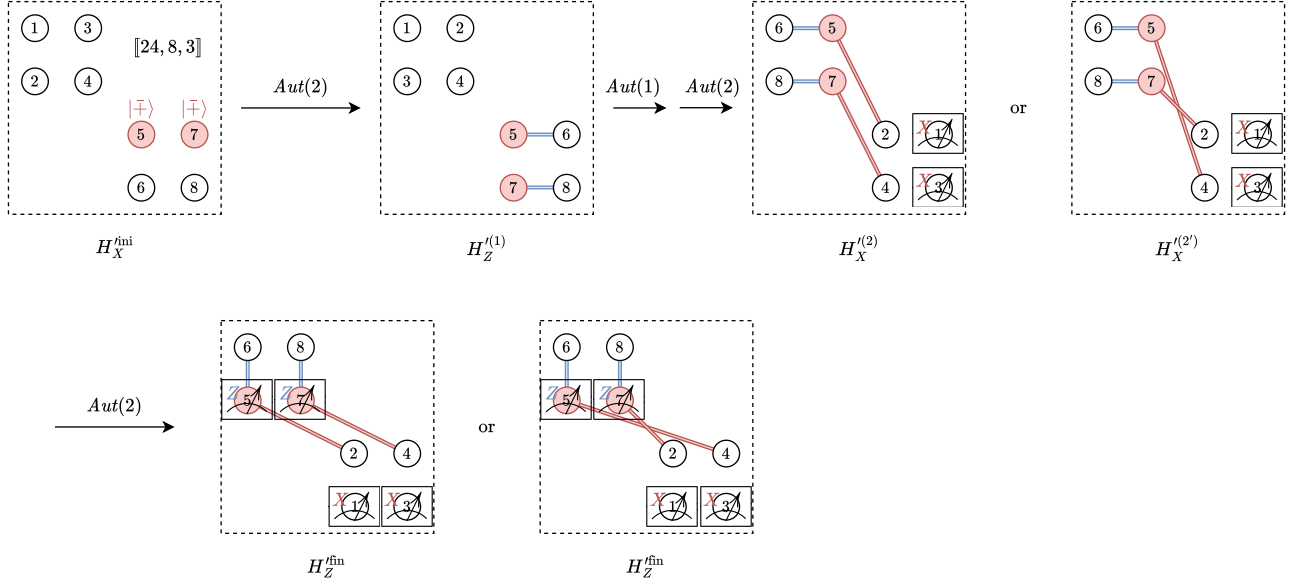


FIG. 5. The procedure for performing logical  $CNOT_{6 \rightarrow 2}$  in parallel with  $CNOT_{8 \rightarrow 4}$  or  $CNOT_{6 \rightarrow 4}$  in parallel with  $CNOT_{8 \rightarrow 2}$  via parallel surgery for the  $[[24, 8, 3]]$  CC code. The uncoloured circles are logical qubits in unknown states, while red coloured circles are the logical qubits initialised in  $|+\rangle$ . The blue double line connects two logical qubits being merged in Z basis, while the red double line connects the logical qubits being merged in X basis.

0. **initialisation of auxiliary logical qubits:** We initialise the 5<sup>th</sup> and 7<sup>th</sup> logical qubits in logical  $|+\rangle$  states via measuring them in the X basis and perform Pauli frame correction. For this step, the product connection code  $\mathcal{P}^{\text{ini}}$  is equipped with X-type parity check matrix

$$H_X^{\text{ini}} = \left( \begin{array}{ccc|cc} 0 & & & 1 & 0 \\ & 0 & & 0 & 0 \\ & & 0 & & 1 & 0 \\ & & & 0 & 0 & 0 \end{array} \right).$$

1. **Joint Z-Pauli measurements:** We first apply  $Aut(2)$  to  $SWAP_{2,3}$  and  $SWAP_{6,7}$ . The joint Z-Pauli measurements are then performed for  $\bar{Z}_5 \otimes \bar{Z}_6$  and  $\bar{Z}_7 \otimes \bar{Z}_8$  via parallel surgery whose product connection code  $\mathcal{P}^{(1)}$  is equipped with Z-type parity check matrix

$$H'_Z{}^{(1)} = \left( \begin{array}{ccc|ccc} 0 & & & 1 & 1 & \\ & 0 & & 1 & 1 & \\ & & 0 & 0 & 0 & 0 \end{array} \right).$$

2. **Joint X-Pauli measurements:** We  $Aut(2)$  again after we applied  $Aut(1)$  to perform a sequence of logical swaps resulting in swapping the logical qubits in the right sector with the logical qubits in the left sector. The joint X-Pauli measurements are then performed for  $\bar{X}_5 \otimes \bar{X}_2$  and  $\bar{X}_7 \otimes \bar{X}_4$  ( $\bar{X}_5 \otimes \bar{X}_4$  and  $\bar{X}_7 \otimes \bar{X}_2$ ) via parallel surgery whose product connection code  $\mathcal{P}^{(2)}$  ( $\mathcal{P}^{(2')}$ ) is equipped with X-type parity check matrix

$$H'_X{}^{(2)} = \left( \begin{array}{ccc|cc} 0 & 1 & & 1 & 0 \\ & 0 & 1 & 0 & 1 \\ & & 0 & & 1 & 0 \\ & & & 0 & 1 \end{array} \right) \text{ or } H'_X{}^{(2')} = \left( \begin{array}{ccc|cc} 0 & 1 & & 0 & 1 \\ & 0 & 1 & 1 & 0 \\ & & 0 & & 0 & 1 \\ & & & 1 & 0 \end{array} \right), \text{ respectively.}$$

3. **Measure out the auxiliary logical qubits in Z basis and complete the CNOT:** We apply  $Aut(2)$  once again in order to utilise  $\mathcal{P}^{\text{fin}}$  to measure out the auxiliary logical qubits in the Z basis, where the parity check matrix is given by

$$H_Z^{\text{fin}} = \left( \begin{array}{cc|cc} 0 & 1 & 0 & \\ 0 & 0 & 0 & \\ & & 0 & 1 \\ & & 0 & 0 \end{array} \right).$$

To complete the logical *CNOT* gates, we apply Pauli frame correction based on the measurement outcomes obtained according to Figure 4.

**Example K.2** (Logical  $CNOT_{2 \rightarrow 6} // CNOT_{4 \rightarrow 8}$ ). Below we illustrate the procedure for performing logical

$CNOT_{2 \rightarrow 6}$  in parallel with  $CNOT_{4 \rightarrow 8}$ ,

in the  $[[24, 8, 3]]$  CC code via parallel surgery.

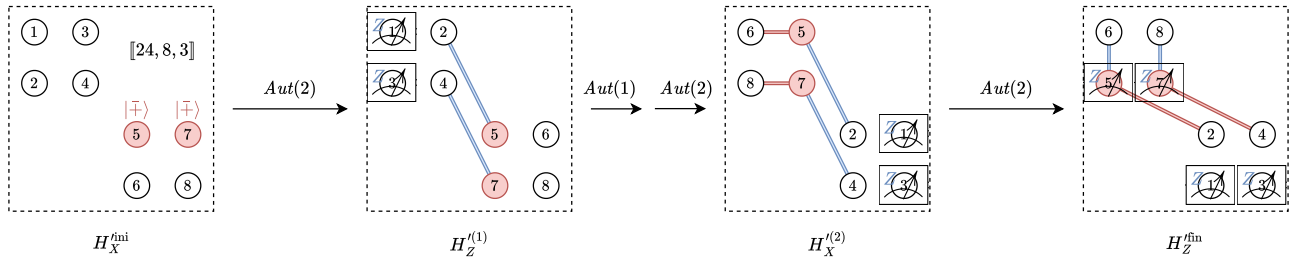


FIG. 6. The procedure for performing logical  $CNOT_{2 \rightarrow 6}$  in parallel with  $CNOT_{4 \rightarrow 8}$ .

For simplicity, we do not expand step by step as in Example K.1, while the relevant parity check matrices are

$$H'_Z{}^{(1)} = \left( \begin{array}{ccc|ccc} 0 & & & 1 & 1 & \\ & 0 & & 1 & 1 & \\ & & 0 & 0 & 0 & 0 \end{array} \right) \text{ and } H'_X{}^{(2)} = \left( \begin{array}{ccc|ccc} 0 & 1 & & 1 & 0 \\ & 0 & 1 & 0 & 1 \\ & & 0 & & 1 & 0 \\ & & & 0 & 1 \end{array} \right),$$

and the  $H_X^{\text{ini}}$  and  $H_Z^{\text{fin}}$  are exactly the same as in Example K.1.

**Example K.3** (Logical  $CNOT_{2 \rightarrow 8} // CNOT_{4 \rightarrow 6}$ ). Below we illustrate the procedure for performing logical

$CNOT_{2 \rightarrow 8}$  in parallel with  $CNOT_{4 \rightarrow 6}$ ,

in the  $[[24, 8, 3]]$  CC code via parallel surgery. The relevant parity check matrices are

$$H'_Z^{(1)} = \left( \begin{array}{cc|cc} 0 & 1 & 0 & 0 \\ 1 & 0 & 0 & 0 \\ & & 0 & 1 \\ & & 1 & 0 \end{array} \right) \text{ and } H'_X^{(2)} = \left( \begin{array}{cc|cc} 1 & 1 & 0 & 0 \\ & 1 & 1 & 0 \\ & & 0 & 0 \\ & & 0 & 0 \end{array} \right),$$

and the  $H_X^{\text{ini}}$  and  $H_Z^{\text{fin}}$  are exactly the same as in Example K.1.

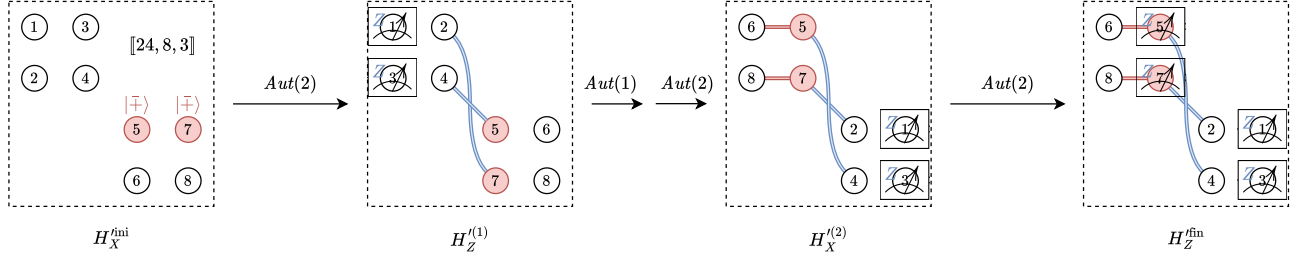


FIG. 7. The procedure for performing logical  $CNOT_{2 \rightarrow 8}$  in parallel with  $CNOT_{4 \rightarrow 6}$ .

**Example K.4** (Logical  $CNOT_{8 \rightarrow 6}$ // $CNOT_{2 \rightarrow 4}$  or logical  $CNOT_{6 \rightarrow 8}$ // $CNOT_{4 \rightarrow 2}$ ). In the  $[[24, 8, 3]]$  CC code, the logical

$$\begin{aligned} &CNOT_{8 \rightarrow 6} \text{ in parallel with } CNOT_{2 \rightarrow 4} \text{ or} \\ &CNOT_{6 \rightarrow 8} \text{ in parallel with } CNOT_{4 \rightarrow 2}, \end{aligned}$$

can be performed via parallel surgery with the logical qubits 1, 3, 5, 7 treated as logical auxiliary qubits. We first apply  $Aut(1)$ ,  $Aut(2)$  and  $Aut(3)$  sequentially to swap the logical qubits in the order shown below. One may be aware, after reordering these logical qubits, the logical  $CNOT$  gates that we intend to perform can be performed with the exact same procedure for the logical  $CNOT$  gates illustrated in Example K.1, Example K.2 or Example K.3, with the 1<sup>st</sup> and 5<sup>th</sup> logical qubits initialised in  $|\bar{\uparrow}\rangle$ .

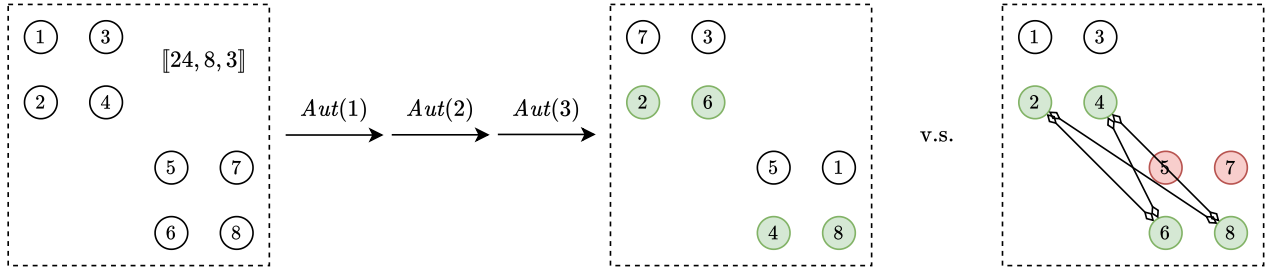
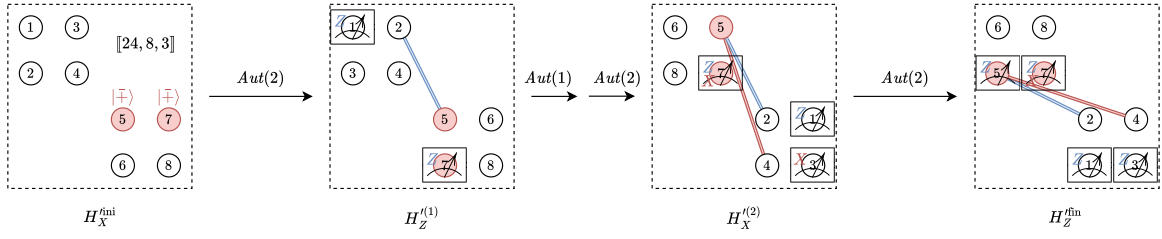


FIG. 8. After reordering of logical qubits, we notice that the intended logical  $CNOT$  gates can be performed with the exact same procedure as in Example K.1, Example K.2 or Example K.3. Here circles coloured green are the logical qubits we intend to involve in some logical  $CNOT$  gates and circles coloured in red are the auxiliary logical qubits initialised in  $|\bar{\uparrow}\rangle$ . The diamond arrows are the logical  $CNOT$  gates we have generated in the previous examples, with diamond aiming at the target of the  $CNOT$  gate.

**Example K.5** (Single logical  $CNOT$  gates controlled by the 2<sup>nd</sup> logical qubit). Below we present the procedure for performing single logical  $CNOT$  gates controlled by the 2<sup>nd</sup> logical qubit. All the initial stage product connection code are the same as in Example K.1.

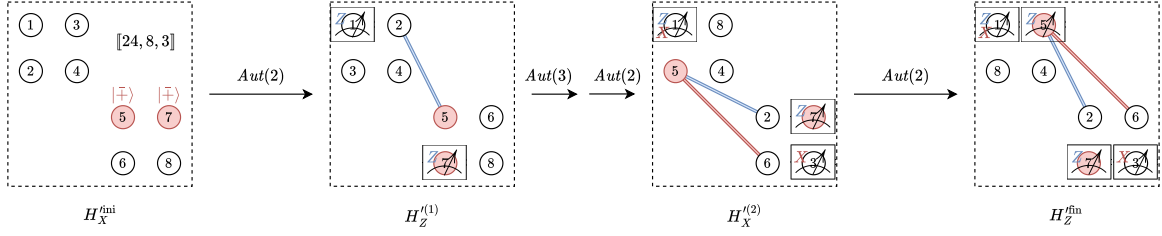
1.  $CNOT_{2 \rightarrow 4}$ : The relevant parity check matrices are

$$H'_Z^{(1)} = \left( \begin{array}{cc|cc} 1 & 0 & 0 & 0 \\ & 0 & 1 & 0 \\ & & 1 & 0 \\ & & 0 & 1 \end{array} \right), H'_X^{(2)} = \left( \begin{array}{cc|cc} 0 & 1 & 0 & 1 \\ & 0 & 1 & 0 \\ & & 0 & 1 \\ & & 0 & 0 \end{array} \right) \text{ and } H'_Z^{\text{fin}} = \left( \begin{array}{cc|cc} 0 & 1 & 0 & 0 \\ & 0 & 0 & 0 \\ & & 0 & 1 \\ & & 0 & 0 \end{array} \right).$$



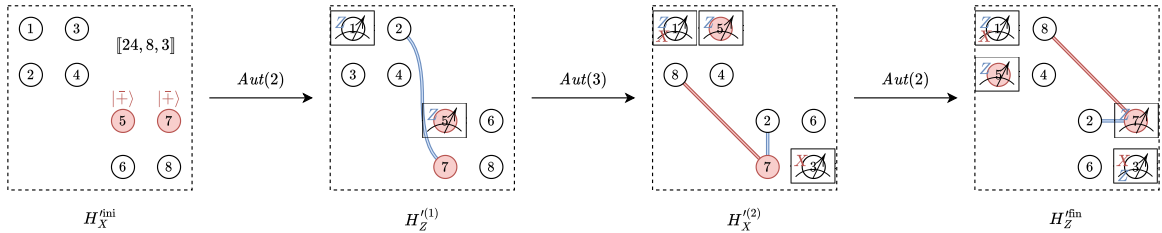
2.  $CNOT_{2 \rightarrow 6}$ : The relevant parity check matrices are

$$H_Z^{(1)} = \left( \begin{array}{cc|ccc} 1 & & 0 & 0 & \\ & 0 & & 0 & \\ & & 1 & & \\ & & & 1 & 0 & 0 \\ & & & & 1 & 0 \\ & & & & & 0 \end{array} \right), H_X^{(2)} = \left( \begin{array}{cc|ccc} 1 & & 0 & 0 & \\ & 1 & & 0 & 0 & \\ & & 0 & 0 & \\ & & & 0 & 0 & \\ & & & & 0 & 1 \end{array} \right) \text{ and } H_Z^{fin} = \left( \begin{array}{cc|ccc} 1 & 0 & & 0 & \\ & 0 & 0 & & \\ & & 1 & 0 & \\ & & & 0 & 0 & \\ & & & & 0 & 0 \end{array} \right).$$



3.  $CNOT_{2 \rightarrow 8}$ : The relevant parity check matrices are

$$H_Z^{(1)} = \left( \begin{array}{cc|ccc} 0 & 0 & & 0 & \\ & 1 & 0 & & \\ & & 0 & 0 & 1 & 1 \\ & & 1 & 0 & & \\ & & & 1 & 1 & 1 \end{array} \right), H_X^{(2)} = \left( \begin{array}{cc|ccc} 1 & & 0 & 0 & \\ & 1 & & 0 & 0 & \\ & & 0 & 0 & \\ & & & 0 & 0 & \\ & & & & 0 & 1 \end{array} \right) \text{ and } H_Z^{fin} = \left( \begin{array}{cc|ccc} 0 & & & 0 & \\ & 0 & 0 & & \\ & & 0 & & \\ & & & 0 & 1 & \\ & & & & & 1 \end{array} \right).$$



**Example K.6** (Single logical CNOTs controlled by the 8<sup>th</sup> logical qubit). We notice that all single logical  $CNOT$  gates controlled by the 8<sup>th</sup> logical qubit can be performed exactly in a same way as the 2<sup>nd</sup> logical qubit controlled  $CNOT$  gates in Example K.5 after applying the logical SWAP gates introduced by  $Aut(3)$ :

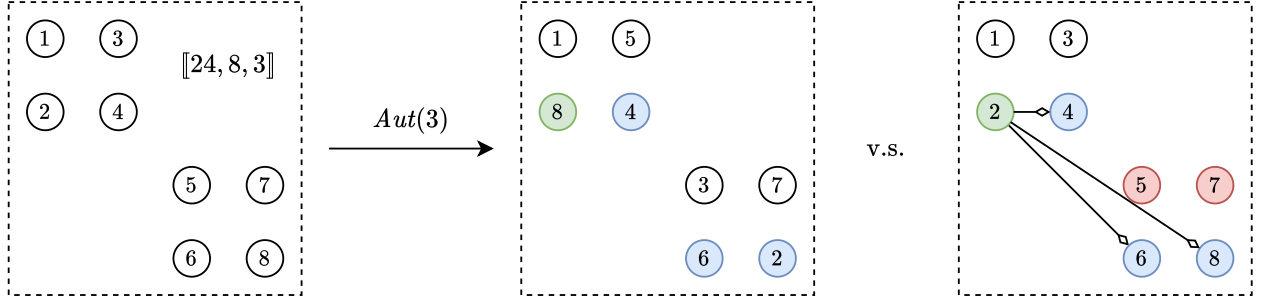


FIG. 9. After  $Aut(3)$ , we notice that the intended logical  $CNOT$  gates can be performed with the exact same procedure as in Example K.5. Here circles coloured green are the logical controls, circles coloured in blue are intended logical targets and circles coloured in red are the auxiliary logical qubits initialised in  $|\bar{0}\rangle$ . The diamond arrows are the logical  $CNOT$  gates we have generated in the previous example, with diamond aiming at the target of the  $CNOT$  gate.

### Appendix L: Full Clifford group over four logical qubits of the $[[24, 8, 3]]$ CC code

In this appendix, we demonstrate the full Clifford group over four logical qubits of the  $[[24, 8, 3]]$  CC code can be realised via parallel surgery, fold-transversal and automorphism gates. To be consistent with Appendix K, we label the logical qubits 2, 4, 6, 8 as data logical qubits while treating the logical qubits 1, 3, 5, 7 as auxiliary logical qubits.

#### 1. Arbitrary $\bar{S}_i\bar{S}_j^\dagger$ gates

We present here for the  $[[24, 8, 3]]$  CC code, we are able to perform arbitrary  $\bar{S}_i\bar{S}_j^\dagger$  gates where  $i, j \in \{2, 4, 6, 8\}$ . By initialising the auxiliary logical qubits 1, 3, 5, 7 in  $|\bar{0}\rangle$  with parallel surgery, we are able to generate these fault-tolerant  $\bar{S}_i\bar{S}_j^\dagger$  gates from the  $CZ-S$  gate introduced in Appendix J 1.

We begin with  $\bar{S}_4\bar{S}_8^\dagger$  generated from the original  $\bar{S}_1\bar{S}_4\bar{S}_5^\dagger\bar{S}_8^\dagger\bar{C}Z_{2,3}\bar{C}Z_{6,7}$ . Together with automorphism logical  $SWAP$  gates introduced in Appendix J 3, we initialise the auxiliary logical qubits 1, 3, 5, 7 in  $|\bar{0}\rangle$  via logical measurement on  $Z$  basis and Pauli frame correction. We then perform the  $CZ-S$  fold-transversal logical gate. However,

$$S|0\rangle = S^\dagger|0\rangle = |0\rangle,$$

the 1<sup>st</sup> and 5<sup>th</sup> auxiliary logical qubits are unchanged. Further, as 3<sup>rd</sup> and 7<sup>th</sup> auxiliary logical qubits are in  $|\bar{0}\rangle$  which leads a trivial action on the 2<sup>nd</sup> and 6<sup>th</sup> data logical qubits through  $\bar{C}Z$ , as

$$CZ_{a,b}(|\psi\rangle_a \otimes |0\rangle_b) = |\psi\rangle_a \otimes |0\rangle_b.$$

We are then left with logical action  $\bar{S}_4\bar{S}_8^\dagger$  only.

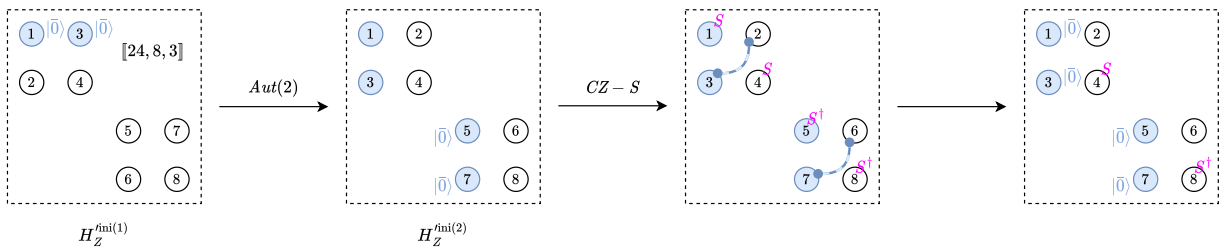


FIG. 10. The procedure for performing logical  $\bar{S}_4\bar{S}_8^\dagger$ , while having the auxiliary logical qubits 1, 3, 5, 7 initialised in  $|\bar{0}\rangle$ .

By utilising logical  $SWAP$  gates, we are able to reorder the logical qubits such that any pair  $(i, j)$  for  $i, j \in \{2, 4, 6, 8\}$  can be on the diagonal in the same configuration. Hence, we are able to generate arbitrary  $\bar{S}_i\bar{S}_j^\dagger$  gates for this  $[[24, 8, 3]]$  CC code.

Importantly, as the  $CZ$  gates are always acting on a pair of data and auxiliary logical qubits, any possible error propagation onto the physical supports of auxiliary logical qubits can be ignored. Hence, the arbitrary  $\bar{S}_i\bar{S}_j^\dagger$  gates on four data logical qubits are fault-tolerant.

## 2. Global $\bar{H}^{\otimes 8}$ gate

We are able to simplify the  $H$ - $SWAP$  fold-transversal logical gate introduced in Appendix J 2 via utilising the logical  $SWAP$  gates introduced in Appendix J 3.

$$\left( \bar{S}WAP_{1,6}\bar{S}WAP_{4,7}\bar{S}WAP_{5,8}\bar{S}WAP_{6,7} \prod_{i=1}^8 \bar{H}_i \right) Aut(1)Aut(3)Aut(1)Aut(1) = \prod_{i=1}^8 \bar{H}_i \equiv \bar{H}^{\otimes 8}.$$

The corresponding physical operation on the physical qubits is

$$\bar{H}_{\text{phys}}^{\otimes 8} = SWAP_{2,3}SWAP_{4,7}SWAP_{5,9}SWAP_{6,8}SWAP_{11,12}SWAP_{13,24}SWAP_{14,23}SWAP_{15,22}SWAP_{16,18}SWAP_{19,21} \prod_{i=1}^{24} H_i.$$

As we label the logical qubits 1, 3, 5, 7 as auxiliary logical qubits, this  $\bar{H}^{\otimes 8}$  automatically acts as  $\bar{H}^{\otimes 4}$  over the four data logical qubits. Together with logical  $CNOT$  gates between arbitrary pairs of data logical qubits as in Appendix K and arbitrary  $S_iS_j^\dagger$  gates, we are able to generate the full Clifford group over these four logical data qubits, following Theorem VII.1.